Bio-basierte Carbon (Nano-)Partikel als Polymerverstärker

Bio-based carbon (nano-)spheres for polymer reinforcement

Dissertation

Zur Erlangung des Doktorgrades

an der Universität für Bodenkultur Wien

Department für Materialwissenschaften und Prozesstechnik

Institut für Holzforschung

Betreuer:
Ao. Univ. Prof. Dipl.-Ing. Dr. Wolfgang Gindl-Altmutter

Beratungsteam:
Assoc. Prof. Dipl.-Chem. Dr. Falk Liebner
Dipl.-Ing. Dr. Stefan Veigel

Eingereicht von:
Janea Kristin Köhnke, MSc.

Wien, Februar 2019

VORWORT

Diese Arbeit wurde von Mai 2015 bis Februar 2019 an der Universität der Bodenkultur im Department für Materialwissenschaften und Prozesstechnik im Institut für Holzforschung erstellt. Die finanzielle Grundlage für die Forschung kam aus dem Brückenschlagprogramm der Österreichischen Forschungsförderungsgesellschaft (FFG) durch das Projekt „Bio-based carbon nanospheres for polymer reinforcement“ Nr. 846543.

Die Erstellung einer Doktorarbeit ist nie das Werk einer einzelnen Person. Deswegen möchte ich mich an dieser Stelle bei all denen bedanken, die mich bei der Anfertigung fachlich und persönlich unterstützt haben und ohne die es nicht möglich gewesen wäre, diese Arbeit zu schreiben. Mein ganz besonderer Dank geht an meinen Betreuer, Prof. Dr. Gindl-Altmutter, für die Idee des Themas, die wissenschaftliche und finanzielle Unterstützung, persönliches Verständnis sowie das mir entgegengebrachte Vertrauen. Danke an Dr. Stefan Veigel, der unermüdlich geholfen und Fragen beantwortet hat, Gerhard Emsenhuber, der viele Messungen unterstützt hat und Dr. Harald Rennhofer, der mit seiner geduldigen Art geholfen, beraten und Proben gemessen hat. Mein Dank geht an Dr. Falk Liebner, der Korrekturen durchgeführt und mich fachlich beraten hat. Ich bedanke mich bei all meinen Kollegen der Holzforschung und weiteren Kollegen, die viele Proben für mich untersucht haben und bei Fragen jederzeit für mich da waren. Ein persönlicher Dank geht an meine Bürokollegen Sabine Herzele und Dr. Jérôme Colson, die immer ein offenes Ohr für Fragen und Probleme hatten, mich vom ersten Tag an herzlich aufgenommen und mich über die drei Jahre treu begleitet haben.

Herzlich bedanke ich mich bei meiner Familie, vor allem meinen Eltern, für die Finanzierung meiner langen Ausbildung, die Unterstützung aller meiner Entscheidungen, das Interesse an meiner Arbeit, anregende Diskussionen und ermunternde Worte. Zuletzt ein großes Dankeschön an meine Freunde, die die Zeit in Wien zu einem unvergesslichen Lebensabschnitt gemacht haben, die mich während der drei Jahre trotz zum Teil großer Entfernung immer wieder motiviert und auch mal abgelenkt und jederzeit ein offenes Ohr für mich hatten.

ZUSAMMENFASSUNG

In dieser Arbeit wurde die Strukturveränderung von Lignin während der Carbonisierung untersucht. Ziel war es, Unterschiede bei der Carbonisierung zwischen verschiedenen Ligninen (Kraft Lignin, Lignosulfonat, Soda Lignin und Organosolv Lignin) und Ablaugen (Sulfit- und Sulfatablauge) herauszufinden, und den Einfluss der Carbonisierungstemperatur (800 °C, 1200 °C, 1600 °C und 2000 °C), sowie der Größe (Nano Lignin im Vergleich zu Mikro Lignin) zu untersuchen. Zusätzlich wurden Forschungen angestellt, um die elektrische Leitfähigkeit der carbonisierten Lignine zu testen und zu erklären. Die hergestellten Carbonpartikel wurden mit Polymeren (PLA, PCL) zu Compositen verarbeiten, um auch diese leitfähig zu machen. Es wurden nicht nur elektrische Leitfähigkeit, sondern auch Veränderungen des E-Moduls und der Zugfestigkeit der hergestellten Composite bestimmt. Es hat sich herausgestellt, dass eine Carbonisierungstemperatur von 2000 °C notwendig ist, um geordnete graphitische Strukturen im Lignin auszubilden. Dies ist am besten mit sprühgetrockneter Schwarzlauge gelungen. Die Leitfähigkeit variierte zwischen allen Proben stark, beste Ergebnisse lieferte hierbei das Kraft Lignin. Leitfähige Composite konnten hergestellt werden mit 30 % carbonisiertem Kraft Lignin und Organosolv Lignin, Lignosulfonat zeigte als Partikel schon schlechte Leitfähigkeit, diese geringe Leitfähigkeit machte sich auch im Composit bemerkbar. Soda Lignin erzielte bei 30 % Füllung keine Leitfähigkeit. Insgesamt konnte gezeigt werden, dass elektrisch leitfähige Carbonpartikel aus Lignin hergestellt werden können, die wiederum die Herstellung vollständig biobasierter funktioneller Polymerverbunde ermöglichen.

ABSTRACT

This dissertation addresses the structural change of lignin particles when carbonised. Differences of the produced carbon particles were compared between diverse lignins (kraft lignin, lignosulfonate, soda lignin and organosolv lignin), two spent liquors (sulphite and kraft pulping liquors), final carbonisation temperature (800 °C, 1200 °C, 1600 °C and 2000 °C) as well as starting size of the lignin particles (macro-sized and sub-macro-sized). Additionally research was done to measure and explain electrical conductivity of carbon particles. Different polymers (PLA, PCL) were used as matrix and filled with produced carbon particles to obtain electrically conductive polymers. The impact of the particles on the produced composites was measured, such as Young´s modulus and tensile strength. Graphitic structures in lignin derived carbon particles were obtained with carbonisation temperatures of 2000 °C, not below. The carbon structure was the best for the spray dried kraft pulping liquor. In general, electrical conductivity had high variations, best values were obtained for the carbon particles derived from kraft lignin. Composites had a percolation threshold for electrical conductivity at 25 %, composites reaching this threshold and filled with carbon particles obtained from kraft lignin or organosolv lignin showed conductivity. All produced composites showed higher stiffness while extensibility and strength generally decreased. Overall, it was demonstrated that electrically conductive carbon can be derived from lignin, enabling the production of fully biobased functional composite materials.

INHALTSVERZEICHNIS

1. Einleitung 1
2. Material und Methoden 6
   2.1. Material 6
   2.2. Polymere für Filme/Herstellung 6
   2.3. Herstellung von Nanolignin 6
   2.4. Thermische Ligninbehandlung 11
   2.5. Charakterisierungsmethoden der Lignine/Carbone 11
   2.6. Charakterisierung der Filme 12
3. Zusammenfassung der Ergebnisse 14
4. Ausblick 31
5. Literaturverzeichnis 32
6. Abbildungsverzeichnis 42
7. Tabellenverzeichnis 43

1. EINLEITUNG

Lignin ist nach Cellulose das zweithäufigste Biopolymer auf der Welt[1]. Nahezu jede Landpflanze besteht zu 12 bis 40 Prozent aus Lignin. Die Aufgabe des Lignins in der Pflanze ist die Herstellung der Druckfestigkeit, Hydrophobierung, Schutz vor Mikroorganismen, sowie Bindemittel zwischen den einzelnen Elementen zu sein. Erst durch das Lignin sind Pflanzen in der Lage, in Richtung Himmel zu wachsen. Trotz des großen Ligninaufkommens sind die Nutzungsmöglichkeiten derzeit noch stark eingeschränkt. Dies liegt an den komplexen und schwer aufzubrechenden chemischen Strukturen des Lignins. Das Lignin ist ein amorphes aromatisches Polymer, welches thermoplastische Eigenschaften hat und dreidimensional vernetzt ist. Lignin setzt sich zusammen aus substituierten Phenylpropanen. Die Vorstufen des Lignins sind Cumarylalkohol (H), Coniferylalkohol (G) und Sinapylalkohol (S). Diese drei Bausteine unterscheiden sich nur durch die Anzahl der Methoxylgruppen ansteigend von H mit null Gruppen zu S mit zwei Gruppen. Die Holzart legt fest, aus welchen Bausteinen das Lignin gebildet wird, so hat Nadelholz einen G-Anteil von über 95 %, Laubholz etwas mehr S- als G-Bausteine und Gräser von allen drei Bausteinen einen ähnlich hohen Anteil. Die einzelnen Bausteine werden mittels Ether- oder C-C-Bindungen miteinander verbunden, wobei der größte Anteil β-O-4-Bindungen sind. Weitere wichtige Bindungstypen sind die β-5- und 5-5‘-Bindungen, insgesamt gibt es neun verschiedene Bindungstypen. Genauso vielfältig wie die Bindungstypen sind die Endgruppen des Lignins; es gibt über elf unterschiedliche Typen. Aufgrund dieser Komplexität und Inhomogenität der Ligninstruktur stellen der Abbau des Lignins und eine Nutzbarmachung eine große Herausforderung dar.

Während der Zellstoffherstellung wird das Lignin von der Cellulose, dem Hauptbestandteil der Pflanzen, getrennt und oftmals zusammen mit den Aufschlusschemikalien verbrannt. Beim Verbrennungsprozess dient Lignin nicht nur als Energielieferant, sondern es ermöglicht auch die Chemikalienrückgewinnung[2]. Dabei geht in modernen Bioraffinerien bis zu 55 % der Holzausgangsmasse in die Energieproduktion, um die Prozessenergie zu gewinnen und somit energetisch autark zu sein. Das weltweit jährliche Aufkommen von Lignin beläuft sich auf ungefähr 50 Millionen Tonnen[3]. Dabei wird pro Kilogramm Lignin durchschnittlich 25 MJ Energie gewonnen[4]. Es wird sowohl thermische Energie, als auch Strom hergestellt. Dieser Wert variiert zwischen Aufschlussvarianten und Art der Energiegewinnung. Bei dem Zellstoffaufschluss entstehen je nach Verfahren vier verschiedene Lignine: Kraft Lignin, Lignosulfonat, Soda Lignin und Organosolv Lignin[5-7].

Kraft Lignin entsteht im Sulfatkochprozess, hierbei wird das Lignin in der Kochlauge gelöst. Die Kochlauge besteht aus Wasser, Natriumsulfid und Natriumhydroxid[8]. Nach dem Aufschluss beinhaltet die Ablauge braune Ligninfragmente mit unterschiedlichem Molekulargewicht[9]. Um das Lignin von den Aufschlusschemikalien zu trennen, kann es ausgefällt werden, wonach das Lignin hohe Aschegehalte, viele Hydroxyl- und Carboxylgruppen sowie viele kondensierte

Strukturen hat[10]. Weltweit entsprechen ungefähr 85 % des produzierten Lignins Kraft Lignin[11].

Lignosulfonate werden im Sulfitkochprozess gewonnen: Das Holz wird in schwefeliger Säure gekocht, wobei das Lignin durch die Sulfonierung der Seitengruppen des Lignins und durch die starke Fragmentierung wasserlöslich wird[12]. Trotz des starken Aufschlusses hat das hellbraune Lignin ein hohes Molekulargewicht und einen hohen Aschegehalt[13]. Der Gehalt an Zuckern ist gering, außerdem ist das Lignin wasserlöslich aufgrund der zum Teil geladenen Seitengruppen[14]. Nur 6 % des weltweiten Ligninaufkommens ist Lignosulfonat[15].

Soda Lignin wird im Sodakochprozess hergestellt. Die Kochlauge besteht aus Natronlauge, in der die Pflanze gelöst wird. Dieser Aufschlussprozess wird meist für Einjahrespflanzen angewendet, selten auch für Laubhölzer[16]. Das Soda Lignin ist komplett schwefelfrei und hat aufgrund der Einjahrespflanzen als Ressource oft hohe Silikat- und Stickstoffgehalte[17,18]. Obwohl Einjahrespflanzen fast ausschließlich mit dem Sodaverfahren aufgeschlossen werden, kommt es weltweit nur zu einem Anteil von 8 %[19].

Der Organosolvprozess basiert auf Wasser kombiniert mit organischen Lösungsmitteln[20]. Bei dieser Aufschlussmethode hat das Lignin ein geringes molekulares Gewicht und eine hohe Reinheit, dadurch dass es schwefelfrei ist und einen geringen Aschegehalt hat[21,22]. Organosolv Lignin wird bisher nicht großindustriell hergestellt, allerdings laufen die ersten Pilotanlagen einwandfrei.

Wie oben erwähnt, wird das Lignin häufig energetisch genutzt. Es gibt allerdings einige Einsatzbereiche, in denen man das Lignosulfonat und Kraft Lignin stofflich statt energetisch verarbeitet. Lignosulfonat zum Beispiel wird stofflich zu über 80 % genutzt. Vor allem als Dispergiermittel kommt Lignosulfonat in verschiedensten Branchen zum Einsatz. Wertsteigernd finden sich Anwendungsgebiete als Bindemittel, wie zum Beispiel in Klebstoffen, wo es aufgrund seiner phenolischen Gruppen als Phenolersatz verwendet wird[23,24]. Auch als Additiv zu Beton und Gips[25], als Emulsionsmittel und Stabilisator, sowie als Gerbstoff oder Komplexierungsmittel wird Lignosulfonat genutzt. In die einzelnen Moleküle aufgebrochen kann aus Lignosulfonat Vanillin hergestellt werden. Die Anwendungsgebiete für Kraft Lignin sind derzeit noch stark beschränkt auf Phenolersatz in Harzen, auf Dispergiermittel mit weit weniger Einsatzgebieten, als Stabilisator, in der Elektroindustrie in Autobatterien[26] und in der Galvanisierung.

In den letzten 20 Jahren gibt es zunehmend Forschungsaktivität auf dem Gebiet der Ligninnutzung, somit werden in Zukunft weitere Verwendungsmöglichkeiten hinzukommen[27-30]. Grob werden die Nutzungsmöglichkeiten in drei Gruppen unterteilt: Die Nutzung als Aromaten[31-33], als Thermoplaste [34] und als Duromere, wie in Abbildung 1 dargestellt. Als Aromat lässt sich Lignin zur Pyrolyse, Hydrierung, Hydrothermolyse, Hydrolyse (Vanillin) oder BTEX (Benzol, Toluol, Ethylbenzol und Xylol) einsetzen[35]. Im Anwendungsgebiet der Thermoplaste kommen WPC (Wood Plastic Composites) oder andere Thermoplaste in Frage[36-39]. Bei den Duromeren gibt es eine große Bandbreite an Einsatzbereichen: in Polyurethanen, in Klebstoffen, als Füllstoff[40-42] oder aber als Carbonfaser oder Carbonpartikel. Die Forschung beschränkt sich nicht nur auf die Suche nach Anwendungsmöglichkeiten, sondern befasst sich auch mit der Reinigung und Modifizierung des Lignins[43-46]. So wurde das Ligno-Boost Verfahren entwickelt, um Kraft Lignin auszufällen und großindustriell herzustellen. Die erste LignoBoost Anlage, die in ein Zellstoffwerk implementiert werden konnte, wurde 2013 in Plymouth, Nordamerika, in Betrieb genommen. Inzwischen ist eine weitere LignoBoost Anlage in Kotka, Finnland, eröffnet worden.

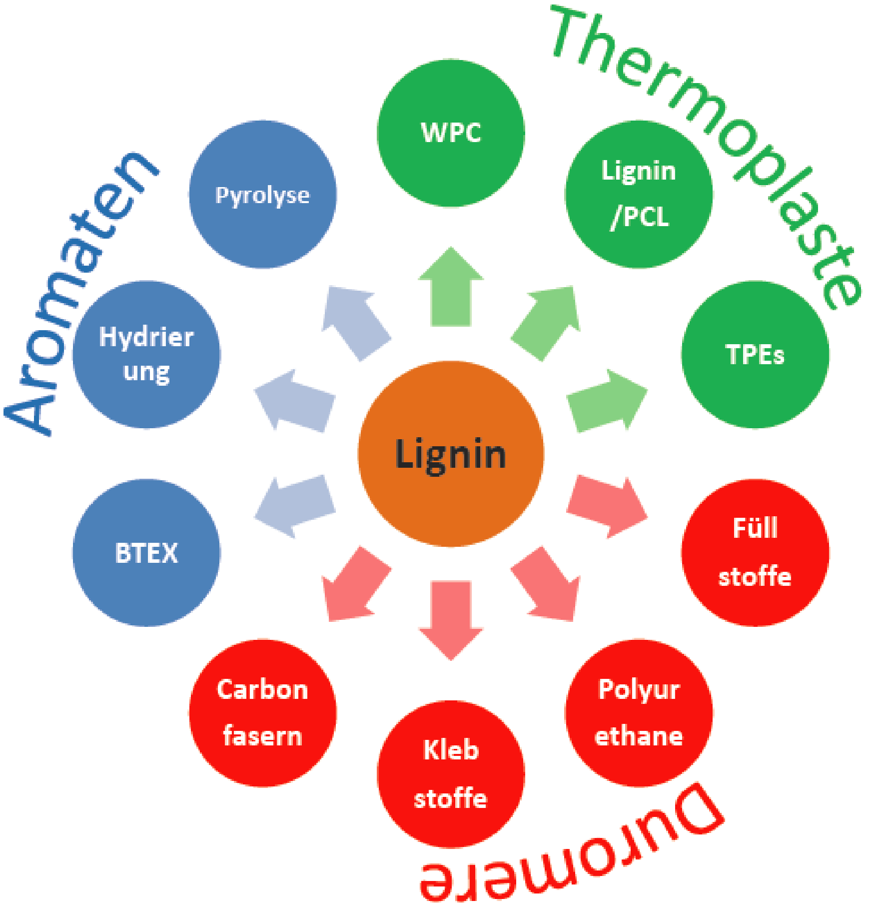

Abbildung 1: Überblick über Ligninnutzung

Trotz der steigenden Forschungsaktivität in den letzten 20 Jahren ist bis heute noch kein deutlich wertsteigernder Nutzungszweig für Lignin großindustriell umgesetzt worden. Allerdings zeichnet sich ein vielversprechender Forschungsbereich in der Lignincarbonisierung immer deutlicher ab. Hierbei gibt es verschiedene Ansätze: Carbonfasern[47-49], Siebe aus den Carbonfasern[50], Carbonpartikel als Füller für leitfähige Composite[51,52], Carbonpartikel in Akkus[53,54], Carbonvorlagen[55] sowie Aktivkohle[56,57], dargestellt in Abbildung 2. Neben verschiedenen eingesetzten Ligninen und Zielen unterscheidet sich vor allem die Herstellungsart. Im Bereich der Herstellung von Carbonfasern aus Lignin wächst die

Forschungsaktivität in den letzten Jahren stark[58-60]. Ziel ist es, günstigere, für die Massenproduktion taugliche Carbonfasern zu erzeugen. Schwierigkeiten hierbei sind insbesondere die Reinheit des Lignins, die Mischkomponenten, die Spinntechnologien und die erzielten mechanischen Eigenschaften[61,62]. Im Bereich der Carbonpartikel gibt es, im Gegensatz zu den Fasern, sehr unterschiedliche Anforderungen an die Eigenschaften, was die Herstellungsprozesse und Problematiken deutlich unterschiedlich macht[63-65]. Rußpartikel werden meist als Zusatzstoff für Reifen eingesetzt und sind sehr günstige Füllmittel. Allerdings können die Partikel auch als Zusatzstoff in Compositen genutzt werden, um Leitfähigkeit zu erzeugen[54,66,67] oder in Zement, für verbesserte Feinverteilung und Interaktion[68]. Andere Einsatzbereiche sind Druckerschwärze, Farbe oder Wärmeleitpasten[65]. Auch gibt es Ansätze, Hybridpartikel aus Lignin und Rußpartikeln herzustellen, bevor diese dann in Compositen eingesetzt werden[69]. All diese Ansätze sind aufgrund der hohen Wertsteigerung des Lignins relevant.

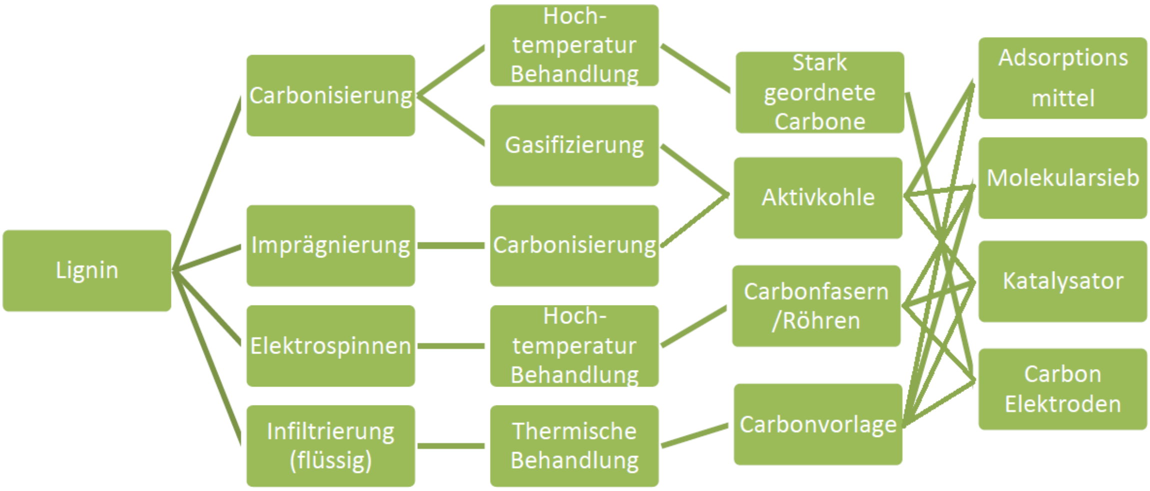

Abbildung 2: Übersicht über Herstellungswege und Verwendungsarten von carbonisiertem Lignin nach Kai[70]

Da die Eigenschaften des erzeugten Carbons aus Lignin von den Eigenschaften des eingesetzten Lignins abhängen, ist es unabdingbar, sich auch mit der Herstellung von Nanopartikeln aus Lignin zu befassen. Hierbei gibt es mechanische und chemische Ansätze, die sich grundlegend unterscheiden: bei mechanischen Ansätzen wird das Lignin gemahlen oder anderweitig in kleinere Partikel aufgespalten, während beim chemischen Ansatz das Lignin aufgelöst wird, um es dann auszufällen und bestimmte Größen zu erreichen. Mechanische Ansätze sind die Verkleinerung der Partikel durch Ultraschall, wobei die Partikel miteinander kollidieren[71-74], und Zerkleinerung durch den Homogenisator[75]. Chemische Ausfällungen variieren durch den Einsatz verschiedener Lösungs- und Ausfällmittel: Ethanol/Wasser[76], Ethylenglycol/wässrige Salzsäure[77], Aceton/superkritisches Kohlenstoffdioxid[78], Wasser/PDADMAC (Polydiallyldimethylammoniumchlorid)[79]. Weiterhin gibt es Ansätze, Kraftlignin nach Größe durch unterschiedliche Ausfällmittel zu sortieren[80].

Das Ziel der vorliegenden Arbeit ist die Herstellung und Charakterisierung von Carbonpartikeln, die aus verschiedenen Ligninen gewonnen werden. Die Carbonpartikel sollen als Füllstoff für Polymere dienen, welche ebenfalls hergestellt und charakterisiert werden. Dieser Forschungsbereich ist vor allem deshalb interessant, weil die Partikelherstellung deutlich einfacher und kostengünstiger als das Faserspinnen aus Lignin ist. Weiterhin bieten carbonisierte Ligninpartikel eine biobasierte Alternative zu den Carbon Blacks, die bisher ausschließlich aus Erdöl gewonnen werden. Erste Untersuchungen ergaben, dass die carbonisierten Ligninpartikel interessante Eigenschaften als Füllstoff aufweisen, das gilt es weiter zu untersuchen und zu erforschen. Ausgehend von verschiedenen Ligninen und Ablaugen wurden Zerkleinerungsmethoden, Thermostabilisierung und Carbonisierung bei unterschiedlichen Temperaturen durchgeführt. Untersuchungen mit mikroskopischen und röntgenstrukturanalytischen Methoden, sowie Leitfähigkeitsmessungen haben stattgefunden. Mit den hergestellten Partikeln als Füllmaterial wurden unterschiedliche Filme hergestellt, die mit mechanischen Prüfverfahren und Leitfähigkeitsmessungen charakterisiert wurden.

Die Ergebnisse dieser vorliegenden Arbeit sind in vier Publikationen veröffentlicht. Die Publikationen I und II befassen sich mit der Fragestellung, welchen Unterschied es bei den verschiedenen Ligninen nach der Carbonisierung gibt und welche Carbonisierungstemperaturen notwendig sind. Die Publikation III erläutert die Frage, ob die Aufreinigung der Lignine notwendig ist oder ob es auch möglich ist, direkt mit der Ablauge in die Carbonisierung zu gehen. Publikation IV behandelt den Unterschied zwischen normalem Lignin und Nanolignin als Ausgangsrohstoff für das Carbon.

Publikation I: Comparison of four technical lignins as resource for electrically conductive carbon particle

Publikation II: Carbon Microparticles from Organosolv Lignin as Filler for Conducting Poly(Lactic Acid)

Publikation III: Electrically conducting carbon microparticles by direct carbonization of spent wood pulping liquor

Publikation IV: Electrically-Conductive Sub-Micron Carbon Particles from Lignin: Elucidation of Nanostructure and Use as Filler in Cellulose Nanopapers

2. MATERIAL UND METHODEN

2.1. MATERIAL

LIGNINE

Es wurden sechs unterschiedliche Lignine genutzt, zwei Kraft Lignine, ein Lignosulfonat, ein Soda Lignin und zwei unterschiedliche Organosolv Lignine. Diese Auswahl entspricht den am Markt gängigen Ligninen. Das erste Kraft Lignin war das Indulin AT, gekauft bei MeadWestvaco (Richmond, Virginia, US), das zweite Kraft Lignin war ebenfalls Indulin AT, aber im Aerosol Flow Reaktor behandelt, zur Verfügung gestellt von Orlando J. Rojas und seinem Team, produziert nach der Methode in M. Ago et al. [81]. Das Lignosulfonat war ein Natrium-Lignosulfonat und wurde bei Borregaard gekauft (Sarpsborg, Norwegen). Das Soda Lignin war das Protobind 2400, hergestellt in Indien und gekauft bei GrenValue (Alpnach Dorf, Schweiz). Das Organosolv Lignin, welches in der zweiten Publikation genutzt wurde, kam aus Indien, Produktnummer CP8068-03-9-BULK von Chemical Point UG (Deisenhofen, Deutschland). Das Organosolv Lignin der ersten Publikation wurde von Frauenhofer (Leuna, Deutschland) zur Verfügung gestellt.

ABLAUGEN

Es wurden eine Sulfitablauge, Bleichabwasser von Sappi, und eine Sulfatablauge, Schwarzlauge von Mondi, zur Verfügung gestellt. Der Sulphitaufschluss, sowie der Sulfataufschluss sind die beiden einzigen in Österreich angewendeten Aufschlussprozesse, weswegen diese Ablaugen eine gute Referenz sind.

2.2. POLYMERE FÜR FILME/HERSTELLUNG

Es wurden ein biobasiertes Polymer Polylactid (PLA) und ein biologisch abbaubares Polymer Polycaprolacton (PCL) als Matrix gewählt. Beide Polymere sind leicht zu verarbeiten. PCL wurde in Toluol mit einer Konzentration von 100 g/L gelöst, PLA mit gleicher Konzentration in Chloroform. Die Carbonpartikel wurden in das flüssige PCL eingerührt mit einem Verhältnis von 30 % Masse Carbonpartikel und 70 % Masse PCL. Bei PLA wurden verschiedene Masseprozente zwischen 0 und 35 % eingemischt. Die Mischungen wurden in Petrischalen abgegossen und das Lösungsmittel ist abgedampft. Die entstandenen Composite wurden zerschnitten und in einer Heißpresse bei 80 °C (PCL)/ 150 °C (PLA) neu verpresst. Dieser Vorgang wurde drei Mal wiederholt, um eine gleichmäßige Verteilung der Partikel zu gewährleisten. Beim letzten Pressvorgang wurde die Filmdicke auf 0,5 mm eingestellt und Teststreifen von 6 mm x 60 mm hergestellt.

2.3. HERSTELLUNG VON NANOLIGNIN

Da kommerziell erhältliche Ligninpulver relativ große Partikel (Größenordnung 100 µm) enthalten, wurden verschiedene Verfahren zur Herstellung kleinerer Partikel erprobt. Auf Grund gut bekannter Zusammenhänge in Partikel-gefüllten Polymerverbundwerkstoffen[82] wurden hier entsprechend vorteilhafte Eigenschaften erwartet. Zur Herstellung von Nanolignin wurden drei mechanische Methoden gewählt: das Ultraschallbad, der Homogenisator und der Mikrofluidizer. Weiterhin wurde im Rahmen dieser Arbeit durch Sprühtrocknung und Ausfällung versucht, Nanolignin herzustellen.

ULTRASCHALLBAD

Für das Ultraschallbad wurde eine Suspension aus Wasser mit 0,7 % Kraft Lignin in ein Gefäß mit Rührfisch gefüllt, wie in Abbildung 3 A) abgebildet. In dieses Gefäß wurde für einige Sekunden eine Ultraschallsonde mit einer Eintauchtiefe von 3 cm gehalten. Die genauen Versuchsparameter der drei Durchläufe sind in Tabelle 1 zu finden.

Tabelle 1: Versuchsparameter Ultraschallbad

	Leistung (W)	Frequenz (kHz)	Amplitude (mm)	Zeit (sek)	Energie absorbiert (J/cm^3)	Energie (J/ml)
Versuch I	8,9	19,02	0,002	60	0,53	6,675
Versuch II	8,9	19,028	0,002	375	0,53	41,718
Versuch III	26,8	19,045	0,005	125	12,9	41,875

HOMOGENISATOR

Eine Suspension aus Wasser und Kraft Lignin mit einem Ligningehalt von 0,5 % wurde durch einen Homogenisator gefahren, der Druck langsam erhöht auf 800 bar und anschließend 15 Durchläufe bei 800 bar durchgeführt. Die schematische Darstellung des Homogenisators ist in Abbildung 3 B zu sehen.

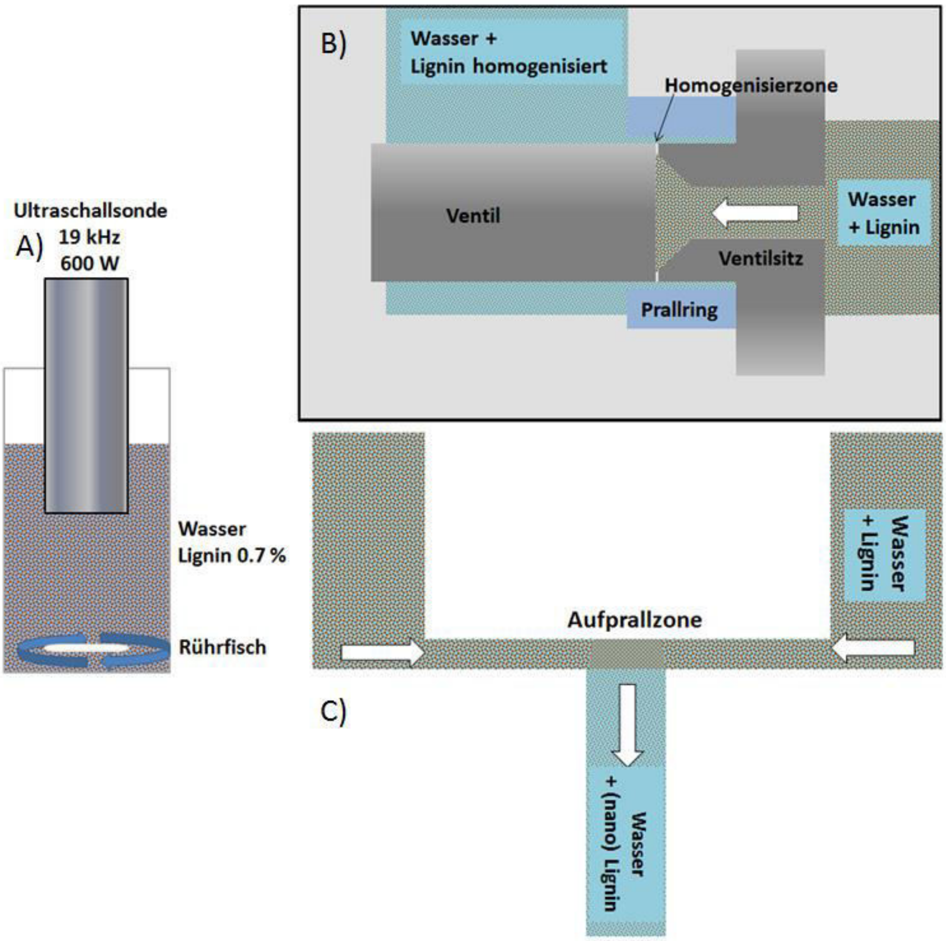

Abbildung 3: Schematische Darstellung A) der Ultraschallsonde, B) des Homogenisators und C) des Mikrofluidizers.

MIKROFLUIDIZER

Im Mikrofluidizer (Abbildung 3 C)) wurde eine Suspension von Wasser mit 10 %/20 % Kraft Lignin mehrfach durch ein oder zwei Zellen gepumpt bei unterschiedlichen Zellengrößen und einer unterschiedlichen Anzahl von Durchläufen. Die genauen Versuchsparameter der Unterschiedlichen Proben sind in Tabelle 2 aufgeführt.

Tabelle 2: Versuchsparameter Mikrofluidizer

Probe	Stoffgehalt	Zelle 1 (µm)	Zelle 2 (µm)	Minuten	Durchläufe
1	10		400	5	8
2	10		400	10	16
3	10		400	15	23
4	10	400	200	5	8
5	10	400	200	10	16

Probe	Stoffgehalt	Zelle 1 (µm)	Zelle 2 (µm)	Minuten	Durchläufe
6	10	400	200	15	23
7	10	200	100	5	8
8	10	200	100	10	16
9	10	200	100	15	23
10	10	100	75	5	8
11	10	100	75	10	16
12	10	100	75	15	23
13	20		400	5	8
14	20		400	10	16
15	20		400	15	23
16	20	400	200	5	8
17	20	400	200	10	16
18	20	400	200	15	23
19	20	400	200	20	30
20	20	400	200	25	38
21	20	400	200	30	45

SPRÜHTROCKNUNG

Die Ablaugen wurden vor dem Sprühtrocknen auf einen bestimmten Feststoffgehalt eingestellt. Danach wurden die Proben mit unterschiedlichen Stoffdichten, Temperaturen und Pumpgeschwindigkeiten getrocknet, ersichtlich in Tabelle 3.

Tabelle 3: Versuchsparameter Sprühtrocknung

Probe	Drüse (mm)	Stoffdichte (%)	Temperatur (°C)	Durchlauf 100ml (min)	Pumpe (%)
1	1,5	11	105	16	20
2	1,5	20	105	20	20
3	2,8	20	115	30	10
4	2,8	20	120	16	20

AUSFÄLLUNG

Beim Ausfällen wurde das Kraft Lignin in verschiedenen Lösungsmitteln aufgelöst, indem das Lignin zum Lösungsmittel hinzugefügt und 72 Stunden bis zum vollständigen Auflösen des Lignins im Ultraschallbad gerührt wurde. Anschließend folgte das Filtern und Zentrifugieren, um Verunreinigungen herauszubekommen. Dann wurde mit einer bestimmten Tropfgeschwindigkeit das Fällungsmittel unter Rühren zur Lösung hinzugegeben, dieses führte zum Ausfällen des Lignins. Eine schematische Darstellung des Ausfällvorgangs ist in Abbildung 4 zu sehen.

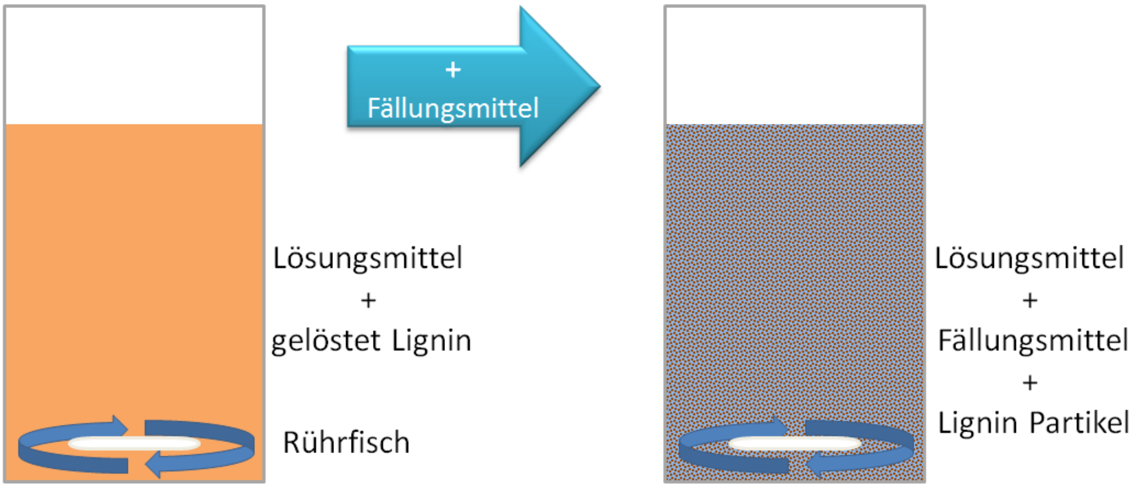

Abbildung 4: Schematische Darstellung des Ausfällvorgangs

Das Lignosulfonat wurde im Wasser gelöst, indem es 24 h gerührt wurde, danach wurde die Lösung filtriert. Das Fällungsmittel wurde unter Rühren mit einer Spritze schnell hinzugefügt, anschließend erfolgte das Rühren der Suspension für weitere 10 Minuten. Die Suspension wurde bei 1500 g 10 Minuten bei 20 °C zentrifugiert und im Überstand befanden sich die Nanopartikel. Die Versuchsparameter sind in Tabelle 4 zu sehen.

Tabelle 4: Versuchsparameter Ausfällversuche

Lignin	Lösungs-mittel	Fällungs-mittel	Lignin (mg/ml)	Tropfgesch-windigkeit (ml/min)	Fällungs-mittel am Ende (%)
Kraft Lignin	Dioxan	Wasser	4	3,3	90
Kraft Lignin	Dioxan	Wasser	4	7,04	90
Kraft Lignin	Dioxan	Wasser	4	9,43	90
Kraft Lignin	Dioxan	Cyclohexan	1	2	1
Kraft Lignin	Dioxan	Cyclohexan	1	2	5
Kraft Lignin	Dioxan	Cyclohexan	1	2	7
Kraft Lignin	Dioxan	Cyclohexan	1	2	9
Kraft Lignin	Dioxan	Cyclohexan	1	2	10
Lignosulfonat	Wasser	Aceton	10	200	90
Lignosulfonat	Wasser	Aceton	10	200	50

DYNAMISCHE LICHTSTREUUNG

Partikelgrößenbestimmung der Partikel in Suspension wurde mit dynamischer Lichtstreuung (DLS) am Zetasizer Nano ZS mit der Software Ver. 7.03 durchgeführt. Die Temperatur der Probe betrug 25 °C, die Zählrate war 231,5 kcps und ein Scan wurde 60 Sekunden durchgeführt.

2.4. THERMISCHE LIGNINBEHANDLUNG

THERMOSTABILISIERUNG

Die Thermostabilisierung erfolgte bei allen Proben gleich. Das Pulver wurde in einer dünnen Schicht gleichmäßig in einer Petrischale verteilt und die Schalen in einem Ofen bei Umgebungsatmosphäre auf 250 °C erhitzt. Dabei wurde der Ofen so programmiert, dass er mit einer Heizrate von 0,01 °C*min^{-1} das Pulver erhitzte.

CARBONISIERUNG

Die Carbonisierung erfolgte in einem GERO HTK8 Ofen, der ein Volumen von 6 Litern hatte. Die Pulver wurden in Graphittiegel eingewogen, über Nacht in einem Ofen bei 103 °C getrocknet, um die restliche Feuchtigkeit verdampfen zu lassen und am nächsten Tag in den Ofen zu stellen. Der Ofen wurde mit einem Volumen von 150 L*h^{-1} mit Argongas gespült und dabei mit einer Heizrate von 1 °C*min^{-1} bis 500 °C erhitzt. Die Temperatur blieb eine Stunde konstant, um die Probe aufzuheizen. Danach wurde mit einer erhöhten Aufheizrate von 5 °C*min^{-1} auf 900 °C erhitzt, wieder eine Stunde gehalten, und bei einem letzten Schritt auf 2000 °C und auch dort eine Stunde gehalten. Anschließend erfolgte die Abkühlung des Ofens und die Proben konnten entnommen werden. Wenn die finale Temperatur der Proben nicht 2000 °C entsprach, wurde trotzdem genau nach diesem Schema erhitzt, allerdings bei der finalen Temperatur gestoppt und die jeweilige Temperatur eine Stunde gehalten.

2.5. CHARAKTERISIERUNGSMETHODEN DER LIGNINE/CARBONE

Die Lignine wurden mit unterschiedlichen Methoden charakterisiert, die im Folgenden kurz aufgeführt und beschrieben sind.

Die Rasterelektronenmikroskopie (REM) und energiedispersive Röntgenspektroskopie (EDX (Engl. Energy dispersive X-ray analysis)) wurden am QuantaTM 250 von FEI (Wien, Österreich) durchgeführt. Das Mikroskop war ausgerüstet mit einer Shottky Feldemissionenkanone mit einer Spannung von 10 kV und einem Vakuum von 1*10-6 mbar. Die Proben wurden auf leitfähige, doppelseitig klebende Carbon- und Kupferpads gestreut, überschüssiges Probenmaterial mit Druckluft entfernt und eine Sputterbeschichtung aus Gold aufgebracht.

Die dynamische Differenzkalorimetrie (DSC (Engl. Differential scanning calorimentry)) wurde am DSC 200F3 Maia von Netzsch (Graz, Österreich) ausgeführt. Die Aufheizrate lag bei 5/10 °C*min^{-1}. Offene Aluminiumtiegel wurden mit der Probe befüllt und unter Stickstoffatmosphäre erhitzt.

Die thermogravimetrische Analyse (TGA) wurde am TA Instruments TGA Q5000 von der Waters GmbH (Eschborn, Deutschland) mit einer Heizrate von 20 °C*min^{-1} ausgeführt.

Die Fourier-Transform-Infrarotspektrometrie wurde am Helios Spektrometer von Ultrafast Systems BV (Amsterdam, Niederlande) durchgeführt. Das Spektrometer war mit einer Tensor 27 und einem Diamanten ausgestattet. Die Auflösung der Spektren betrug $4 cm^{-1}$. Für diese wurde eine Basislinienkorrektur durchgeführt.

Für die Raman-Spektroskopie wurde auf einem Raman Mikroskop alpha300RA von der WITec GmbH (Deutschland) genutzt. Ein grüner Laser mit der Wellenläng e von λ=532 nm, ein Spektrometer mit 600 g*mm-1 UHTS 300 ebenfalls von WITec und einer CCD Kamera von Andor DU401ABV (Belfast, Nordirland). Der Laser wurde mit 5 mW betrieben und auf einer Fläche von $20x20\ \mu m^2$ wurde alle 250 nm ein Spektrum gemessen, was 6400 Spektren pro Fläche ergibt. Am Ende wurden durchschnittliche Spektren (19200 Spektren/Probe) errechnet und verglichen.

Röntgendiffraktion (XRD) wurde am Diffraktometer SmartLab von Rigaku (Ettlingen, Deutschland) gemessen. Das Diffraktometer war ausgestattet mit Cu Kα-Strahlung, einem Parabolspiegel im Hauptstrahl und einem zweiten Grafitmonochromator. Es wurden 2Theta Schritte mit 0,02 ° bei einer Verweildauer von 4 Sekunden gewählt.

Die Elementaranalyse wurde an dem AE 1108 CHNS-O von Carlo Erba (Fisons Instruments, Thermo_Quest) durchgeführt. Es wurden Zinnkapseln verwendet und bei Temperaturen von 1020 °C die Proben mineralisiert. Helium fungierte als Träger für den Substanzstrom, Trennung und Quantifizierung wurde mittels Gaschromatografie durchgeführt. Die Detektion erfolgte mit einem Wärmeleitfähigkeitsdetektor.

Die Leitfähigkeit der Pulver und die Dichtebestimmung erfolgte nach Sanchez-Gonzalez[83]. Eine Plastikröhre mit einem inneren Durchmesser von 6,22 mm wurde auf einem Metallkolben befestigt, mit ca. 12 mm der Probe befüllt, was 50 mg bis 100 mg entsprach. Die Höhe, sowie das Gewicht der Probe wurden gemessen und ein zweiter Metallkolben mit dem Innendurchmesser der Röhre von oben auf die Röhre gelegt. Dieser hat die Druckkammer geschlossen. Nun wurde die Leitfähigkeit an den Kolben gemessen. Danach wurde durch Gewichte auf dem oberen Kolben der Druck auf das Pulver erhöht und die Leitfähigkeit/Dichte in Abhängigkeit vom Druck gemessen. Die unterschiedlichen Gewichte, sowie der resultierende Druck sind in Tabelle 5 aufgezeichnet.

Tabelle 5: Resultierender Druck unterschiedlicher Gewichte bei der Messung elektrischer Leitfähigkeit

Gewicht (kg)	0,2	0,5	0,7	2,0	2,5
Druck (kPa)	65	161	226	645	807

2.6. CHARAKTERISIERUNG DER FILME

Die Compositstreifen wurden auf Zugfestigkeit in einer Zwick Roell 20 kN (Zwick GmbH & Co. KG, Ulm) getestet. Die Zwick hatte einen Kraftaufnehmer von 2,5 kN. Die Leitfähigkeit der Filme wurde an derselben Maschine getestet, allerdings wurde ein Spannungsmessgerät zwischen Probenhalter und Compositfilm durch ein Kupferblech angeschlossen, wie in Abbildung 5 ersichtlich. Dadurch konnte während der Zugprüfung laufend die Leitfähigkeit der Filme ermittelt werden.

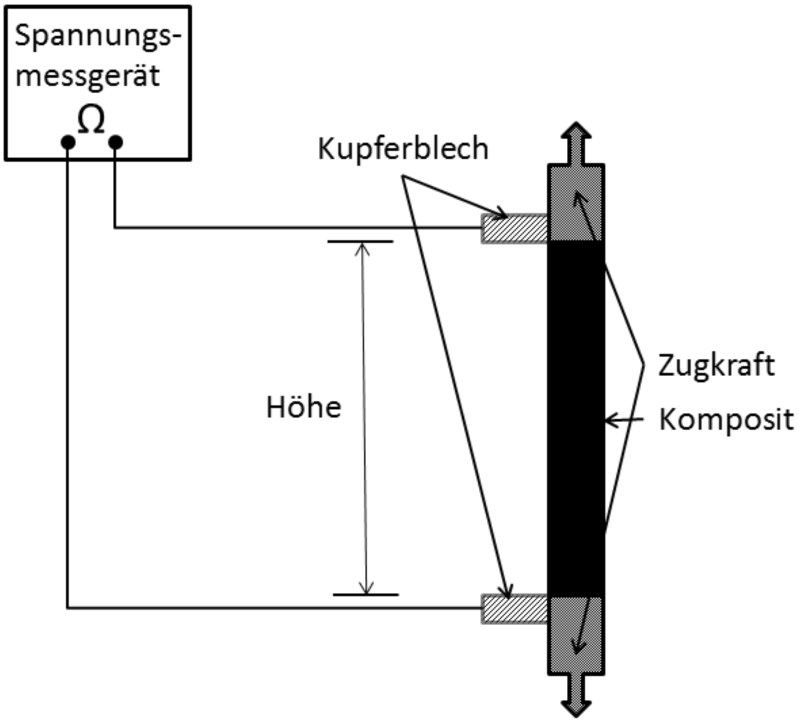

Abbildung 5: Schematische Darstellung der Messung der elektrischen Leitfähigkeit von Filmen

3. ZUSAMMENFASSUNG DER ERGEBNISSE

Im Rahmen der vorliegenden Arbeit wurde die Herstellung von Carbonpartikeln aus Lignin untersucht. Da die Eigenschaften des hergestellten Carbons wesentlich von den Eigenschaften des eingesetzten Lignins abhängen, wurde eine möglichst große Variabilität der Lignine gewählt, wie in Abbildung 6 dargestellt.

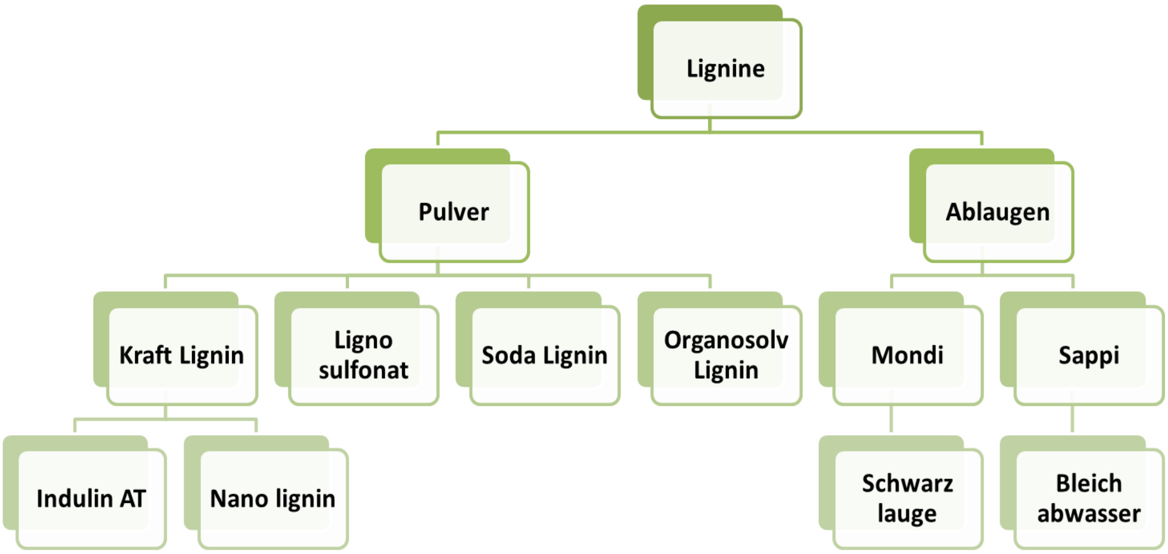

Abbildung 6: Überblick über eingesetzte Rohstoffe für die Carbonisierung

Insgesamt wurden sieben verschiedene Grundstoffe eingesetzt, wobei diese unterschiedlicher Verarbeitung unterlagen. Das Kraft Lignin (Indulin AT) wurde für mechanische Zerkleinerung eingesetzt. Kraft Lignin (Indulin AT) und Lignosulfonat wurden für Ausfällversuche genutzt. Die Ablaugen wurden bei der Sprühtrocknung eingesetzt. Ein Großversuch mit verschiedenen Carbonisierungstemperaturen wurde mit den vier unterschiedlichen Ligninen in Pulverform (Kraft Lignin, Lignosulfonat, Soda Lignin und Organosolv Lignin(Leuna)) durchgeführt, diese vier Lignine sind in Abbildung 7 dargestellt. Die anderen Proben (Kraft Lignin aus dem Aerosol Flow Reaktor und die sprühgetrockneten Ablaugen) wurden jeweils bei 2000 °C carbonisiert.

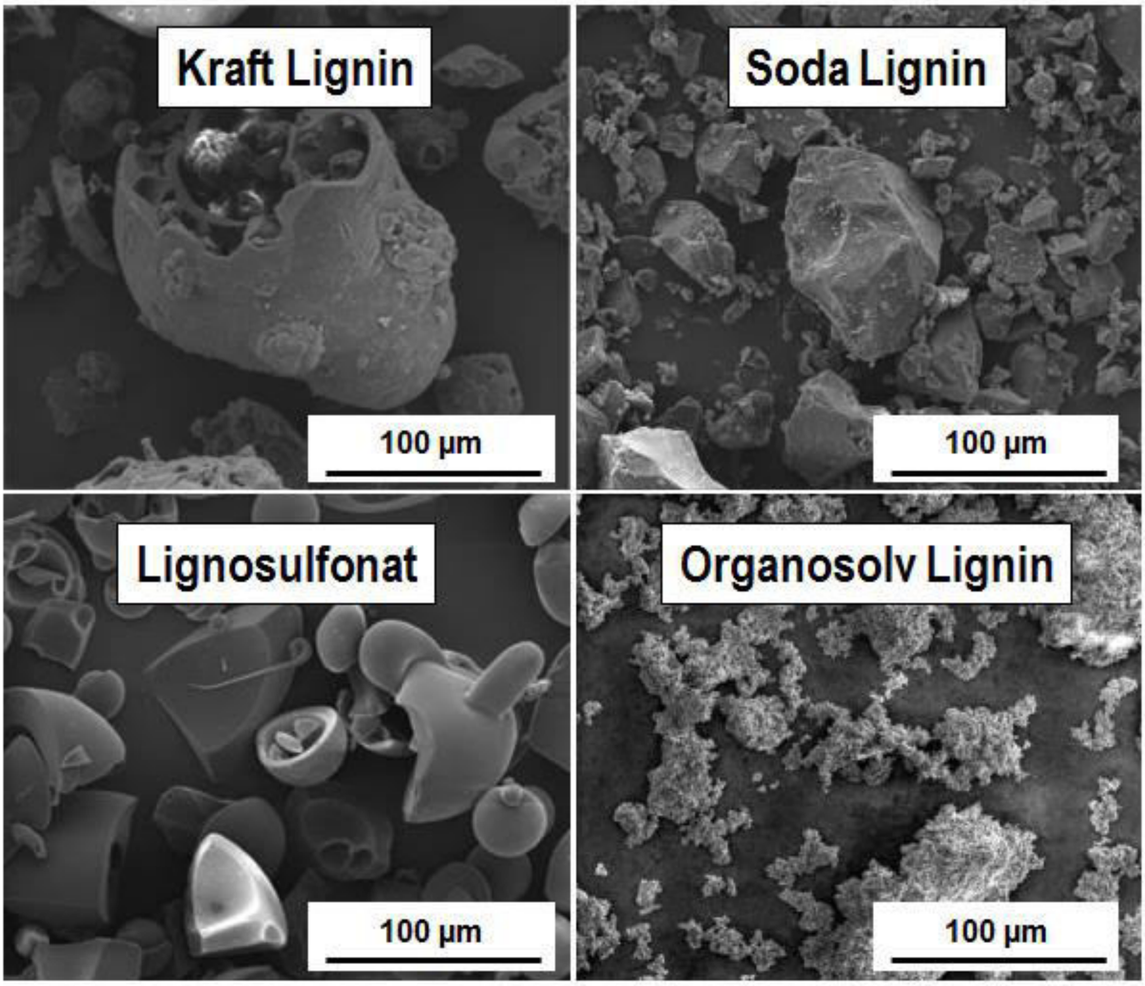

Abbildung 7: SEM-Aufnahmen von Kraft Lignin, Soda Lignin, Lignosulfonat und Organosolv Lignin.

Wie in der Tabelle 7 ersichtlich, unterscheiden sich die vier Lignine nicht nur stark in der Morphologie, sondern auch in der Elementzusammensetzung.

Die Lignine wurden vor der Weiterverarbeitung außerdem mit thermogravimetrischer Analyse und dynamischer Differenzkalorimetrie charakterisiert, Abbildung 8. Hierbei wurde deutlich, dass sich beim Erhitzen das Kraft Lignin, Soda Lignin und Organosolv Lignin ähnlich verhalten: bei 100 °C verdampft Wasser, welches sich noch in der Probe befindet, was zu einem Gewichtsverlustführt und eine endotherme Reaktion ist. Ab 250 °C beginnt die Zersetzung unter leicht exothermen Bedingungen bis 400 °C, danach erfolgt nur noch ein kleiner Masseverlust. Das Lignosulfonat hat eine etwas stärker endotherme Reaktion bei 130 °C, und eine sehr stark exotherme Reaktion zwischen 300 °C und 400 °C, hier wird SO_2 freigesetzt, was zu der starken Reaktion führt(Publikation III).

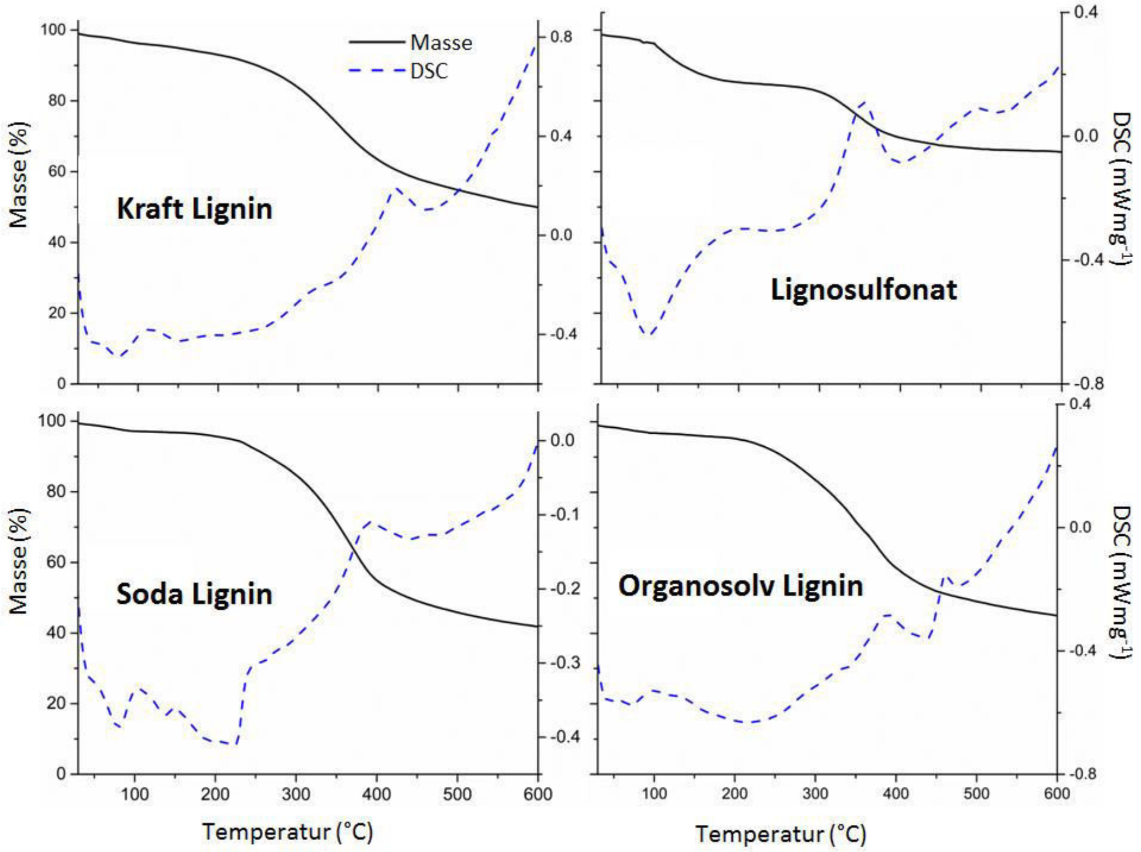

Abbildung 8: DSC und TGA von Kraft Lignin, Soda Lignin, Lignosulfonat und Organosolv Lignin

Wie oben erwähnt, wurde das Kraft Lignin (Indulin AT) zur mechanischen Zerkleinerung eingesetzt. Es wurden drei verschiedene Methoden mit unterschiedlichen Versuchsparametern verwendet: Ultraschallsonde, Homogenisator und Mikrofluidizer. Durch diese Methoden wurden Verkleinerungen erzielt, jedoch bei keiner der Methoden eine homogene Partikelgrößenverteilung erreicht. So wurde zum Beispiel im Mikrofluidizer die Probe 12 (Stoffgehalt 10 %, Zellengröße 75 und Durchlaufzeit 15 Minuten, vergleiche Tabelle 2) von vorher 5286 nm auf 160 nm (32 % Masse) und 600 nm (68 % Masse) verkleinert. Wie in Abbildung 9 zu sehen, waren die Partikel von sehr unterschiedlicher Form und Größe nach der Behandlung im Mikrofluidizer. Die Ergebnisse des Ultraschallbades und des Homogenisators sahen ähnlich aus. Infolgedessen wird es nicht weiter ausgeführt, es kam auch als Rohstoff für die Carbonisierung nicht in Frage.

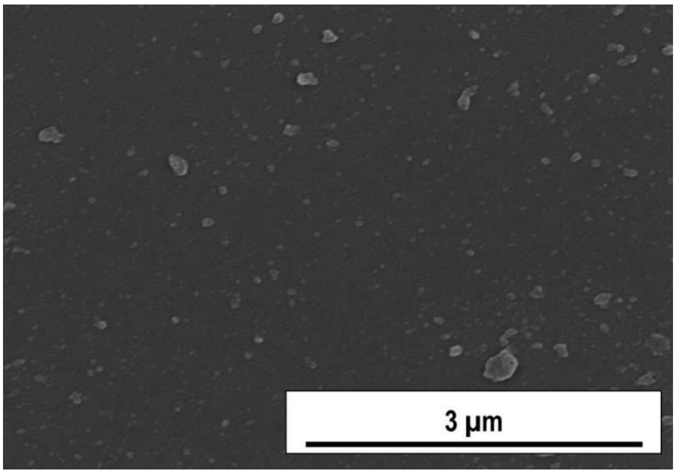

Abbildung 9: SEM-Aufnahme von Kraft Lignin nach der Behandlung im Mikrofluidizer

Da durch die mechanische Zerkleinerung von Partikeln keine zufriedenstellenden Ergebnisse erzielt wurden, war der nächste Schritt, die gewünschte Partikelgröße über eine Ausfällung zu erreichen. Wie in den Methoden beschrieben, wurden verschiedenste Lignine, Löse- und Ausfällmittel ausprobiert. In Abbildung 10 ist zu sehen, dass das Ausfällen in mehreren Fällen gut funktioniert hat, zum Beispiel bei Lignosulfonat, gelöst in Wasser und ausgefällt mit Aceton (B). Auch Kraft Lignin in Dioxan zu lösen und mit Cyclohexan auszufällen hat sich als Methode bewährt. Jedoch zeigten die Proben wieder sehr unterschiedliche Partikelgrößenverteilungen. Das Problem beim Einsatz dieser Partikel zur Carbonisierung lag in der Trocknung: Vor dem Carbonisierungsvorgang muss das Lignin zum Thermostabilisieren getrocknet werden. Weder das Abdampfen Abbildung 10(D), noch das Sprühtrocknen oder Gefriertrocknen hat funktioniert, sodass die Partikel erhalten geblieben wären. Sie haben sich agglomeriert und neue, viel größere, Formen gebildet. Damit waren auch diese Partikel für die Carbonisierung nicht brauchbar.

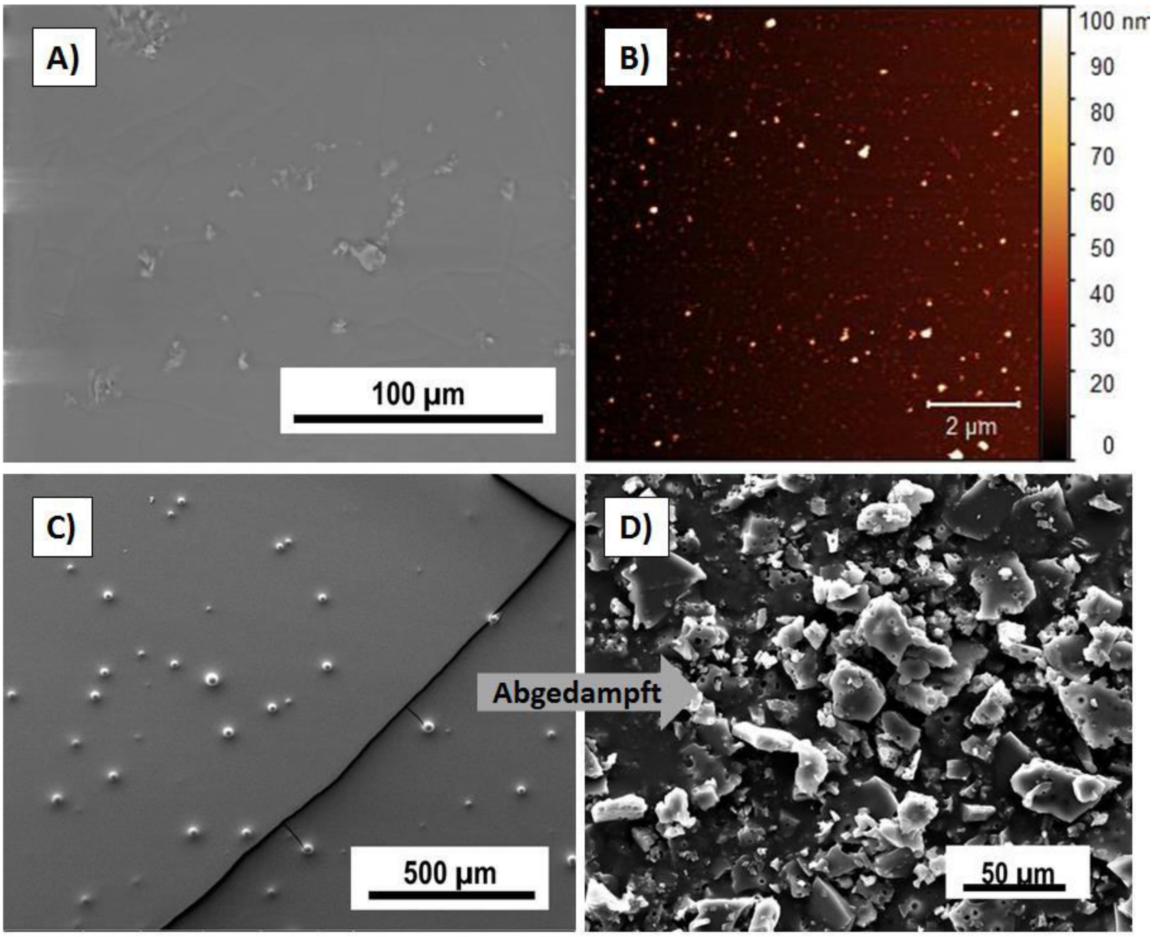

Abbildung 10: Ergebnisse des Ausfällens: A) Kraft Lignin mit Dioxan/Wasser (REM), B) Lignosulfonat mit Wasser/Aceton (AFM), C) Kraft Lignin mit Dioxan/Cyclohexan (REM), D) Probe C) abgedampft (REM)

Nachdem verschiedene Methoden zur Partikelverkleinerung nicht zufriedenstellend funktionierten, da es vor allem Probleme mit der Trocknung gab, wurden vorerst nur vier unbehandelte Lignine für den Carbonisierungsvorgang eingesetzt (Kraft Lignin, Soda Lignin, Lignosulfonat, Organosolv Lignin). Diese Ergebnisse wurden in den Publikationen I-III veröffentlicht. Nach diesen Versuchen ergab sich die Möglichkeit, mit dem Team von Orlando Rojas von der Aalto Universität zusammenzuarbeiten, die durch das Einsetzen eines Aerosol-Strömungsreaktors Nanolignin herstellen konnten[81]. Es wurden Nanoligninproben zur Verfügung gestellt, die carbonisiert werden konnten.

Der Carbonisierung voran ging die Thermostabilisierung, wie sie in den Methoden beschrieben wurde. Durch die Thermostabilisierung wurde das Lignin chemisch so verändert, dass es bei der schnellen Erhitzung zur Carbonisierung formstabil blieb und nicht mehr schmolz. Durch Kondensation, Dehydration, Vernetzung, Autoxidation und Eliminierungsreaktionen kam es im thermostabilisierten Material zu geringerem Gehalt an Kohlenstoff, Sauerstoff und Wasserstoff, wobei Wasser, Kohlenstoffmonoxid und Kohlestoffdioxid gebildet und abgetragen wurden. Funktionelle Gruppen am Lignin wurden abgespalten, während sich das Grundgerüst stärker vernetzt hat. Diese Veränderungen sind in den FT-IR Spektren in Abbildung 11 zu sehen und in der Publikation II genauer erklärt.

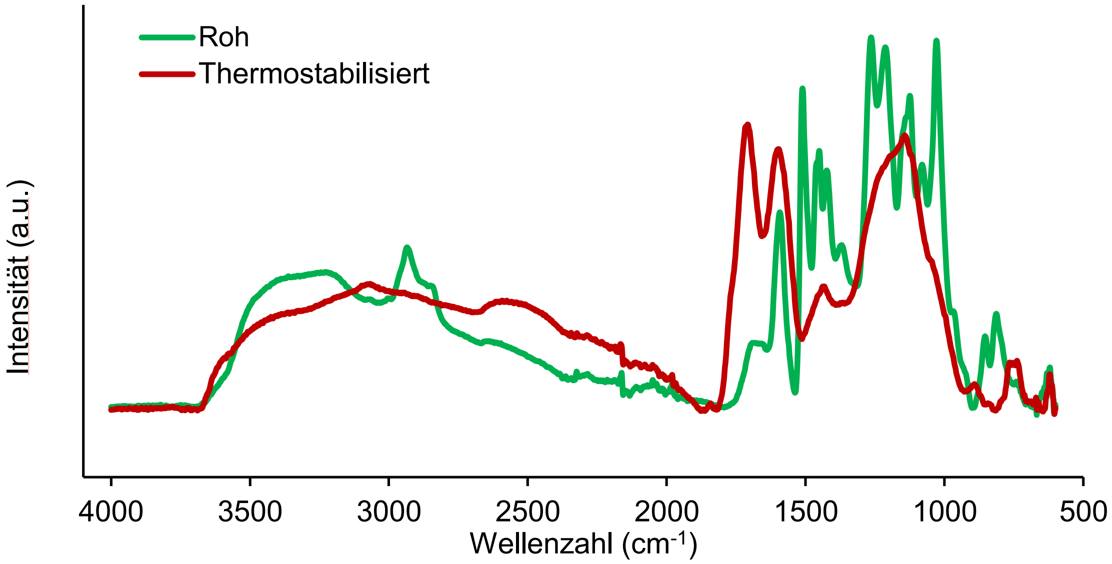

Abbildung 11: FT-IR Spektrum des unbehandelten und thermostabilisierten Kraft Lignins

Die Thermostabilisierung, wie auch die Carbonisierung, führten zu einem Masseverlust. Dieser schwankte bei der Thermostabilisierung zwischen 25 % und 60 %, wobei die Organosolv Lignine die geringsten Ausbeuten hatten, vergleiche Tabelle 6. Nach der Carbonisierung varriierte die Ausbeute kaum zwischen den Carbonisierungstemperaturen von 1200 °C und 2000 °C, wobei die Gesamtausbeute eine hohe Variabilität aufwies, sie schwankte zwischen 6 % und 24 %. Besonders gering war die Ausbeute des sprühgetrockneten Kraft Lignins, hoch hingegen die Ausbeute des sprühgetrockneten Lignosulfonates. Während der Gewichtsverlust bei der Thermostabilisierung durch Oxidationsreaktionen hervorgerufen wird, wie oben beschrieben, ist der Gewichtsverlust bei der Carbonisierung vor allem auf das Aufbrechen der chemischen Verbindungen zurückzuführen, die dann im weiteren Verlauf zur Repolymerisation und zum Entstehen von graphitischen Strukturen führen. Weiterhin werden fast alle Anorganika abgespalten und über das Trägergas Argon aus der Probe befördert, was zu einem erheblichen Gewichtsverlust führen kann, je nach Beschaffenheit der Probe. Eine Besonderheit des Lignosulfonates ist es, dass bei der Erhitzung zwischen 300 °C und 450 °C eine stark exotherme Reaktion entsteht, wie im Paper VI ausgeführt wurde. Diese exotherme Reaktion wird von dem freigesetzten SO_2 verursacht, welches in großen Mengen nur im Lignosulfonat vorkommt.

Tabelle 6: Gesamtausbeuten der Thermostabilisierung und Carbonisierung aller Lignine

	250 °C	800 °C	1200 °C	1600 °C	2000 °C
Kraft Lignin	55,75	27,94	24,12	24,94	24,47
Soda Lignin	49,12	24,61	21,47	22,34	22,14
Lignosulfonat	64,97	39,24	26,22	22,24	22,04
Organosolv Lignin Leuna	39,21	17,56	15,69	16,89	16,25
Organosolv Lignin Indien	42,24				18,86
Kraft Lignin sprühgetrocknet	74,19				5,55
Lignosulfonat sprühgetrocknet	44,31				30,61
Nanolignin (Kraft)	47,58				

Dass die Ausbeuten mit dem Verlust der Anorganika zusammenhängen, lässt sich beweisen durch die Elementaranalyse der Proben in Tabelle 7. Nach der Thermostabilisierung senkt sich der Kohlenstoff- und Wasserstoffgehalt, während sich der Schwefelgehalt erhöht. Dies liegt an den oben erwähnten oxidativen Vorgängen im Lignin. Kohlenstoff und Wasserstoffmoleküle werden abgespalten, während Schwefelmoleküle im Lignin verbleiben, da sich SO_2 erst ab 300 °C bildet, weswegen die Gesamtmasse abnimmt und so der %-Anteil an Schwefel zunimmt. Nach der Carbonisierung bei 2000 °C ist in allen Proben über 99,5 % Kohlenstoff vorhanden, andere Elemente unter der Nachweisgrenze oder nur in sehr geringen Anteilen. Bei sehr hohen Carbonisierungstemperaturen werden die Strukturen so stark verändert, dass nur noch das Kohlenstoffgrundgerüst stehen bleibt und eine graphitische Gitterstruktur bildet, so dass andere Elemente nur an den am Rande liegenden Kohlenstoffatomen eine Möglichkeit haben, sich zu binden. Alle anderen Elemente werden während des Carbonisierungsvorgangs von dem Material abgespalten und durch das Trägergas herausgespült.

Tabelle 7: Elementaranalyse verschiedener Proben vor- und nach der Thermostabilisierung und Carbonisierung

	Element (%w/w)								
	C	H	N	S	O	K	Na	Ca	Mg
Kraft Lignin roh	62,80	5,80	0,90	0,10					
Kraft Lignin 250 °C	55,28	2,17	0,87	1,31	36,50	<0,05	0,46		
Kraft Lignin 2000 °C	99,87	<0,05	<0,05	<0,02		0,03	0,03	0,05	<0,02
Soda Lignin roh	61,90	5,90	0,90	<0,02					
Soda Lignin 2000 °C	99,18	0,03	<0,05	0,23		0,03	0,03	0,03	<0,02
Lignosulfonat roh	47,90	3,70	0,20	2,00					
Lignosulfonat 250 °C	43,46	3,10	0,25	4,04	34,17	< 0,05	4,16		
Lignosulfonat 2000 °C	99,55	<0,05	<0,05	0,04		<0,02	<0,02	0,06	<0,02
Organosolv Lignin roh	61,10	5,90	0,3	<0,02					
Organosolv Lignin 2000 °C	99,58	<0,05	<0,05	<0,02		0,05	<0,02	0,03	<0,02
Kraft sprühgetrocknet	30,59	4,05	0,13	4,84	38,50	2,85	13,43	0,59	0,18
Kraft sprühgetrocknet 250 °C	27,51	2,04	0,12	6,28	38,67	3,62	17,51	0,77	0,24
Lignosulfonat sprühgetrocknet	46,88	5,77	0,21	5,20	37,08	0,30	0,15	0,75	1,81
Lignosulfonat sprühgetrocknet 250 °C	37,19	3,91	0,16	5,74	37,87	1,96	8,83	0,76	1,02

Die SEM-Bilder der unbehandelten Lignine zeigen sehr unterschiedliche Strukturen. Zu sehen sind alle Lignine in den Abbildung 12-17. Bei allen ähnlich ist aber die Veränderung während der Carbonisierung: Zum einen schrumpfen alle Partikel, zum anderen wird die Oberfläche rauer, verglichen mit dem unbehandelten Lignin. Wie schon angesprochen wurde, verändert sich die Struktur der Lignine stark, wodurch die Partikel kompakter werden. Die abgespalteten Nebenprodukte diffundieren an die Oberfläche, dadurch entsteht eine Porosität, die die Oberfläche rau aussehen lässt.

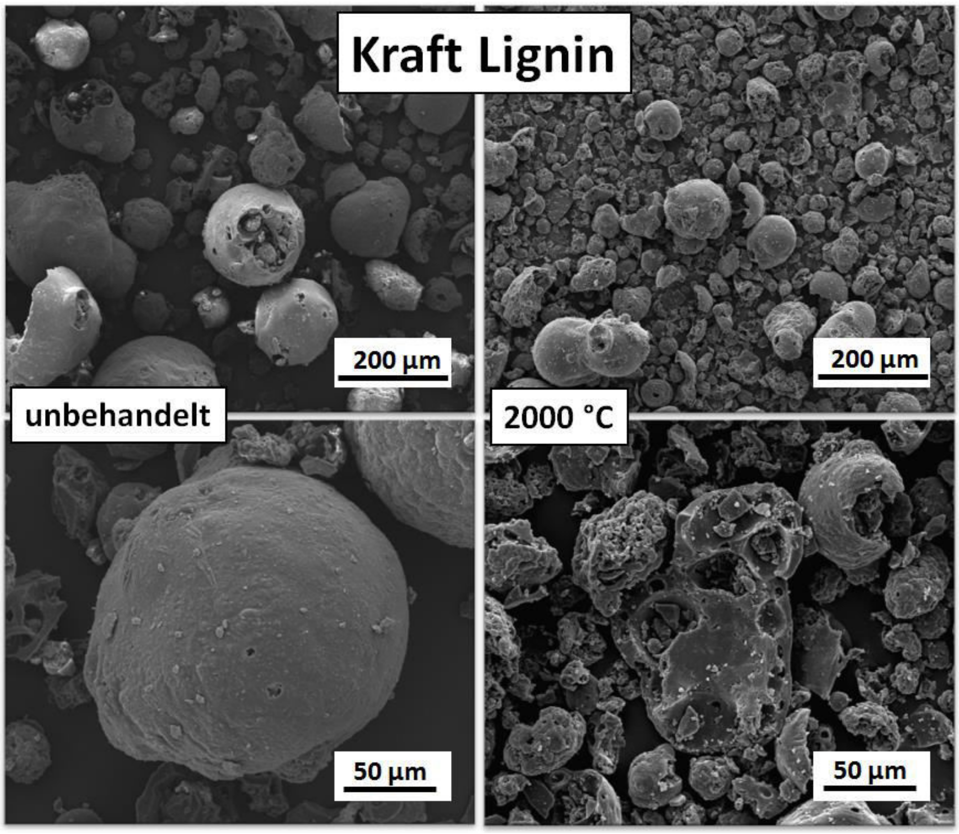

Abbildung 12: SEM-Bilder des Kraft Lignins unbehandelt und carbonisiert (2000 °C)

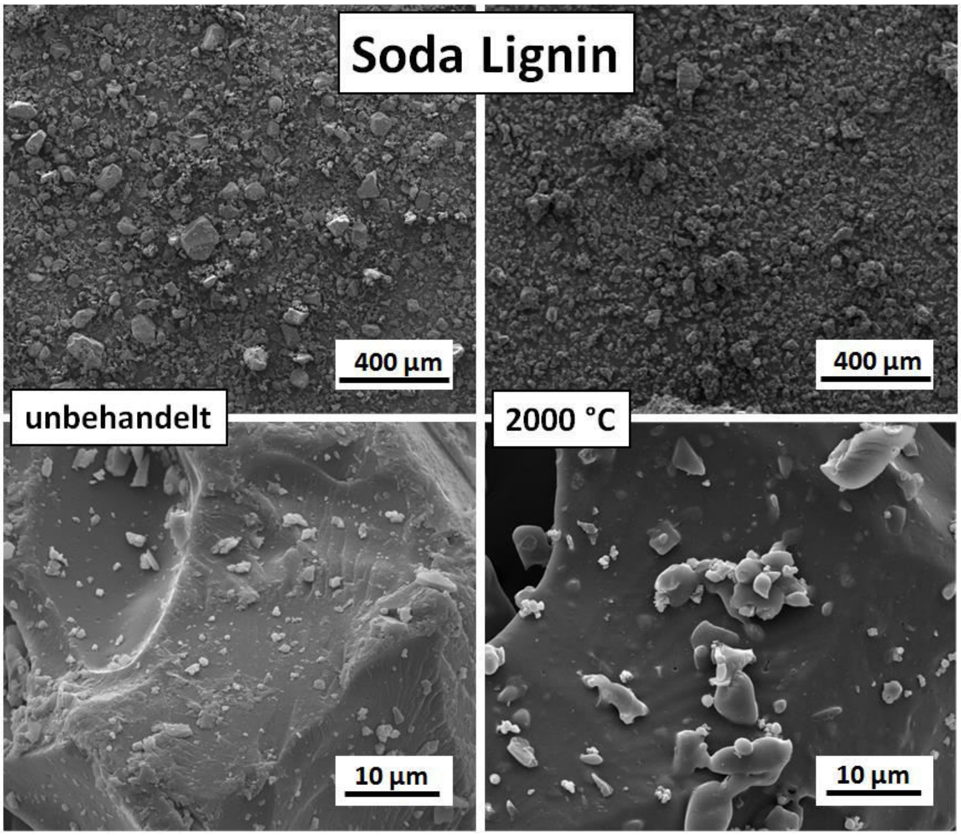

Abbildung 13: SEM-Bilder des Soda Lignins unbehandelt und carbonisiert (2000 °C)

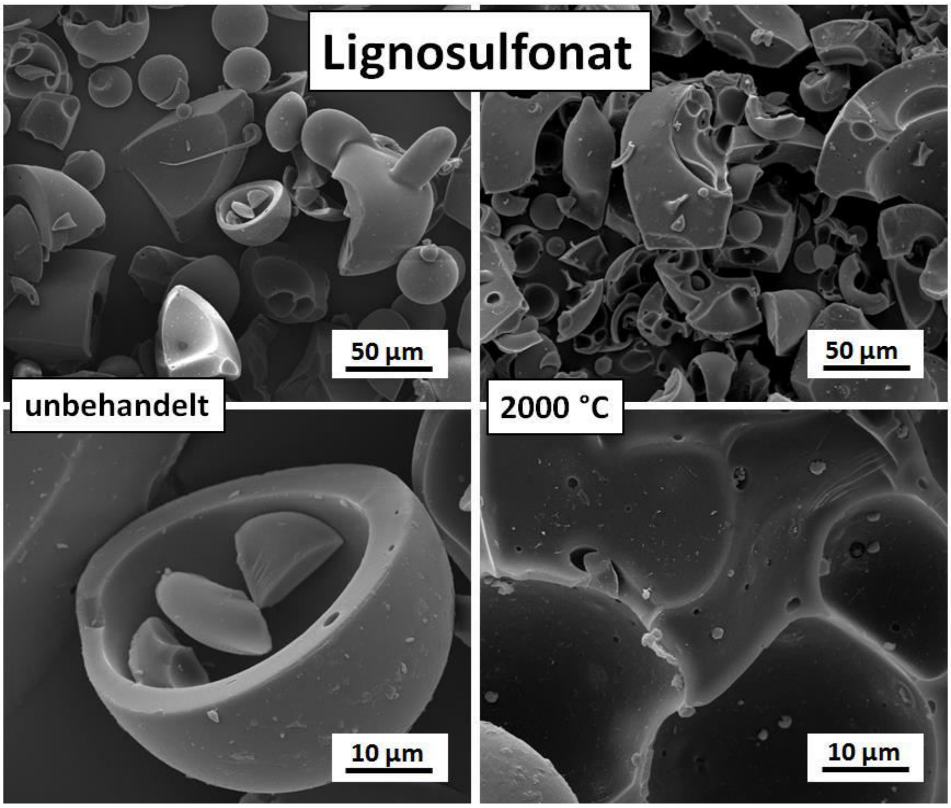

Abbildung 14: SEM-Bilder des Lignosulfonats unbehandelt und carbonisiert (2000 °C)

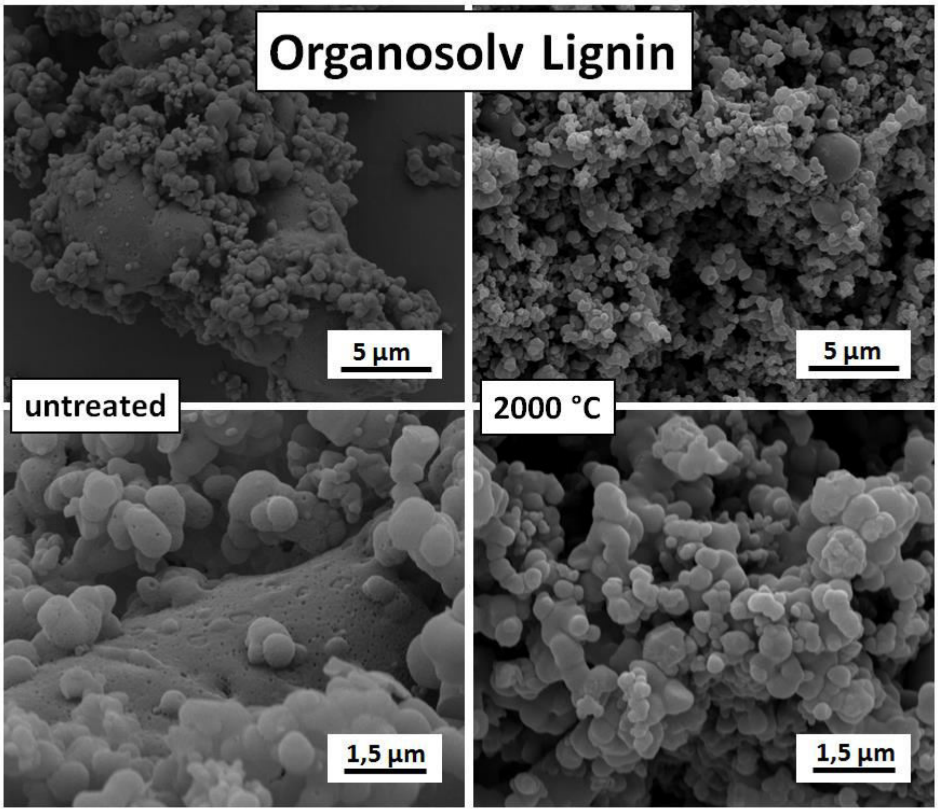

Abbildung 15: SEM-Bilder des Organosolv Lignins unbehandelt und carbonisiert (2000 °C)

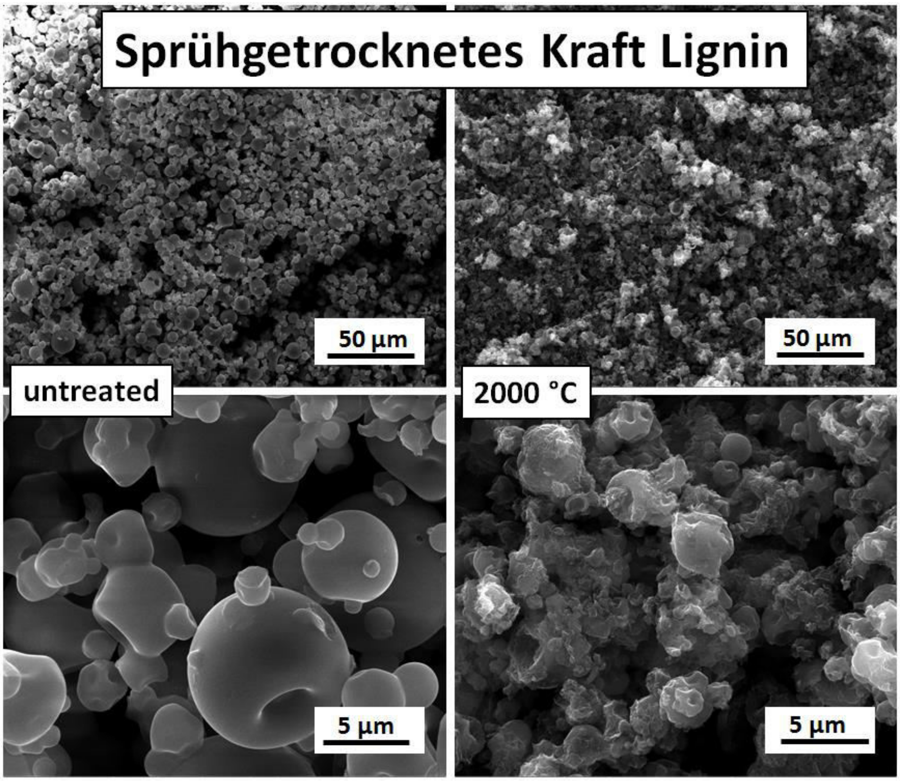

Abbildung 16: SEM-Bilder des sprühgetrockneten Kraft Lignins unbehandelt und carbonisiert (2000 °C)

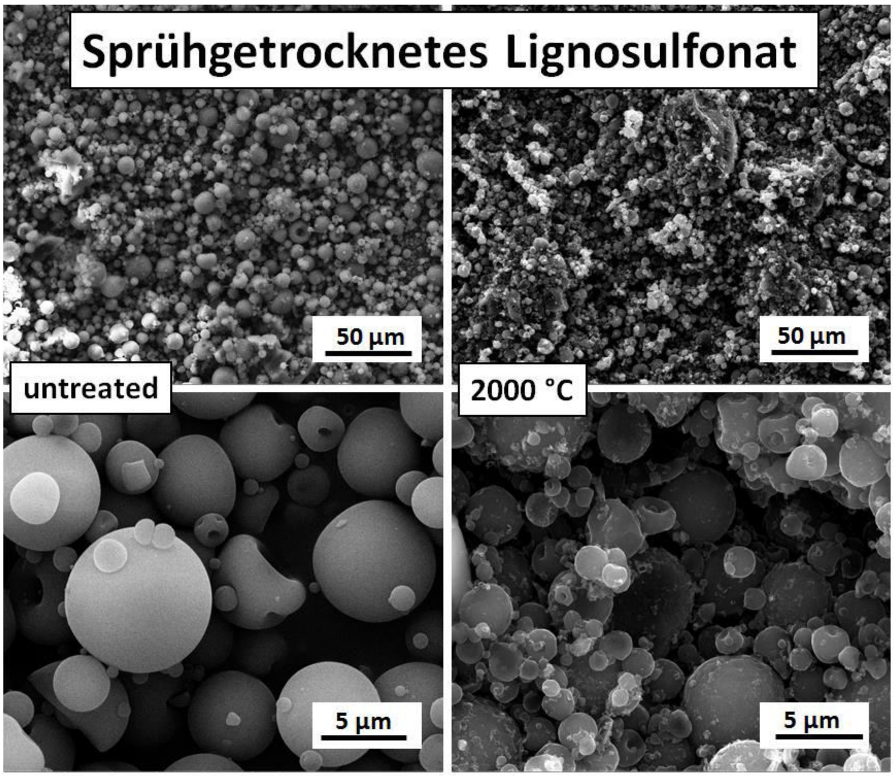

Abbildung 17: SEM-Bilder des sprühgetrockneten Lignosulfonats unbehandelt und carbonisiert (2000 °C)

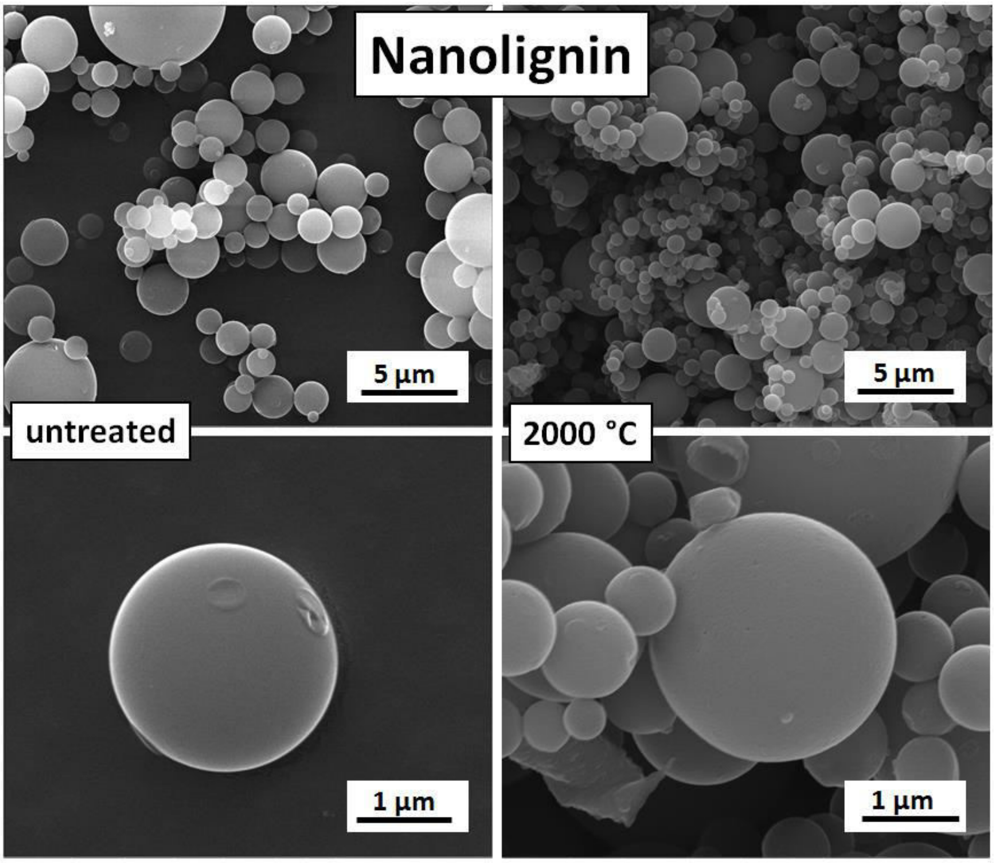

Abbildung 18: SEM-Bilder des Kraft Nanolignins unbehandelt und carbonisiert (2000 °C)

Durch die Carbonisierung wurden die Ligninpartikel elektrisch leitfähig, Abbildung 19. Das Entstehen der Leitfähigkeit der carbonisierten Ligninpartikel lässt auf einen Strukturwandel während der Carbonisierung schließen. Generell werden Stoffe elektrisch leitfähig, wenn frei bewegliche, geladene Teilchen vorhanden sind. Wie oben beschrieben, besteht der carbonisierte Ligninpartikel zu über 99 % aus Kohlenstoffatomen. Die Eigenschaften des Partikels werden also dadurch bestimmt, wie diese Kohlenstoffatome angeordnet sind. Jedes Kohlenstoffatom hat 4 Valenzelektronen. In einem Idealfall also 3 weitere Verbindungen zu anderen Kohlenstoffatomen und damit ein viertes Elektron, welches frei beweglich oder auch delokalisiert ist, und somit die elektrische Leitfähigkeit erzeugt. Wenn dieses in nur einer Ebene geschieht, dann erhält man Graphen, welches ein wabenförmiges Netz mit sechsgliedrigen Ringen dieser Kohlenstoffatome ist. Mehrere Schichten Graphen übereinander gelagert ergeben Graphit, wobei die Schichten selber mit Wasserstoffbrückenbindungen aneinander gebunden sind. Aufgrund dieser Morphologie ist Graphit nur innerhalb der Schichten leitfähig, zwischen den Schichten selber ist kein Stromfluss vorhanden. In dem Fall der carbonisierten Ligninpartikel bilden sich Graphenschichten aus, die allerdings nicht perfekt sind, und auch nicht perfekt übereinander gelagert sind. Es entstehen Löcher im Netz aus Kohlenstoff. Außerdem sind die einzelnen Schichten (zum Teil) willkürlich zueinander ausgerichtet, so dass Leitfähigkeit in alle Richtungen entsteht und auch nicht unendlich hoch ist, eben weil die freien Elektronen zwar sehr beweglich sind, aber doch Einschränkungen zwischen den einzelnen Schichten oder innerhalb der einzelnen Schichten bestehen. Aus diesem Grund ist die Leitfähigkeit der verschiedenen carbonisierten Lignine auch unterschiedlich. Jedoch steigt die Leitfähigkeit mit der Erhöhung der Carbonisierungstemperatur an, Abbildung 19, weil die höhere Temperatur dafür sorgt, dass sich die einzelnen Netze besser formieren und ausrichten können, und somit dem graphitischen Gitter immer näher kommen. Während Kraft Lignin bei einem Druck von 0,6 MPa einen spezifischen Widerstand von 0,45 Ωcm hat, kommt das Nano Lignin bei gleichem Druck auf 6,6 MPa spezifischen Widerstand, auch bei höherem Druck von 1,5 MPa erreicht das Nano Lignin nur 2,68 Ωcm.

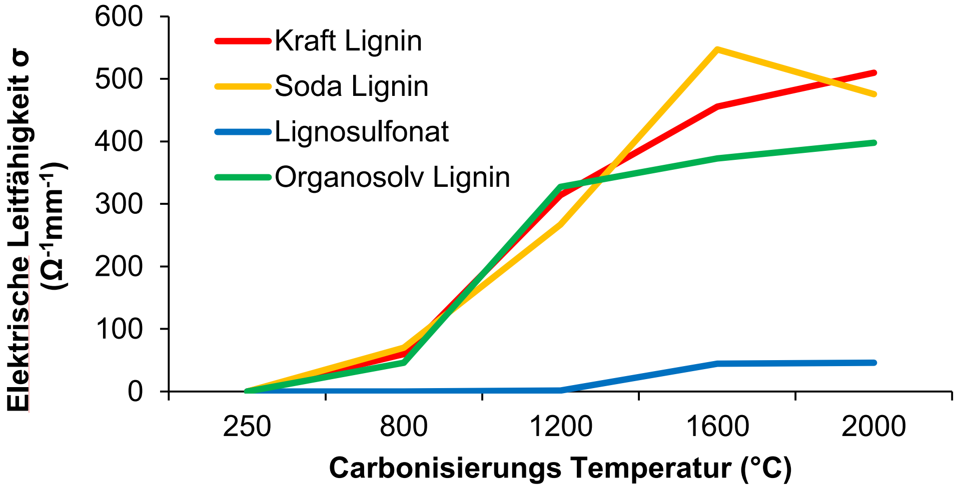

Abbildung 19: Leitfähigkeit der Lignine in Abhängigkeit von der Carbonisierungstemperatur

Um die Theorie der Veränderung des Kohlenstoffgerüstes nachzuweisen, wurden Röntgenuntersuchungen gemacht. Die Kristallstrukturanalyse hat gezeigt, dass sich schon ab 800 °C Carbonisierungstemperatur klare graphitische Strukturen zeigen, diese sich allerdings bei allen Ligninen stärker ausprägen, wenn die Temperaturen steigen. Außerdem gab es Unterschiede zwischen den einzelnen Ligninen, siehe Abbildung 20, wobei das sprühgetrocknete Kraftlignin und das Nanolignin die deutlichste Ausprägung des (002)-Peaks zeigen, also die am besten geordneten graphitischen Strukturen während der Carbonisierung ausgebildet hat. Im Gegensatz dazu zeigen die anderen hier abgebildeten Lignine sehr breite (002)-Peaks, was auf amorphe Carbonstrukturen schließen lässt.

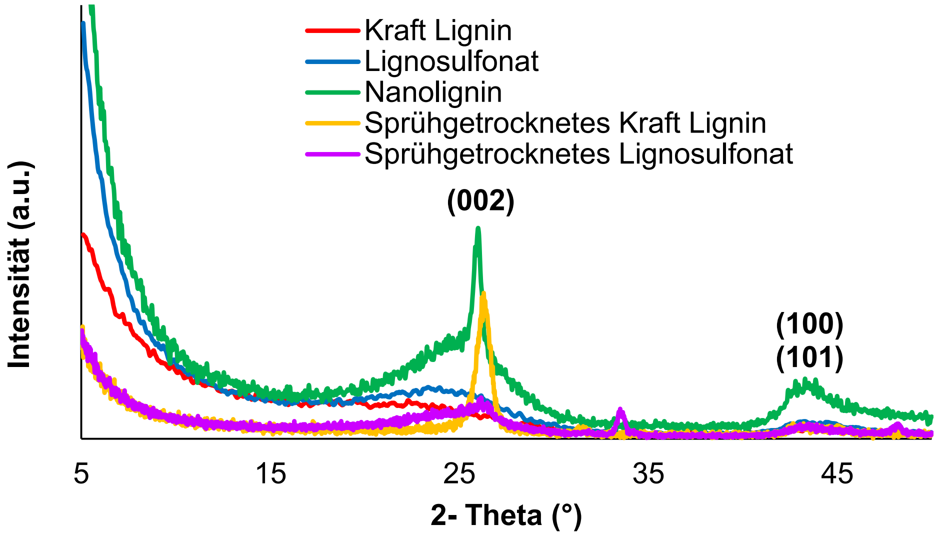

Abbildung 20: XRD-Spektren des Kraft Lignins, Lignosulfonats, Nanolignins, sprühgetrockneten Kraft Lignins und sprühgetrockneten Lignosulfonats

Ein weiterer Nachweis der gebildeten Strukturen gibt die Raman-Spektroskopie. Auch hierbei wurde nachgewiesen, dass die hergestellten Partikel graphitische Strukturen haben. Wie in Abbildung 21 zu sehen ist, treten zwei verschiedene Peaks auf, der D-Peak bei 1350 cm^{-1} und der G-Peak bei 1580 cm^{-1}. Hierbei kann auch ein Rückschluss auf die Art des graphitischen Materials gemacht werden: Der D-Peak steht für ungeordnete Strukturen, der G-Peak für perfekt geordnete graphitische Strukturen. Durch das Verhältnis dieser beiden Peaks zueinander kann man die Proben quantitativ vergleichen:

Tabelle 8: Vergleich des D- und G-Peaks der Ramanspektren

	Kraft Lignin	Soda Lignin	Lignosulfonat	Organosolv Lignin
I_D/I_G	1,45	1,26	1,48	1,10

	Nanolignin	Kraft Lignin sprühgetrocknet	Lignosulfonat sprühgetrocknet
I_D/I_G	1,01	0,25	0,62

Es wird in Tabelle 8 deutlich, dass im direkten Vergleich aller Lignine das sprühgetrocknete Kraft Lignin mit Abstand die am meisten geordneten Strukturen hat, während das normale Kraft Lignin und Lignosulfonat am meisten ungeordnete Strukturen aufweisen.

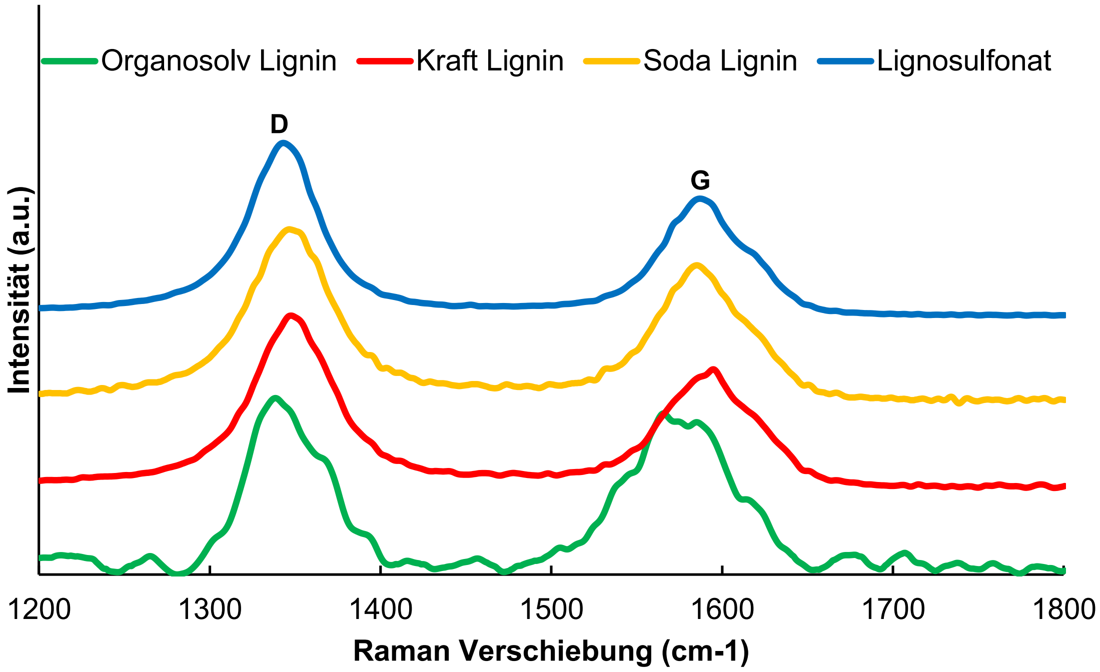

Abbildung 21: Raman-Spektren des Kraft Lignins, Lignosulfonats, Soda Lignins und Organosolv Lignins mit dem D-Peak und G-Peak

Diese Strukturuntersuchungen belegen, dass ein graphitisches Material entstanden ist, und dass diese Kohlenstoffformation tatsächlich die Ursache der Leitfähigkeit ist. Im nächsten Schritt wurde untersucht, ob leitfähige Composite hergestellt werden können, wieviel Füllmaterial man braucht und ob es Unterschiede bei dem eingesetzten Lignin gibt. Die Ergebnisse wurden im Paper III diskutiert. In Abbildung 22 ist deutlich zu sehen, dass erst ab 30 % carbonisiertem Lignin eine Leitfähigkeit gemessen wurde, so dass für alle weiteren Versuche immer mit 30 % Füllmenge gearbeitet werden konnte.

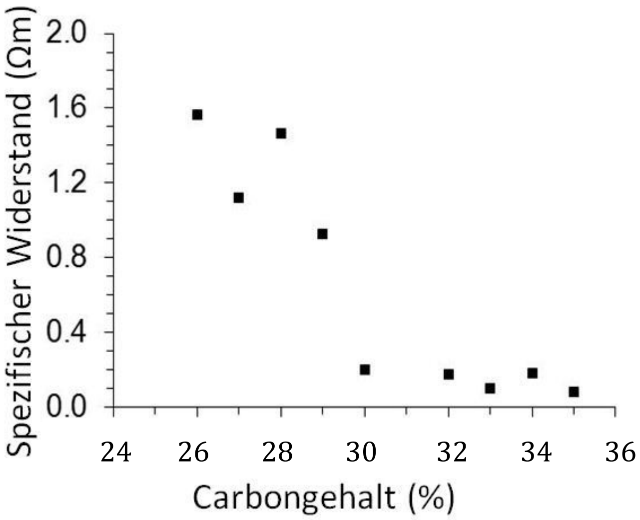

Abbildung 22: Feststellung der Mindestfüllmenge von Carbon Partikeln (Organosolv Lignin Partikel, carbonisiert bei 2000 °C) im Polymer (PLA), um elektrische Leitfähigkeit zu erzeugen.

Die Leitfähigkeit der hergestellten Composite unterscheidet sich stark, abhängig vom eingesetzten Lignin, Abbildung 23. Generell ist zu sehen, dass bei höherer Spannung die spezifische Leitfähigkeit abnimmt. Dies ist für alle Lignine identisch. Die höchste Leitfähigkeit erzielt das Kraft Lignin, während das Lignosulfonat nur geringe Leitfähigkeit im Composit aufweist und das Soda Lignin gar keine. Da das Lignosulfonatpulver auch geringe Leitfähigkeiten hatten, erstaunt es nicht, dass dies im Composit nicht anders ist. Die geringe Leitfähigkeit des Soda Lignins im PCL ist überraschender, lässt sich aber durch die hohe Dichte des Lignins erklären. Da im Versuch Massenprozent eingewogen wurden, wurde vom Soda Lignin dementsprechend ein geringeres Volumenprozent genutzt. Durch dieses geringe Volumen konnte kein Elektronenfluss zwischen den leitfähigen Partikeln entstehen, da dafür eine gewisse Nähe und somit Berührungspunkte der Partikel gewährleistet sein mussten.

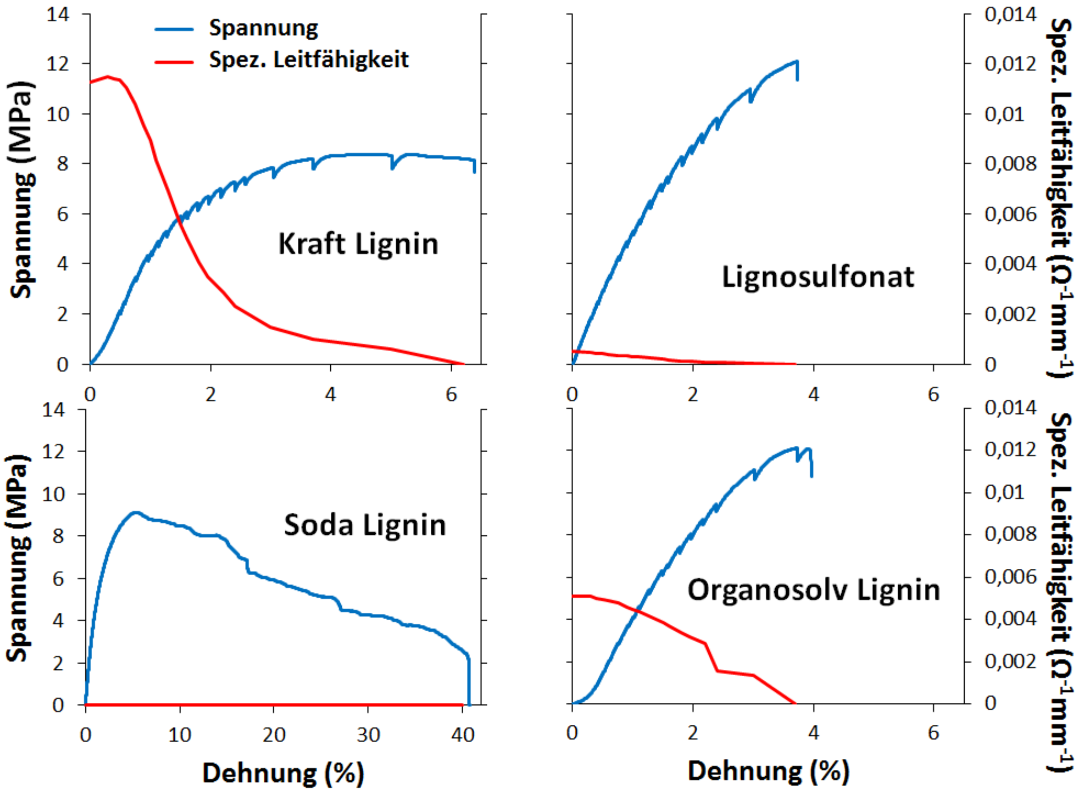

Abbildung 23: Abnahme der Leitfähigkeit der Composite bei zunehmender Zugspannung

Die Eigenschaften des PCL wurden durch die carbonisierten Ligninpartikel beeinflusst. Während die Zugfestigkeit stark abnimmt, steigt das Elastizitätsmodul an: Das Material wird stärker, aber steifer (Tabelle 9). Während der Elastizitätsmodul bei den Proben mit Kraft Lignin und Soda Lignin nur wenig steigt, verdoppelt es sich nahezu für die Proben mit Lignosulfonat und Organosolv Lignin. Die Zugfestigkeit reduziert sich am stärksten für das Kraft Lignin, die kleinste maximale Dehnung hingegen tritt bei dem mit Soda Lignin und Lignosulfonat gefüllten PCL auf.

Tabelle 9: Ergebnisse der Zugversuche des PCL gefüllt mit 30 % carbonisierter Ligninpartikel

	Elastizitätsmodul (MPa)	Zugfestigkeit (MPa)	Maximale Dehnung (%)
Kraft Lignin	347 ± 32	6,59 ± 0,12	9,83 ± 2,27
Soda Lignin	382 ± 19	9,09 ± 0,08	2,88 ± 0,18
Lignosulfonat	598 ± 73	12,06 ± 0,69	3,22 ± 0,16
Organsolv Lignin	604 ± 58	11,75 ± 1,19	16,86 ± 2,68
Polycaprolacton	354 ± 20	28,16 ± 3,64	696,61 ± 74,75

4. AUSBLICK

Die vorliegende Arbeit zeigt, dass es möglich ist, aus verschiedenen Ligninen und sogar aus Ablaugen elektrisch leitfähige Carbonpartikel mit graphitischer Struktur herzustellen. Hiermit ergibt sich eine weitere mögliche Nutzungsform für Lignin und ligninhaltige Prozesslaugen in der Zukunft. Erstmals ließen sich komplett biobasierte Composite anfertigen, die leitfähig sind. Dieses ergibt sich durch den Einsatz der aus Lignin gewonnenen Carbonpartikel kombiniert mit PLA, einem Polymer, welches aus erneuerbaren Ressourcen gewonnen werden kann, wie zum Beispiel Maisstärke. Es wurden große Unterschiede zwischen den verschiedenen Ligninen aufgezeigt, wobei das sprühgetrocknete Kraftlignin die am besten geordneten Strukturen nach der Carbonisierung aufweist. Der Vergleich zwischen Nano- und Mikrolignin hat gezeigt, dass es Unterschiede gibt, wobei das Mikrolignin bessere Leitfähigkeiten erzielt, das Nanolignin aber ausgeprägtere graphitische Strukturen entwickelt. Langfristig ist eine Substituierung von Carbon black, welches aus Erdöl gewonnen wird, denkbar, allerdings ist hierfür noch einiges an Optimierungsarbeit notwendig, da die Ausbeuten und auch die Variabilität des Lignins große Herausforderungen in dieser Arbeit darstellten. Folgende Einsatzbereiche der hergestellten Composite sind möglich: Die Reifenindustrie, die Coatingindustrie, sowie die Elektronikindustrie, dabei sollte das Rohmaterial entsprechend ausgewählt werden. Einen großen Anteil am Gelingen der zukünftigen Projekte beim direkten Einsatz von Prozessablaugen wird die Chemikalienrückgewinnung haben.

5. LITERATURVERZEICHNIS

1. Boerjan, W.; Ralph, J.; Baucher, M. Lignin biosynthesis. *Annu Rev Plant Biol* **2003**, *54*, 519-546.
2. Berglin, N.; Berntsson, T. Chp in the pulp industry using black liquor gasification: Thermodynamic analysis. *Applied Thermal Engineering* **1998**, *18*, 947-961.
3. Hu, J.; Zhang, Q.; Lee, D.J. Kraft lignin biorefinery: A perspective. *Bioresour Technol* **2018**, *247*, 1181-1183.
4. Naqvi, M.; Yan, J.; Dahlquist, E. Black liquor gasification integrated in pulp and paper mills: A critical review. *Bioresour Technol* **2010**, *101*, 8001-8015.
5. Constant, S.; Wienk, H.L.J.; Frissen, A.E.; Peinder, P.d.; Boelens, R.; van Es, D.S.; Grisel, R.J.H.; Weckhuysen, B.M.; Huijgen, W.J.J.; Gosselink, R.J.A.*, et al.* New insights into the structure and composition of technical lignins: A comparative characterisation study. *Green Chemistry* **2016**, *18*, 2651-2665.
6. Watkins, D.; Nuruddin, M.; Hosur, M.; Tcherbi-Narteh, A.; Jeelani, S. Extraction and characterization of lignin from different biomass resources. *Journal of Materials Research and Technology* **2015**, *4*, 26-32.
7. Sahoo, S.; Seydibeyoğlu, M.Ö.; Mohanty, A.K.; Misra, M. Characterization of industrial lignins for their utilization in future value added applications. *Biomass and Bioenergy* **2011**, *35*, 4230-4237.
8. Chakar, F.S.; Ragauskas, A.J. Review of current and future softwood kraft lignin process chemistry. *Industrial Crops and Products* **2004**, *20*, 131-141.
9. Betancur, M.; Bonelli, P.R.; Velasquez, J.A.; Cukierman, A.L. Potentiality of lignin from the kraft pulping process for removal of trace nickel from wastewater: Effect of demineralisation. *Bioresour Technol* **2009**, *100*, 1130-1137.
10. Vainio, U.; Maximova, N.; Hortling, B.; Laine, J.; Stenius, P.; Simola, L.K.; Gravitis, J.; Serimaa, R. Morphology of dry lignins and size and shape of dissolved kraft lignin particles by x-ray scattering. *Langmuir* **2004**, *20*, 9736-9744.
11. Tejado, A.; Pena, C.; Labidi, J.; Echeverria, J.M.; Mondragon, I. Physico-chemical characterization of lignins from different sources for use in phenol-formaldehyde resin synthesis. *Bioresour Technol* **2007**, *98*, 1655-1663.
12. Areskogh, D.; Li, J.; Gellerstedt, G.; Henriksson, G. Investigation of the molecular weight increase of commercial lignosulfonates by laccase catalysis. *Biomacromolecules* **2010**, *11*, 904-910.
13. Yang, H.; Yan, R.; Chen, H.; Lee, D.H.; Zheng, C. Characteristics of hemicellulose, cellulose and lignin pyrolysis. *Fuel* **2007**, *86*, 1781-1788.
14. Shulga, G.; Rekner, F.; Varslavan, J. Sw—soil and water. *Journal of Agricultural Engineering Research* **2001**, *78*, 309-316.
15. El Mansouri, N.E.; Salvado, J. Structural characterization of technical lignins for the production of adhesives: Application to lignosulfonate, kraft, soda-anthraquinone, organosolv and ethanol process lignins. *Industrial Crops and Products* **2006**, *24*, 8-16.
16. González-García, S.; Teresa Moreira, M.; Artal, G.; Maldonado, L.; Feijoo, G. Environmental impact assessment of non-wood based pulp production by

soda-anthraquinone pulping process. *Journal of Cleaner Production* **2010**, *18*, 137-145.

17. García, A.; Toledano, A.; Serrano, L.; Egüés, I.; González, M.; Marín, F.; Labidi, J. Characterization of lignins obtained by selective precipitation. *Separation and Purification Technology* **2009**, *68*, 193-198.
18. Rodríguez, A.; Sánchez, R.; Requejo, A.; Ferrer, A. Feasibility of rice straw as a raw material for the production of soda cellulose pulp. *Journal of Cleaner Production* **2010**, *18*, 1084-1091.
19. Sixta, H. *Handbook of pulp*. Wiley-VCH Verlag GmbH: Weinheim, 2006.
20. Pan, X.; Arato, C.; Gilkes, N.; Gregg, D.; Mabee, W.; Pye, K.; Xiao, Z.; Zhang, X.; Saddler, J. Biorefining of softwoods using ethanol organosolv pulping: Preliminary evaluation of process streams for manufacture of fuel-grade ethanol and co-products. *Biotechnol Bioeng* **2005**, *90*, 473-481.
21. Çetin, N.S.; Özmen, N. Use of organosolv lignin in phenol–formaldehyde resins for particleboard production. *International Journal of Adhesion and Adhesives* **2002**, *22*, 477-480.
22. Wang, M.; Leitch, M.; Xu, C. Synthesis of phenol–formaldehyde resol resins using organosolv pine lignins. *European Polymer Journal* **2009**, *45*, 3380-3388.
23. Ji, X.; Guo, M. Preparation and properties of a chitosan-lignin wood adhesive. *International Journal of Adhesion and Adhesives* **2018**, *82*, 8-13.
24. Del Saz-Orozco, B.; Alonso, M.V.; Oliet, M.; Domínguez, J.C.; Rojo, E.; Rodriguez, F. Lignin particle- and wood flour-reinforced phenolic foams: Friability, thermal stability and effect of hygrothermal aging on mechanical properties and morphology. *Composites Part B: Engineering* **2015**, *80*, 154-161.
25. Kalliola, A.; Vehmas, T.; Liitiä, T.; Tamminen, T. Alkali-o2 oxidized lignin – a bio-based concrete plasticizer. *Industrial Crops and Products* **2015**, *74*, 150-157.
26. Jeon, J.W.; Zhang, L.; Lutkenhaus, J.L.; Laskar, D.D.; Lemmon, J.P.; Choi, D.; Nandasiri, M.I.; Hashmi, A.; Xu, J.; Motkuri, R.K.*, et al.* Controlling porosity in lignin-derived nanoporous carbon for supercapacitor applications. *ChemSusChem* **2015**, *8*, 428-432.
27. Schulze, P.; Seidel-Morgenstern, A.; Lorenz, H.; Leschinsky, M.; Unkelbach, G. Advanced process for precipitation of lignin from ethanol organosolv spent liquors. *Bioresour Technol* **2016**, *199*, 128-134.
28. Hulin, L.; Husson, E.; Bonnet, J.P.; Stevanovic, T.; Sarazin, C. Enzymatic transesterification of kraft lignin with long acyl chains in ionic liquids. *Molecules* **2015**, *20*, 16334-16353.
29. Qin, W.; Wu, L.; Zheng, Z.; Dong, C.; Yang, Y. Lignin hydrolysis and phosphorylation mechanism during phosphoric acid-acetone pretreatment: A dft study. *Molecules* **2014**, *19*, 21335-21349.
30. Qian, Y.; Zhang, Q.; Qiu, X.; Zhu, S. Co2-responsive diethylaminoethyl-modified lignin nanoparticles and their application as surfactants for co2/n2-switchable pickering emulsions. *Green Chem.* **2014**, *16*, 4963-4968.
31. Brittain, A.D.; Chrisandina, N.J.; Cooper, R.E.; Buchanan, M.; Cort, J.R.; Olarte, M.V.; Sievers, C. Quenching of reactive intermediates during mechanochemical depolymerization of lignin. *Catalysis Today* **2018**, *302*, 180-189.

32. Shen, X.-J.; Huang, P.-L.; Wen, J.-L.; Sun, R.-C. A facile method for char elimination during base-catalyzed depolymerization and hydrogenolysis of lignin. *Fuel Processing Technology* **2017**, *167*, 491-501.
33. Zhou, C.H.; Xia, X.; Lin, C.X.; Tong, D.S.; Beltramini, J. Catalytic conversion of lignocellulosic biomass to fine chemicals and fuels. *Chem Soc Rev* **2011**, *40*, 5588-5617.
34. Yang, W.; Rallini, M.; Wang, D.-Y.; Gao, D.; Dominici, F.; Torre, L.; Kenny, J.M.; Puglia, D. Role of lignin nanoparticles in uv resistance, thermal and mechanical performance of pmma nanocomposites prepared by a combined free-radical graft polymerization/masterbatch procedure. *Composites Part A: Applied Science and Manufacturing* **2018**, *107*, 61-69.
35. Dutta, S.; Wu, K.C.W.; Saha, B. Emerging strategies for breaking the 3d amorphous network of lignin. *Catal. Sci. Technol.* **2014**, *4*, 3785-3799.
36. Hilburg, S.L.; Elder, A.N.; Chung, H.; Ferebee, R.L.; Bockstaller, M.R.; Washburn, N.R. A universal route towards thermoplastic lignin composites with improved mechanical properties. *Polymer* **2014**, *55*, 995-1003.
37. Xu, G.H.; Ren, S.X.; Wang, D.; Su, L.; Fang, G.Z. Fabrication and properties of alkaline lignin / poly (vinyl alcohol) blend membranes. *Bioresources* **2013**, *8*, 2510-2520.
38. Su, L.; Xing, Z.H.; Wang, D.; Xu, G.H.; Ren, S.X.; Fang, G.Z. Mechanical properties research and structural characterization of alkali lignin/poly(vinyl alcohol) reaction films. *Bioresources* **2013**, *8*, 3532-3543.
39. Reza Barzegari, M.; Alemdar, A.; Zhang, Y.; Rodrigue, D. Mechanical and rheological behavior of highly filled polystyrene with lignin. *Polymer Composites* **2012**, *33*, 353-361.
40. Shah, T.; Gupta, C.; Ferebee, R.L.; Bockstaller, M.R.; Washburn, N.R. Extraordinary toughening and strengthening effect in polymer nanocomposites using lignin-based fillers synthesized by atrp. *Polymer* **2015**, *72*, 406-412.
41. Kang, Y.; Chen, Z.; Wang, B.; Yang, Y. Synthesis and mechanical properties of thermoplastic films from lignin, sebacic acid and poly(ethylene glycol). *Industrial Crops and Products* **2014**, *56*, 105-112.
42. Rosch, J.; Mulhaupt, R. Mechanical-properties of organosolv-lignin-filled thermoplastics. *Polym Bull* **1994**, *32*, 361-365.
43. Mattinen, M.L.; Valle-Delgado, J.J.; Leskinen, T.; Anttila, T.; Riviere, G.; Sipponen, M.; Paananen, A.; Lintinen, K.; Kostiainen, M.; Osterberg, M. Enzymatically and chemically oxidized lignin nanoparticles for biomaterial applications. *Enzyme Microb Technol* **2018**, *111*, 48-56.
44. Figueiredo, P.; Lintinen, K.; Hirvonen, J.T.; Kostiainen, M.A.; Santos, H.A. Properties and chemical modifications of lignin: Towards lignin-based nanomaterials for biomedical applications. *Progress in Materials Science* **2018**, *93*, 233-269.
45. Lourençon, T.V.; Hansel, F.A.; da Silva, T.A.; Ramos, L.P.; de Muniz, G.I.B.; Magalhães, W.L.E. Hardwood and softwood kraft lignins fractionation by simple sequential acid precipitation. *Separation and Purification Technology* **2015**, *154*, 82-88.

46. Alekhina, M.; Ershova, O.; Ebert, A.; Heikkinen, S.; Sixta, H. Softwood kraft lignin for value-added applications: Fractionation and structural characterization. *Industrial Crops and Products* **2015**, *66*, 220-228.
47. Foston, M.; Nunnery, G.A.; Meng, X.; Sun, Q.; Baker, F.S.; Ragauskas, A. Nmr a critical tool to study the production of carbon fiber from lignin. *Carbon* **2013**, *52*, 65-73.
48. Baker, D.A.; Rials, T.G. Recent advances in low-cost carbon fiber manufacture from lignin. *Journal of Applied Polymer Science* **2013**, *130*, 713-728.
49. Kubo, S.; Uraki, Y.; Sano, Y. Preparation of carbon fibers from softwood lignin by atmospheric acetic acid pulping. *Carbon* **1998**, *36*, 1119-1124.
50. Gao, G.; Ko, F.; Kadla, J.F. Synthesis of noble monometal and bimetal-modified lignin nanofibers and carbon nanofibers through surface-grafted poly(2-(dimethylamino)ethyl methacrylate) brushes. *Macromolecular Materials and Engineering* **2015**, *300*, 836-847.
51. Gindl-Altmutter, W.; Fürst, C.; Mahendran, A.r.; Obersriebnig, M.; Emsenhuber, G.; Kluge, M.; Veigel, S.; Keckes, J.; Liebner, F. Electrically conductive kraft lignin-based carbon filler for polymers. *Carbon* **2015**, *89*, 161-168.
52. Rodríguez-Mirasol, J.; Cordero, T.; Rodríguez, J.J. High-temperature carbons from kraft lignin. *Carbon* **1996**, *34*, 43-52.
53. Ago, M.; Borghei, M.; Haataja, J.S.; Rojas, O.J. Mesoporous carbon soft-templated from lignin nanofiber networks: Microphase separation boosts supercapacitance in conductive electrodes. *RSC Advances* **2016**, *6*, 85802-85810.
54. Saha, D.; Li, Y.; Bi, Z.; Chen, J.; Keum, J.K.; Hensley, D.K.; Grappe, H.A.; Meyer, H.M., 3rd; Dai, S.; Paranthaman, M.P.*, et al.* Studies on supercapacitor electrode material from activated lignin-derived mesoporous carbon. *Langmuir* **2014**, *30*, 900-910.
55. Valero-Romero, M.J.; Márquez-Franco, E.M.; Bedia, J.; Rodríguez-Mirasol, J.; Cordero, T. Hierarchical porous carbons by liquid phase impregnation of zeolite templates with lignin solution. *Microporous and Mesoporous Materials* **2014**, *196*, 68-78.
56. Myglovets, M.; Poddubnaya, O.I.; Sevastyanova, O.; Lindström, M.E.; Gawdzik, B.; Sobiesiak, M.; Tsyba, M.M.; Sapsay, V.I.; Klymchuk, D.O.; Puziy, A.M. Preparation of carbon adsorbents from lignosulfonate by phosphoric acid activation for the adsorption of metal ions. *Carbon* **2014**, *80*, 771-783.
57. Fu, K.; Yue, Q.; Gao, B.; Sun, Y.; Zhu, L. Preparation, characterization and application of lignin-based activated carbon from black liquor lignin by steam activation. *Chemical Engineering Journal* **2013**, *228*, 1074-1082.
58. Norberg, I.; Nordström, Y.; Drougge, R.; Gellerstedt, G.; Sjöholm, E. A new method for stabilizing softwood kraft lignin fibers for carbon fiber production. *Journal of Applied Polymer Science* **2013**, *128*, 3824-3830.
59. Brodin, I.; Ernstsson, M.; Gellerstedt, G.; Sjöholm, E. Oxidative stabilisation of kraft lignin for carbon fibre production. *Holzforschung* **2012**, *66*.
60. Baker, D.A.; Gallego, N.C.; Baker, F.S. On the characterization and spinning of an organic-purified lignin toward the manufacture of low-cost carbon fiber. *Journal of Applied Polymer Science* **2012**, *124*, 227-234.

61. Frank, E.; Steudle, L.M.; Ingildeev, D.; Spörl, J.M.; Buchmeiser, M.R. Carbonfasern: Präkursor-systeme, verarbeitung, struktur und eigenschaften. *Angewandte Chemie* **2014**, *126*, 5364-5403.
62. Lin, J.; Kubo, S.; Yamada, T.; Koda, K.; Uraki, Y. Chemical thermostabilization for the preparation of carbon fibers from softwood lignin. *Bioresources* **2012**, *7*, 5634-5646.
63. Li, Y.; Cui, D.; Tong, Y.; Xu, L. Study on structure and thermal stability properties of lignin during thermostabilization and carbonization. *Int J Biol Macromol* **2013**, *62*, 663-669.
64. Gonugunta, P.; Vivekanandhan, S.; Mohanty, A.K.; Misra, M. A study on synthesis and characterization of biobased carbon nanoparticles from lignin. *World Journal of Nano Science and Engineering* **2012**, *02*, 148-153.
65. Snowdon, M.R.; Mohanty, A.K.; Misra, M. A study of carbonized lignin as an alternative to carbon black. *ACS Sustainable Chemistry & Engineering* **2014**, *2*, 1257-1263.
66. Ren, D.; Zheng, S.; Wu, F.; Yang, W.; Liu, Z.; Yang, M. Formation and evolution of the carbon black network in polyethylene/carbon black composites: Rheology and conductivity properties. *Journal of Applied Polymer Science* **2014**, *131*, n/a-n/a.
67. Ma, L.-F.; Bao, R.-Y.; Huang, S.-L.; Liu, Z.-Y.; Yang, W.; Xie, B.-H.; Yang, M.-B. Electrical properties and morphology of carbon black filled pp/epdm blends: Effect of selective distribution of fillers induced by dynamic vulcanization. *Journal of Materials Science* **2013**, *48*, 4942-4951.
68. Peyvandi, A.; Soroushian, P.; Abdol, N.; Balachandra, A.M. Surface-modified graphite nanomaterials for improved reinforcement efficiency in cementitious paste. *Carbon* **2013**, *63*, 175-186.
69. Bahl, K.; Miyoshi, T.; Jana, S.C. Hybrid fillers of lignin and carbon black for lowering of viscoelastic loss in rubber compounds. *Polymer* **2014**, *55*, 3825-3835.
70. Kai, D.; Tan, M.J.; Chee, P.L.; Chua, Y.K.; Yap, Y.L.; Loh, X.J. Towards lignin-based functional materials in a sustainable world. *Green Chem.* **2016**, *18*, 1175-1200.
71. Gilca, I.A.; Popa, V.I.; Crestini, C. Obtaining lignin nanoparticles by sonication. *Ultrason Sonochem* **2015**, *23*, 369-375.
72. Tortora, M.; Cavalieri, F.; Mosesso, P.; Ciaffardini, F.; Melone, F.; Crestini, C. Ultrasound driven assembly of lignin into microcapsules for storage and delivery of hydrophobic molecules. *Biomacromolecules* **2014**, *15*, 1634-1643.
73. García, A.; Erdocia, X.; González Alriols, M.; Labidi, J. Effect of ultrasound treatment on the physicochemical properties of alkaline lignin. *Chemical Engineering and Processing: Process Intensification* **2012**, *62*, 150-158.
74. Garcia, A.; Alriols, M.G.; Labidi, J. Evaluation of the effect of ultrasound on organosolv black liquor from olive tree pruning residues. *Bioresour Technol* **2012**, *108*, 155-161.
75. Nair, S.S.; Sharma, S.; Pu, Y.; Sun, Q.; Pan, S.; Zhu, J.Y.; Deng, Y.; Ragauskas, A.J. High shear homogenization of lignin to nanolignin and thermal stability of nanolignin-polyvinyl alcohol blends. *ChemSusChem* **2014**, *7*, 3513-3520.
76. Stewart, H.; Golding, M.; Matia-Merino, L.; Archer, R.; Davies, C. Manufacture of lignin microparticles by anti-solvent precipitation: Effect of preparation

temperature and presence of sodium dodecyl sulfate. *Food Research International* **2014**, *66*, 93-99.

77. Frangville, C.; Rutkevicius, M.; Richter, A.P.; Velev, O.D.; Stoyanov, S.D.; Paunov, V.N. Fabrication of environmentally biodegradable lignin nanoparticles. *Chemphyschem* **2012**, *13*, 4235-4243.
78. Lu, Q.; Zhu, M.; Zu, Y.; Liu, W.; Yang, L.; Zhang, Y.; Zhao, X.; Zhang, X.; Zhang, X.; Li, W. Comparative antioxidant activity of nanoscale lignin prepared by a supercritical antisolvent (sas) process with non-nanoscale lignin. *Food Chemistry* **2012**, *135*, 63-67.
79. Jiang, C. Nano-lignin filled natural rubber composites: Preparation and characterization. *Express Polymer Letters* **2013**, *7*, 480-493.
80. Duval, A.; Vilaplana, F.; Crestini, C.; Lawoko, M. Solvent screening for the fractionation of industrial kraft lignin. *Holzforschung* **2015**, *0*.
81. Ago, M.; Huan, S.; Borghei, M.; Raula, J.; Kauppinen, E.I.; Rojas, O.J. High-throughput synthesis of lignin particles (approximately 30 nm to approximately 2 mum) via aerosol flow reactor: Size fractionation and utilization in pickering emulsions. *ACS Appl Mater Interfaces* **2016**, *8*, 23302-23310.
82. Fu, S.-Y.; Feng, X.-Q.; Lauke, B.; Mai, Y.-W. Effects of particle size, particle/matrix interface adhesion and particle loading on mechanical properties of particulate–polymer composites. *Composites Part B: Engineering* **2008**, *39*, 933-961.
83. Sánchez-González, J.; Macías-García, A.; Alexandre-Franco, M.F.; Gómez-Serrano, V. Electrical conductivity of carbon blacks under compression. *Carbon* **2005**, *43*, 741-747.

6. ABBILDUNGSVERZEICHNIS

Abbildung 1: Überblick über Ligninnutzung ... 3
Abbildung 2: Übersicht über Herstellungswege und Verwendungsarten von carbonisiertem Lignin nach Kai[70] ... 4
Abbildung 3: Schematische Darstellung A) der Ultraschallsonde, B) des Homogenisators und C) des Mikrofluidizers. ... 8
Abbildung 4: Schematische Darstellung des Ausfällvorgangs ... 10
Abbildung 5: Schematische Darstellung der Messung der elektrischen Leitfähigkeit von Filmen ... 12
Abbildung 6: Überblick über eingesetzte Rohstoffe für die Carbonisierung ... 14
Abbildung 7: SEM-Aufnahmen von Kraft Lignin, Soda Lignin, Lignosulfonat und Organosolv Lignin. ... 15
Abbildung 8: DSC und TGA von Kraft Lignin, Soda Lignin, Lignosulfonat und Organosolv Lignin ... 16
Abbildung 9: SEM-Aufnahme von Kraft Lignin nach der Behandlung im Mikrofluidizer ... 17
Abbildung 10: Ergebnisse des Ausfällens: A) Kraft Lignin mit Dioxan/Wasser (REM), B) Lignosulfonat mit Wasser/Aceton (AFM), C) Kraft Lignin mit Dioxan/Cyclohexan (REM), D) Probe C) abgedampft (REM) ... 18
Abbildung 11: FT-IR Spektrum des unbehandelten und thermostabilisierten Kraft Lignins ... 19
Abbildung 12: SEM-Bilder des Kraft Lignins unbehandelt und carbonisiert (2000 °C) ... 22
Abbildung 13: SEM-Bilder des Soda Lignins unbehandelt und carbonisiert (2000 °C) ... 22
Abbildung 14: SEM-Bilder des Lignosulfonats unbehandelt und carbonisiert (2000 °C) ... 23
Abbildung 15: SEM-Bilder des Organosolv Lignins unbehandelt und carbonisiert (2000 °C) ... 23
Abbildung 16: SEM-Bilder des sprühgetrockneten Kraft Lignins unbehandelt und carbonisiert (2000 °C) ... 24
Abbildung 17: SEM-Bilder des sprühgetrockneten Lignosulfonats unbehandelt und carbonisiert (2000 °C) ... 24
Abbildung 18: SEM-Bilder des Kraft Nanolignins unbehandelt und carbonisiert (2000 °C) ... 25
Abbildung 19: Leitfähigkeit der Lignine in Abhängigkeit von der Carbonisierungstemperatur ... 26
Abbildung 20: XRD-Spektren des Kraft Lignins, Lignosulfonats, Nanolignins, sprühgetrockneten Kraft Lignins und sprühgetrockneten Lignosulfonats ... 27
Abbildung 21: Raman-Spektren des Kraft Lignins, Lignosulfonats, Soda Lignins und Organosolv Lignins mit dem D-Peak und G-Peak ... 28
Abbildung 22: Feststellung der Mindestfüllmenge von Carbon Partikeln (Organosolv Lignin Partikel, carbonisiert bei 2000 °C) im Polymer (PLA), um elektrische Leitfähigkeit zu erzeugen. ... 29
Abbildung 23: Abnahme der Leitfähigkeit der Composite bei zunehmender Zugspannung ... 30

7. TABELLENVERZEICHNIS

Tabelle 1: Versuchsparameter Ultraschallbad 7
Tabelle 2: Versuchsparameter Mikrofluidizer 8
Tabelle 3: Versuchsparameter Sprühtrocknung 9
Tabelle 4: Versuchsparameter Ausfällversuche 10
Tabelle 5: Resultierender Druck unterschiedlicher Gewichte bei der Messung elektrischer Leitfähigkeit 12
Tabelle 6: Gesamtausbeuten der Thermostabilisierung und Carbonisierung aller Lignine 20
Tabelle 7: Elementaranalyse verschiedener Proben vor- und nach der Thermostabilisierung und Carbonisierung 21
Tabelle 8: Vergleich des D- und G-Peaks der Ramanspektren 27
Tabelle 9: Ergebnisse der Zugversuche des PCL gefüllt mit 30 % carbonisierter Ligninpartikel 30

PUBLIKATIONEN

Publikation I: Comparison of four technical lignins as resource for electrically conductive carbon particle

Publikation II: Carbon Microparticles from Organosolv Lignin as Filler for Conducting Poly(Lactic Acid)

Publikation III: Electrically conducting carbon microparticles by direct carbonization of spent wood pulping liquor

Publikation IV: Electrically-Conductive Sub-Micron Carbon Particles from Lignin: Elucidation of Nanostructure and Use as Filler in Cellulose Nanopapers

I

Köhnke, J., Gierlinger, N., Prats-Mateu, B., Unterweger, C., Solt, P., Mahler, A., Schwaiger, E., Liebner, F. and Gindl-Altmutter, W. (2019) "**Comparison of four technical lignins as a resource for electrically conductive carbon particles**," *BioRes*. 14(1), 1091-1109. DOI: 10.15376/biores.14.1.1091-1109

Comparison of Four Technical Lignins as a Resource for Electrically Conductive Carbon Particles

Janea Köhnke,[a,*] Notburga Gierlinger,[b] Batirtze Prats Mateu,[b] Christoph Unterweger,[c] Pia Solt,[a,c] Arnulf Kai Mahler,[d] Elisabeth Schwaiger,[e] Falk Liebner,[a] and Wolfgang Gindl-Altmutter [a]

Carbon microparticles were produced from different technical lignins, *i.e.*, kraft lignin, soda lignin, lignosulfonate, and organosolv lignin, at different carbonisation temperatures (800 °C, 1200 °C, 1600 °C, and 2000 °C). Before carbonisation, oxidative thermostabilization was performed. The combination of thermostabilization and carbonisation led to a high mass loss and shrinkage, but no major effect on the particle morphology was apparent. The carbon particles obtained from all four lignin variants developed disordered graphitic structures at high carbonisation temperatures, and good electrical conductivities in the carbon powders were observed for all lignin variants, with the exception of lignosulfonate. The polycaprolactone composite films filled with 30% lignin-derived carbon exhibited various conductivities, with the best results achieved using the kraft lignin-derived carbon.

Keywords: Lignin; Conductivity; Carbonisation; Carbon particles

Contact information: a: BOKU-University of Natural Resources and Life Science Vienna, Konrad Lorenz Strasse 24, A-3430 Tulln, Austria; b: BOKU-University of Natural Resources and Life Science Vienna, Muthgasse 11/II, A-1190 Wien, Austria; c: Wood K plus - Competence Center of Wood Composites and Wood Chemistry, Altenbergerstrasse 69, A-4040 Linz, Austria; d: Sappi Europe, Brucker Strasse 21, A-8101 Gratkorn, Austria; e: Mondi Paper Sales GmbH, Head of R&D Business Unit Packaging Paper, Frantschach 5, A-9413 St. Gertraud, Austria;
** Corresponding author: janea.koehnke@boku.ac.at*

INTRODUCTION

Lignin, a major constituent in wood cell walls, is the second most abundant natural polymer after cellulose (Boerjan *et al.* 2003). When wood is digested in the pulp and paper industry with the aim of utilising cellulose and eventually hemicellulose, huge amounts of lignin become available as a secondary product from the pulping process. This results in an annual global lignin production of approximately 50 million tons (Gosselink *et al.* 2004). Because large-scale, high-value uses of lignin products are not available, lignin is mostly used for the production of heat and energy (Kai *et al.* 2016). With increasing prices for fossil oil and a growing trend towards renewable and sustainable resources, lignin becomes increasingly attractive as a potential low-cost source for value-added products. Consequently, there is an ongoing and steadily intensifying discussion about alternative usages of lignin, such as polymer production, biorefinery development, biofuels, and chemicals (Doherty *et al.* 2011; Chatterjee *et al.* 2014; Duval and Lawoko 2014; Laurichesse and Avérous 2014; Thakur *et al.* 2014; Xu *et al.* 2014; Bruijnincx *et al.* 2015; Kai *et al.* 2016).

Currently there are four major technical lignins produced from pulping, which are kraft lignin (85% of the lignin produced worldwide (Tejado *et al.* 2007)), soda lignin (9%

(Sixta 2006)), lignosulfonate (6% (Mansouri and Salvadó 2006)), and organosolv lignin (not yet commercially available on a large scale). The structure, reactivity, molecular weight, and chemical composition of the resulting lignins are diverse. Kraft lignin originates from the sulphate cooking process, which involves sodium hydroxide and sodium sulphide as the main reagents (Chakar and Ragauskas 2004). The cooking liquor (black liquor) from this process contains fragments of lignin with different molecular weights (Betancur *et al.* 2009). It has high ash, hydroxyl, and carboxyl contents, as well as abundant condensed structures (Vainio *et al.* 2004). Soda lignin derives from the soda cooking process, which is free of sulphur (García *et al.* 2009). The soda cooking process is predominantly used for non-wood plants (grasses, bamboo, *etc.*) and only rarely applied to hardwood species (González-García *et al.* 2010). Hence, soda lignin is often characterised by high silicate and nitrogen contents (Rodríguez *et al.* 2010). Lignosulphonates arise from sulphite cooking processes. Acidic cooking liquor contains HSO_3^- and SO_3^{2-} with variable counter ions (Areskogh *et al.* 2010). In contrast with other technical lignins, lignosulphonates are water soluble because of sulphonation and degradation during the cooking process (Shulga *et al.* 2001). They show a high diversity in functional groups, some of which are charged. Compared with other technical lignins, lignosulphonates show a high molecular weight, high ash content, and low amounts of carbohydrates (Yang *et al.* 2007). Organosolv lignin is produced in a pulping process in which the cooking liquor contains water and organic solvents, *e.g.*, ethanol (Pan *et al.* 2005). Dissolved lignin characteristically has a low molecular weight (Çetin and Özmen 2002). Organosolv lignin has a high purity and is sulphur-free (Wang *et al.* 2009).

Lignin-derived carbon is an intensely researched route for generating additional value from technical lignins. In this context, potential applications include the substitution of fossil-based carbon black (Snowdon *et al.* 2014), lignin-based carbon fibres (Kadla *et al.* 2002; Ruiz-Rosas *et al.* 2010; Foston *et al.* 2013), carbon nanoparticles (Gonugunta *et al.* 2012), and activated carbon (Hayashi *et al.* 2000; Suhas *et al.* 2007). Recently it was determined that lignin-derived carbon particles may act as functional fillers in conductive polymers, similar to carbon black (Gindl-Altmutter *et al.* 2015; Ago *et al.* 2016; Köhnke *et al.* 2016; Köhnke *et al.* 2018). Carbon black is commercially produced by the thermal breakdown of hydrocarbons. Different processes lead to five different carbon blacks that are mass-produced (Bourrat 1993), and their particles vary considerably in terms of their shape, size, surface, conductivity, and porosity (Huang 2002). Different properties are important depending on the application, such as inks, polymer fillers (as reinforcing filler, conductive filler, stabilizer, antioxidant, pigment, and colorant), coatings, and electronic components (Balberg 2002).

In the present study, the suitability of four technical lignins as precursors for carbon microparticles were compared. In particular, the suitability of lignin-derived carbon as a functional, electrically conductive filler for polymers was evaluated. Here, lignin-based fillers could serve as a bio-based alternative to currently used conductive polymers such as polypyrrole (Das and Prusty 2012) and conductive polymer fillers such as carbon black (Jin *et al.* 2013) or carbon nanotubes (Castellino *et al.* 2016).

EXPERIMENTAL

Production of the Carbon Microparticles

Kraft lignin (Indulin AT) was purchased from MeadWestvaco (Richmond, USA). The lignin originated from a kraft cooking process of southern pine and was purified with acidic hydrolysis, where sodium and hemicelluloses were removed. Soda lignin (Protobind 2400), produced from wheat straw, was obtained from GreenValue (Alpnach Dorf, Switzerland). Softwood lignosulfonate (sodium lignosulfonate) was bought from Borregaard (Sarpsborg, Norway). The lignosulphonate was ultra-filtered, desulphonated, and oxidised. Organosolv lignin was provided by Fraunhofer (Leuna, Germany). Polycaprolactone (PCL) and toluene were purchased from Carl Roth GmbH & Co. KG (Karlsruhe, Germany). Treatment of the lignins began with a thermostabilization step that involved heating using a drying oven at an ambient atmosphere and a heating rate of 0.01 °C/min from 20 °C to 250 °C. Carbonisation was performed with four different target temperatures of 800 °C, 1200 °C, 1600 °C, and 2000 °C in a GERO HTK8 oven (Carbolite Gero, Sheffield, UK) with a volume of 6 L and an argon gas flow rate of 150 L/h. The heating rate was 1 °C/min up to 500 °C and was followed by a 1-h holding step. After that, the heating rate was increased to 5 °C/min, with a 1-h holding step at 900 °C and another 1-h holding step at the final temperature.

Characterisation of the Carbonised Lignin Particles

Scanning electron microscopy (SEM) was performed on a QuantaTM 250 field-emission environmental scanning electron microscope (FEI Europe B.V., Eindhoven, Netherlands) with a Schottky field emission gun at 10 kV and a high vacuum of 1 x 10^{-6} mbar. The samples were prepared on a copper conductive double-coated tab and were sputter-coated with a thin film of gold.

Elemental analysis was done on an elemental analyser (EA 1108 CHNS-O, Carlo Erba Instruments, Waltham, USA) at temperatures between 1020 °C and 1400 °C in tin capsules. Gas chromatography was used for separation with highest purity helium gas as a carrier. Quantification and detection were done with a thermal conductivity detector (6890GC with TCD, Agilent, Vienna, Austria).

Thermogravimetric analysis (TGA) and differential scanning calorimetry (DSC) were performed simultaneously on a Netzsch DSC 200 F3 Maia (Netzsch Group, Selb, Germany). Open aluminium crucibles were filled with carbon powder and heated at a rate of 5 °C/min under a nitrogen atmosphere.

The Raman spectra were measured on a Raman microscope (alpha300RA, WITec GmbH, Ulm, Germany) using a green laser (λ = 532 nm), a spectrometer with a 600-g/mm grating (UHTS 300, WITec GmbH, Ulm, Germany), and a charge coupled device camera (DU401ABV, Andor Technology, Belfast, UK). A laser power of 5 mW was used. With an integration time of 0.05 s, single spectra were collected every 250 nm over a region of 20 µm × 20 µm (6400 spectra/region) using a 100x oil immersion objective (numerical aperture = 1.4). Finally, the average spectra of all four samples were calculated (19200 spectra/sample).

The electrical conductivity of the carbon powders was measured according to Sánchez-González *et al.* (2005). A plastic cylinder with an inner diameter of 6.22 mm was fixed onto a stationary metal piston. The cavity of the plastic cylinder was filled with 50 mg to 100 mg of carbon powder, up to a height of approximately 12 mm. The total height was measured and a second movable metal piston with the diameter the size of the cylinder hole was inserted into the cylinder. Upon closure of the cylinder, various loads were applied to the upper piston to reach pressures of 65 kPa, 161 kPa, 226 kPa, 645 kPa, and 807 kPa. The conductivity and height of the powder were measured repeatedly after each increase in pressure. The conduction was ohmic; therefore, the electrical conductivity (σ; Ω^{-1}mm^{-1}) of the samples was calculated with Eq. 1 (Sánchez-González *et al.* 2005),

$$\sigma = l / (R \times A) \tag{1}$$

where l is the distance between the pistons (cm), R is the electrical resistance (Ω), and A is the area of the piston surface (m²).

Polycaprolactone-carbon Composite Films

The PCL was dissolved in toluene at a concentration of 100 g/L under constant stirring at room temperature. The carbon particles were blended into the PCL and toluene mixture at a ratio of 30% carbon (mass) to 70% PCL (mass). The compound was decanted into a crystallising dish, and the toluene evaporated overnight. After 2 h in a vacuum drying chamber, the compound was folded and hot-pressed twice at 90 °C to achieve a more homogeneous and even distribution of carbon particles.

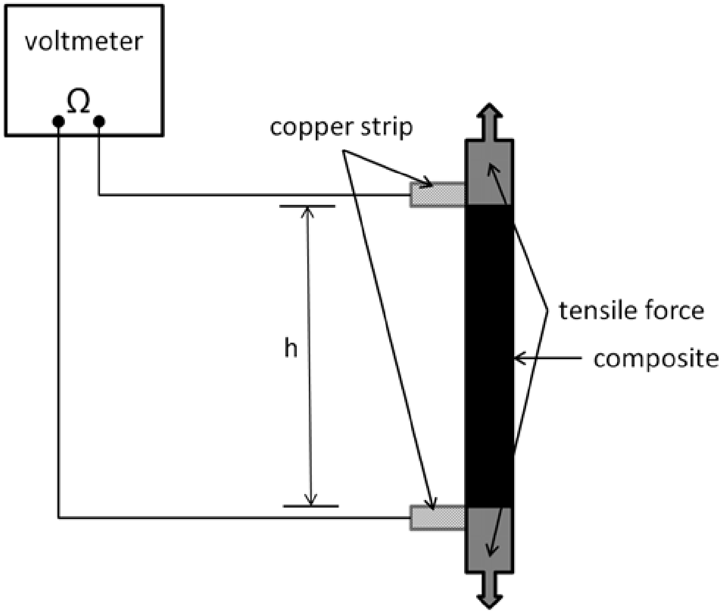

Fig. 1. Experimental device for the resistivity measurements of the composites during tensile loading

Thereafter, the composite was cut into strips 80 mm in length and 8 mm in width and inserted into a Zwick Roell 20-kN universal testing machine (Ulm, Germany) with a 2.5-kN load cell for tensile testing, as is seen in Fig. 1. For the resistivity measurements, two copper strips were added between the composite and grip at a distance (h) of 35 mm. The resistivity was measured during tensile loading.

RESULTS AND DISCUSSION

Gravimetric Yield and Structural Changes during Carbonisation

Overall, considerable mass losses occurred during all of the thermal treatment stages in the present study. Thermostabilization in an ambient atmosphere was performed to avoid fusing the lignin particles because of the inherent thermoplasticity of lignin during carbonisation (Braun *et al.* 2005; Norberg *et al.* 2013). The mass loss resulting from this treatment varied considerably for the four types of lignin (Fig. 2). With a 35% mass loss, lignosulfonate was most stable, whereas organosolv lignin showed the highest mass loss at 61%. During thermostabilization, a number of processes contributed to the mass loss. First, the initial mass loss was caused by the removal of moisture. Thereafter, the oxidation of lignin caused further mass loss that was associated with the loss of phenolic, alcoholic, methyl, carbonyl, and methoxyl groups (Braun *et al.* 2005; Norberg *et al.* 2013). While these phenomena primarily led to a loss of oxygen, hydrogen, and carbon, the inorganic compounds were not affected. This might have contributed to the fact that the organosolv lignin, which was virtually free of inorganics, showed the highest mass loss during thermostabilization.

The carbonisation treatment under an argon atmosphere, which followed thermostabilization, caused remarkable additional mass loss. For all of the lignins, severe mass loss was observed after the first two carbonisation steps with the target temperatures of 800 °C and 1200 °C, whereas only minor mass changes occurred at the higher temperatures (Fig. 2). In principal, mass loss during carbonisation is caused by the breaking of bonds, first the weaker bonds (*e.g.*, C-OH or hydrogen bonds) and then the stronger ones (*e.g.*, ß-O-4 linkages), which directs the depolymerisation of lignin (Liu *et al.* 2015). Random repolymerisation of the remaining carbon structures occurs following depolymerisation and leads to graphitic and graphite-like structures (Song *et al.* 2017; Yi *et al.* 2017).

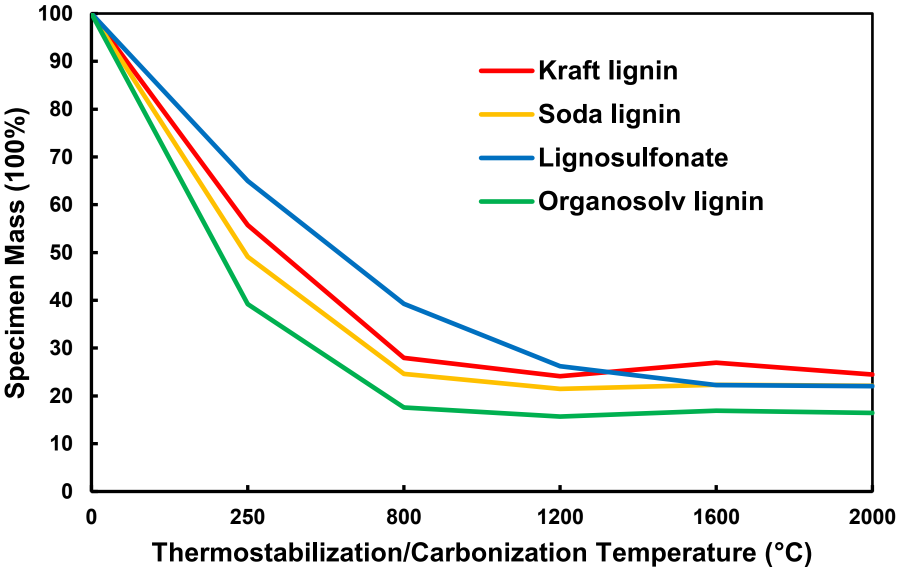

Fig. 2. Mass loss for all of the lignin samples during the thermal treatment of thermostabilization (250°C) and carbonization (800 °C and higher)

Table 1 shows an overview of the changes in the elemental composition of the four lignin variants used and compared the untreated lignin and specimens carbonised at 2000 °C. Regardless of the initial elemental composition, the carbon content of all of the lignin-derived carbons was above 99%, which indicated that inorganics were also largely volatilised at high carbonisation temperatures, which contributed to the overall mass loss. Trace amounts of inorganics, that were not detected in the untreated lignins, appeared after carbonisation, which was probably caused by impurities present in the carbonisation oven or graphite containers used during the carbonisation experiments.

Table 1. Elemental Analysis of the Untreated Lignins and Lignins Carbonised at 2000 °C

Material		Element (% w/w)							
		C	H	N	S	K	Na	Ca	Mg
Kraft lignin	untreated	62.8	5.8	0.9	0.1	-	-	-	-
	2000 °C	99.9	< 0.05	< 0.05	< 0.02	0.03	0.03	0.05	< 0.02
Soda lignin	untreated	61.9	5.9	0.9	< 0.02	-	-	-	-
	2000 °C	99.2	< 0.05	< 0.05	0.23	0.03	0.03	0.03	< 0.02
Lignosulfonate	untreated	47.9	3.7	0.2	2.0	-	-	-	-
	2000 °C	99.6	< 0.05	< 0.05	0.04	< 0.02	< 0.02	0.06	< 0.02
Organosolv lignin	untreated	61.1	5.9	0.3	< 0.02	-	-	-	-
	2000 °C	99.6	< 0.05	< 0.05	< 0.02	0.05	< 0.02	0.03	< 0.02

Simultaneous TGA and DSC analysis provided more information on the dynamics of the thermal decomposition over a limited temperature range of 600 °C (Fig. 3). Notably, the mass loss measured at 250 °C during TGA was less than the mass loss observed during thermostabilization. This was easily explained by the fact that TGA was done in a nitrogen atmosphere to prevent oxidation, whereas thermostabilization was performed with the intention of slow oxidisation and thus inherently caused more mass loss than the TGA.

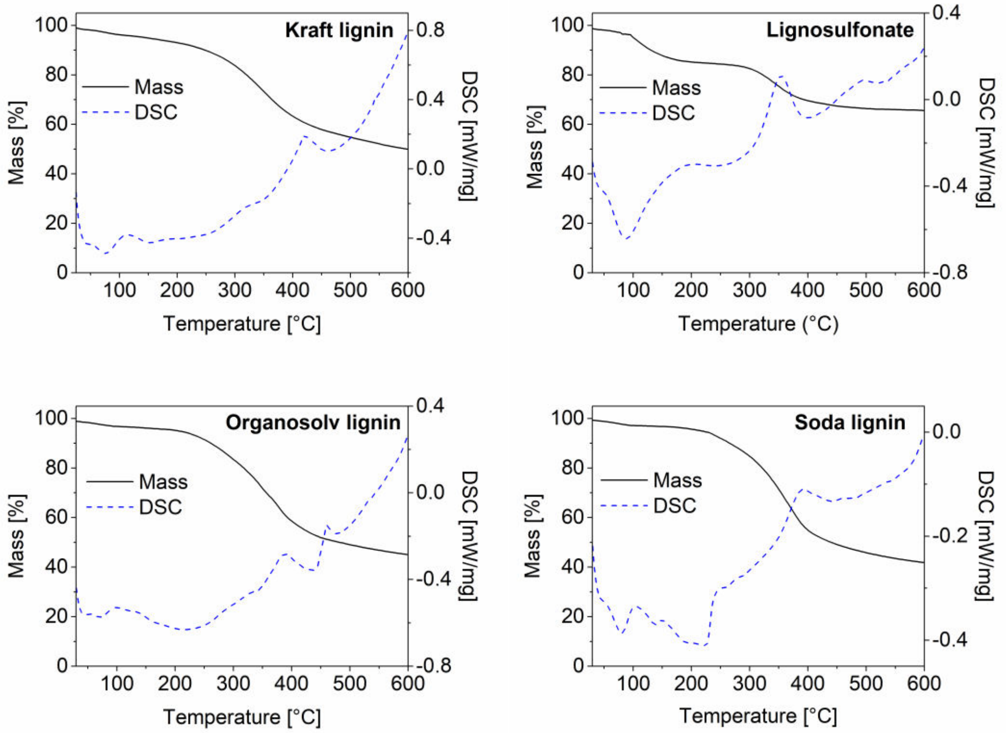

Fig. 3. TGA and DSC curves of all four untreated lignins: (a) kraft lignin; (b) lignosulfonate; (c) soda lignin; and (d) organosolv lignin

After a small initial mass loss because of moisture evaporation, a major mass loss began in the TGA between 200 °C and 300 °C and continued until 400 °C (Fig. 3). While this general trend applied to three of the lignins, lignosulfonate somewhat differed in that a first major mass loss was already seen at lower temperatures of 100 °C and 170 °C. The DSC analysis that was done simultaneously revealed the exothermal behaviour of the concurrent major mass loss in the temperature region of 300 °C to 400 °C. This exothermal peak was the most intense for lignosulphonate and was probably caused by the release of SO_2 during thermal degradation, which released the energy recorded during DSC (Köhnke *et al.* 2018). This high decomposition intensity of the lignosulfonate correlated well with the observation that out of all of the lignins, lignosulfonate showed the highest mass loss between the end of the thermostabilization phase and the final carbonisation step at 2000 °C (Fig. 2).

The Raman spectroscopy provided information about the degree of graphitic order in the carbon structures (Fig. 4). The Raman data showed the typical spectra of a graphitic lattice, which confirmed that carbonaceous structures were produced in the heating process (Dresselhaus *et al.* 2010). The G-band at approximately 1580 cm^{-1}, which corresponded to the single graphite crystal or ideal graphitic lattice, and the D-band at approximately 1350 cm^{-1}, which indicated the presence of polycrystalline graphite and therefore a disordered graphitic lattice, were the most important signals (Tuinstra and Koenig 1970; Sadezky *et al.* 2005). All of the lignin-derived carbon samples produced in the present study were characterised by a higher D-peak compared with the G-peak. This indicated that a noticeable degree of disorder was present in the graphitic structures. An evaluation of the ratio of the peak intensities that is shown in Fig. 4 indicated only minor differences between the four lignin-derived carbons. Among the carbons studied, lignosulfonate showed the lowest G-band intensity compared with the D-band intensity, which was in good agreement with the specific thermal decomposition behaviour of this technical lignin variant (Köhnke *et al.* 2018). In contrast, for the carbon derived from spray-dried kraft black liquors, a clear dominance of the G-band over the D-band was observed by Köhnke *et al.* (2018), which indicated a high degree of graphitic order.

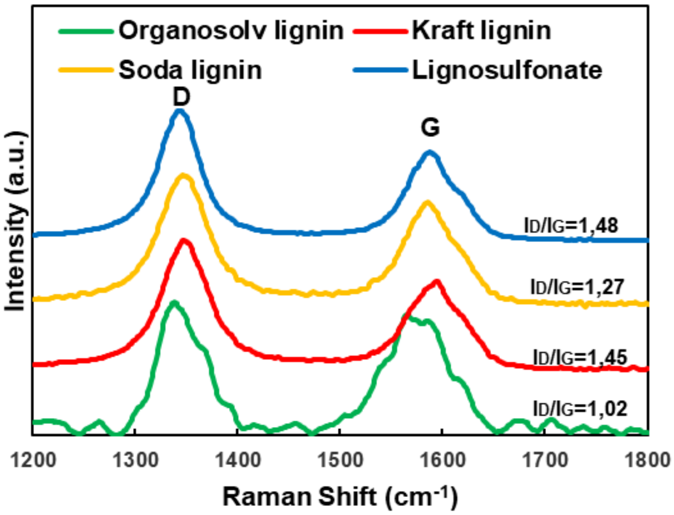

Fig. 4. Raman spectra of the lignin-derived carbon particles carbonised at 2000 °C

Morphological Characterisation by SEM

The different lignins received showed high variable particle sizes and particle morphologies, as is shown in Figs. 5 to 8.

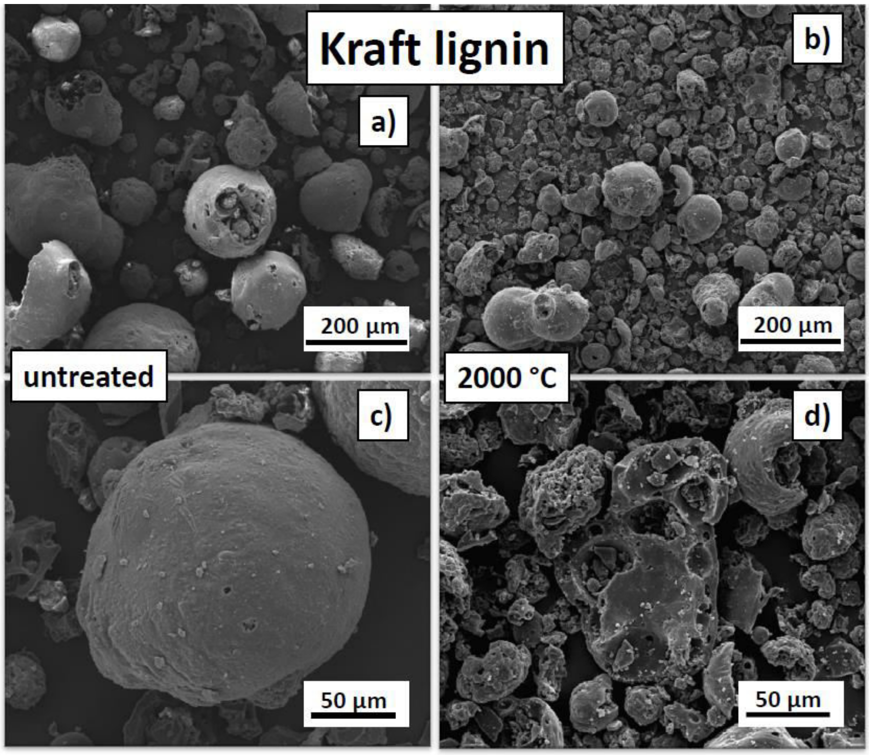

Fig. 5. SEM images of the untreated (a and c) and carbonised (2000 °C) kraft lignin (b and d)

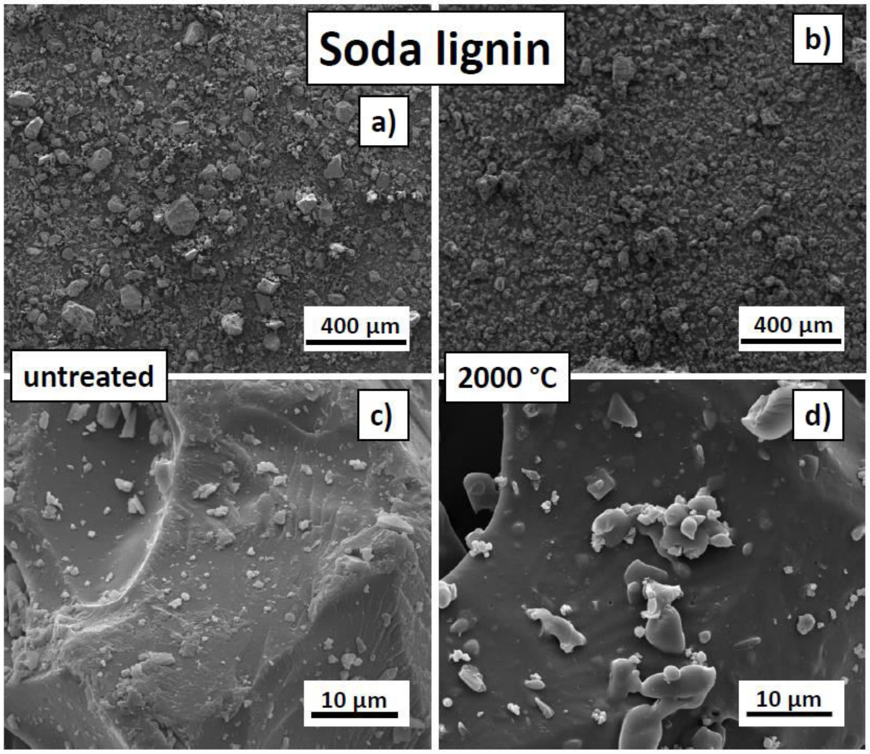

Fig. 6. SEM images of the untreated (a and c) and carbonised (2000 °C) soda lignin (b and d)

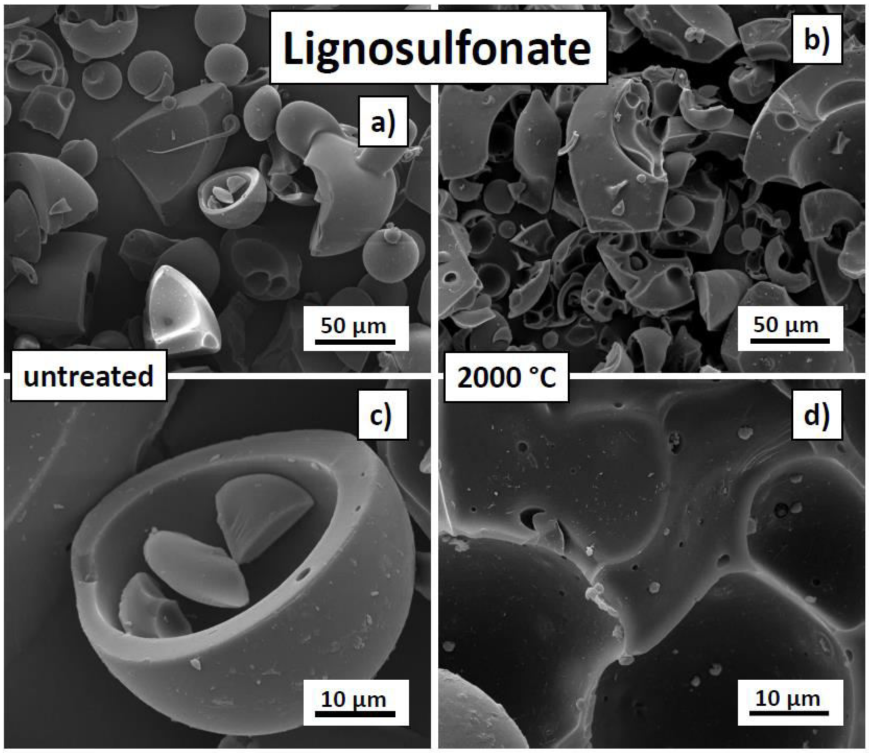

Fig. 7. SEM images of the untreated (a and c) and carbonised (2000 °C) lignosulfonate (b and d)

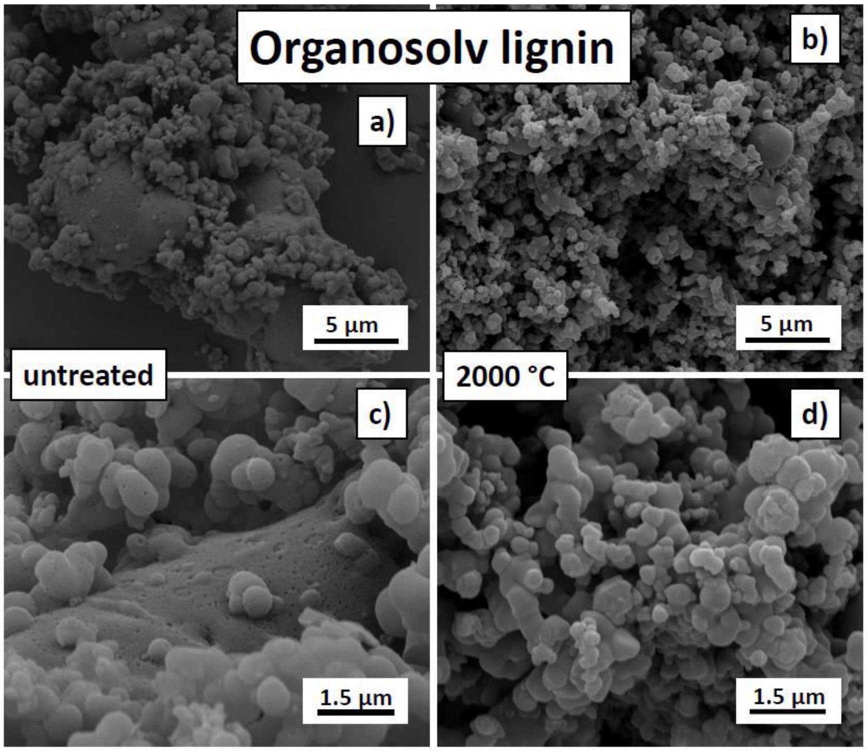

Fig. 8. SEM images of untreated (a and c) and carbonised (2000 °C) organosolv lignin (b and d)

The kraft lignin particles were spherical in shape and had internal cavities (Fig. 5). The particles had a broad particle size distribution with an average size of 59.0 µm, which was the largest diameter of all four lignin variants studied. After carbonisation, the particles shrank to an average diameter of 25.5 µm, which corresponded to a 56.8% shrinkage, which was the highest shrinkage of all of the lignins. Other than the shrinkage, small spots with high electron density contrast crumbs that adhered to the particle surfaces was the only apparent difference after carbonisation. These spots are most probably agglomerations of inorganic residues originating from wood constituents or process chemicals used during pulping (Köhnke *et al.* 2016).

Compared with all of the other lignins, the soda lignin was characterised by an irregular particle morphology, which indicated that it was probably milled (Fig. 6). Furthermore, the particles did not reveal any porosity detectable at the resolution used during SEM. The untreated soda lignin particles had a wide-ranging particle size distribution, with an average size of 14.2 µm, as is displayed in Fig. 6. After carbonisation, the particles shrank to 12.8 µm, which was an average shrinkage of 10.3%. This was the lowest shrinkage of all of the lignins and might have correlated with the absence of noticeable micropores in the particles. Other than shrinkage, no morphological changes because of carbonisation were observed.

The lignosulfonate observed by SEM (Fig. 7) appeared to be fragments of initially spherical, hollow particles. The surface of the fragments had a smooth appearance and porosity was present in small amounts. The size and wall thickness of the fragments showed a high variability. The untreated lignosulfonate particles had a particle size distribution with an average equivalent diameter of 46.2 µm. After carbonisation, the particles shrank to 30.2 µm, which was an average shrinkage of 34.7%. In addition to considerable shrinkage, a clearly visible increase in the porosity occurred during carbonisation (Fig. 7).

The organosolv lignin particle morphology was different compared with the morphologies of the other three lignins, in that it consisted of particles of two different size classes (Fig. 8). Agglomerates with a characteristic size of 30 µm to 35 µm were apparent. Upon closer inspection, these agglomerates consisted of small lignin spheres with smooth surfaces and occasionally hollow structures. These small spheres had an average particle size of 0.5 µm and shrank down to 0.3 µm after carbonisation, which was a shrinkage of 39.7%. Those were the smallest particles found in this study. After carbonisation, changes in the morphology were absent.

Electrical Conductivity of the Carbon Powders and Carbon-polycaprolactone Composite Films

The electrical conductivity was determined for all of the samples, with the exception of the untreated and thermostabilised lignin. Because the conductivity of carbon powders varies with their density (Sánchez-González *et al.* 2005), measurements were taken at different pressures applied to the powders. The change in the conductivity as a result of increasing pressure was determined for the carbons derived from the four technical lignins using the carbons treated at 2000 °C (Fig. 9). All of the characterised specimens showed a roughly linear increase in the conductivity with an increasing pressure. Notably, the densities of the carbon powders were different, with the soda lignin-derived particles showing the highest density and organosolv-derived powder showing the lowest density. The high density of the soda-derived powder correlated with the morphology and pore-free characteristic of the particles (Fig. 6).

The values measured at a fixed pressure of 807 kPa were used for comparing the different lignin variants at all of the carbonisation target temperatures (Fig. 10). The lignosulfonate-derived carbon powder stood out with an electrical conductivity 10 times lower than that of the other carbon powders (Fig. 10). While all of the other carbon types showed a measurable, albeit moderate, electric conductivity at the first carbonisation target temperature of 800 °C, lignosulfonate carbon only appeared to be electrically conductive when prepared at 1600 °C and higher. Even then, a comparably lower level of conductivity was measured. This result was in good agreement with the carbonisation experiments done with spray-dried lignosulfonate liquor, where it was shown that a low degree of graphitic structure in this type of lignin-derived carbon correlated with the comparably low electrical conductivity (Köhnke *et al.* 2018). The hypothesis was put forward that due to the specific chemistry of lignosulfonate, substantial amounts of SO_2 are released during carbonization, which severely degrade the lignin structure, preventing formation of polycyclic moieties required for the build-up of graphitic structures.

The three other lignin-derived carbon powders showed comparable electrical conductivity values. With a characteristic conductivity in the order of 500 $\Omega^{-1}mm^{-1}$, the lignin-derived carbons produced in the present study showed clearly inferior performances to those of industrially produced carbon black, with conductivities in the order of 40 x 10^3 $\Omega^{-1}mm^{-1}$ and up to 250 x 10^3 $\Omega^{-1}mm^{-1}$ measured with a comparable set-up (Sánchez-González *et al.* 2005).

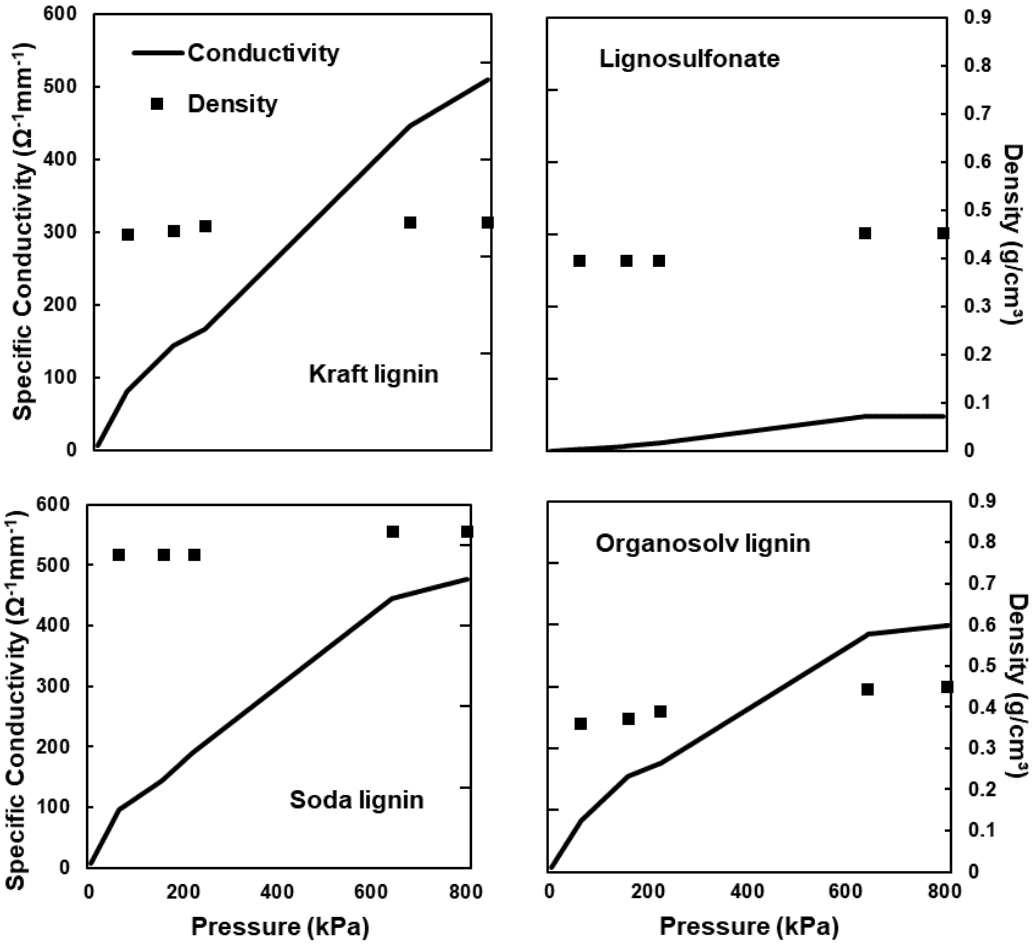

Fig. 9. Electrical conductivity of the four different lignins carbonised at 2000 °C with different pressures, as well as the parallel evolution of density: (a) kraft lignin; (b) lignosulfonate; (c) soda lignin; and (d) organosolv lignin

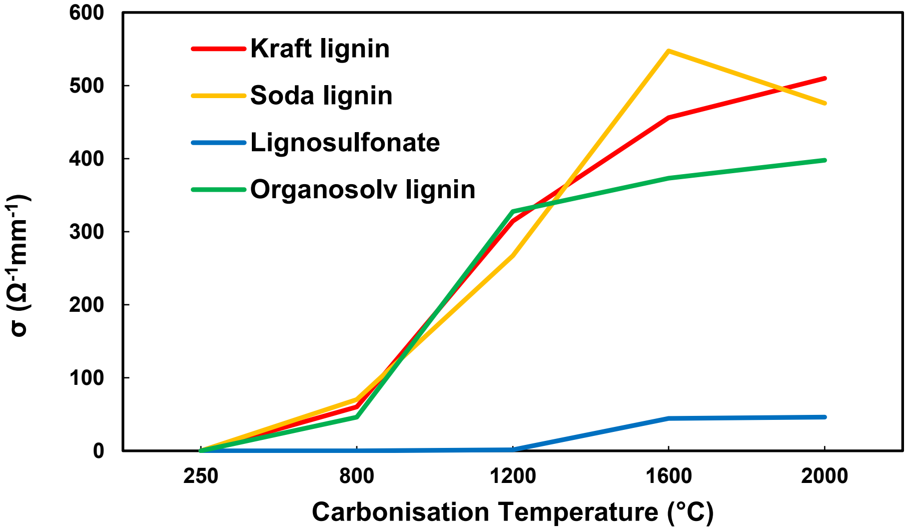

Fig. 10. Electrical conductivity of the four different lignins with different carbonisation temperatures and a pressure of 807 kPa

Having established that carbon powders derived from lignin showed electrical conductivity in principle, their suitability as functional fillers in a polymeric matrix was evaluated using PCL composites. Because of the comparably poor electrical conductivity, remarkable amounts (greater than 20% mass) of carbon needed to be added to the polymer to achieve electrical conductivity (Li *et al.* 2000; Gindl-Altmutter *et al.* 2015; Köhnke *et al.* 2016). Therefore, the PCL films were produced with a 30% carbon content for all of the lignin powders carbonised at 2000 °C, which were the carbon variants that showed the best conductivity (Fig. 10). Polycaprolactone was chosen as the matrix polymer because of its easy handling, biodegradability, and wide range of applications, such as in the biomedical and packaging industries (Woodruff and Hutmacher 2010). Polycaprolactone is a comparably soft and highly extensible polymer, which was confirmed by means of tensile testing (Table 2). As was expected based on the effect of particulate fillers in polymers in general (Fu *et al.* 2008), the addition of the particulate carbon filler resulted in a reduced strength and elongation at break, as well as an increase in the initial modulus of elasticity in most cases (Table 2).

Table 2. Properties of a Pure Polycaprolactone (PCL) Film Compared to the Properties of PCL Filled with 30% Carbon Content

	Modulus of Elasticity (MPa)	Tensile Strength (MPa)	Strain at Failure (%)
Kraft lignin	347 ± 32	6.59 ± 0.12	9.83 ± 2.27
Soda lignin	382 ± 19	9.09 ± 0.08	2.88 ± 0.18
Lignosulfonate	598 ± 73	12.06 ± 0.69	3.22 ± 0.16
Organosolv lignin	604 ± 58	11.75 ± 1.19	16.86 ± 2.68
Polycaprolactone without filler	354 ± 20	28.16 ± 3.64	696.61 ± 74.75

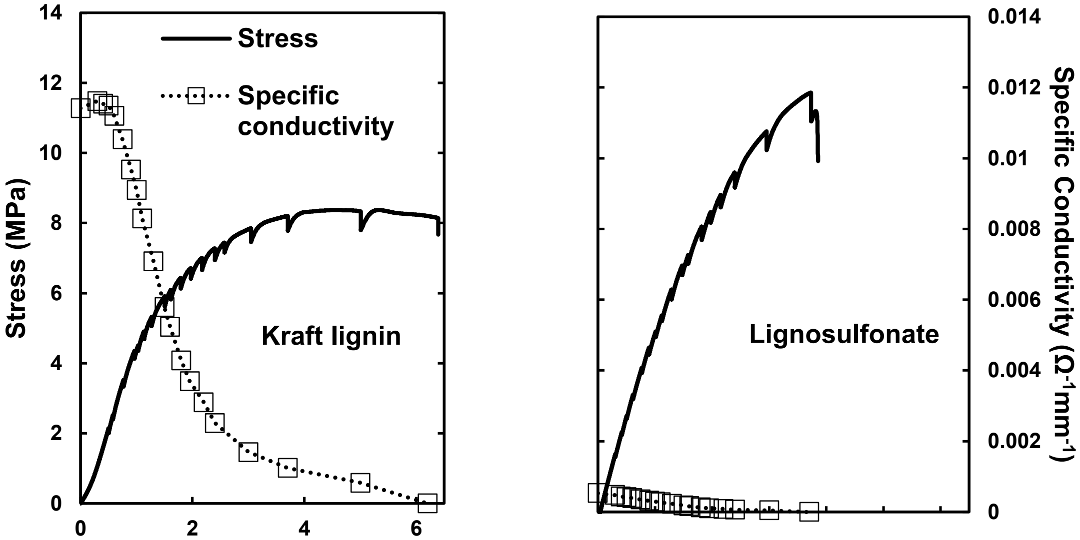

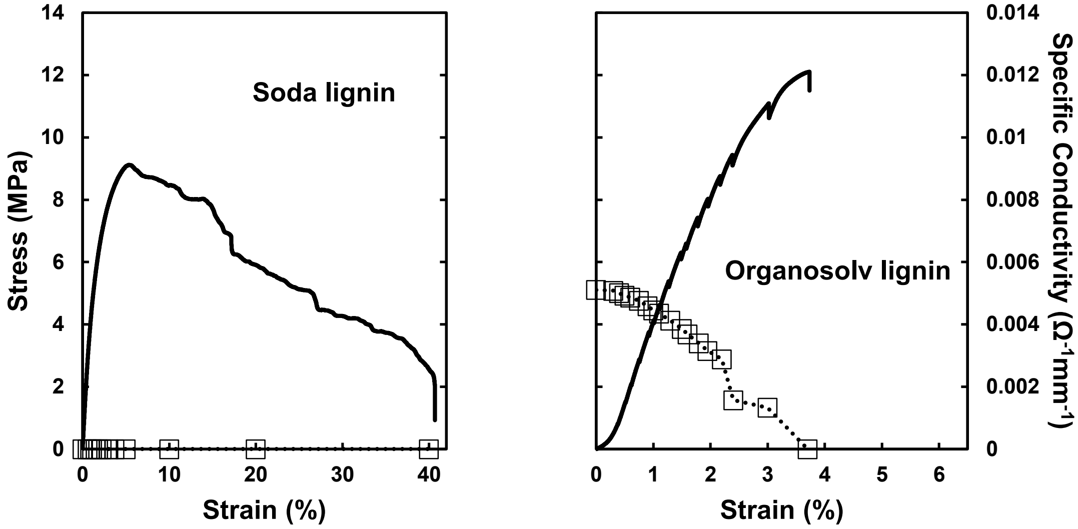

Fig. 11. Stress and specific conductivity of the PCL-carbon composite during the step-wise tensile testing: (a) kraft lignin; (b) lignosulfonate; (c) soda lignin; and (d) organosolv lignin

The PCL-carbon composite films filled with 30% carbon showed remarkably different electrical conductivity values (Fig. 11). First, the poor conductivity of the lignosulfonate-based variant correlated well with the poor conductivity of the lignosulfonate-derived carbon powder (Fig. 10). Considering the conductivity values measured for the carbon powders, the absence of conductivity in the films filled with the soda lignin-derived carbon was surprising. However, it had to be considered that to achieve a strong conductivity, a particulate filler must be both conductive and able to dispose of a high specific volume to enable the formation of a percolating filler network within a polymeric matrix. Because soda lignin-derived carbon was of a considerably higher density compared with all of the other variants (Fig. 9), it was concluded that the soda lignin-derived carbon lacked the volume filling required to achieve percolation at the given mass-based filling ratio. For the remaining variants derived from kraft and organosolv lignin, appreciable electric conductivity values were achieved. Upon stretching the carbon-filled polymer films, the conductivity decreased because the stiffer carbon particles experienced less strain than the surrounding polymer matrix, which resulted in less particle-to-particle contact and reduced the conductivity with an inceasing tensile strain on the composite (Celzard *et al.* 2002; Chung 2004).

CONCLUSIONS

1. The characterisations of the properties and structures of the carbons produced by carbonisation of four different lignin samples indicated that the properties and structure depended on the lignin type and carbonisation temperature.
2. In all of the carbon powders, the graphitic structures were highly disordered. The lignosulfonate-derived carbon in particular showed a poor performance in terms of the electrical conductivity.

3. The kraft lignin- and organosolv lignin-derived carbons were shown to be suitable in principle for application as functional fillers in polymers, even exhibiting strain sensing capability.

ACKNOWLEDGMENTS

The authors are grateful for the funding from the Austrian Science Promotion Agency (FFG) (Bridge Project 846543). Part of this work was carried out within the project BioCarb-K, co-financed by the European Regional Development Fund (EFRE) and the province of Upper Austria through the programme IWB 2014-2020.

REFERENCES CITED

Ago, M., Borghei, M., Haataja, J. S., and Rojas, O. J. (2016). "Mesoporous carbon soft-templated from lignin nanofiber networks: Microphase separation boosts supercapacitance in conductive electrodes," *RSC Adv.* 6(89), 85802-85810. DOI: 10.1039/C6RA17536H

Areskogh, D., Li, J., Gellerstedt, G., and Henriksson, G. (2010). "Investigation of the molecular weight increase of commercial lignosulfonates by laccase catalysis," *Biomacromolecules* 11(4), 904-910. DOI: 10.1021/bm901258v

Balberg, I. (2002). "A comprehensive picture of the electrical phenomena in carbon black-polymer composites," *Carbon* 40(2), 139-143. DOI: 10.1016/S0008-6223(01)00164-6

Betancur, M., Bonelli, P. R., Velásquez, J. A., and Cukierman, A. L. (2009). "Potentiality of lignin from the kraft pulping process for removal of trace nickel from wastewater: Effect of demineralisation," *Bioresource Technol.* 100(3), 1130-1137. DOI: 10.1016/j.biortech.2008.08.023

Boerjan, W., Ralph, J., and Baucher, M. (2003). "Lignin biosynthesis," *Annu. Rev. Plant Biol.* 54, 519-546. DOI: 10.1146/annurev.arplant.54.031902.134938

Bourrat, X. (1993). "Electrically conductive grades of carbon black: Structure and properties," *Carbon* 31(2), 287-302. DOI: 10.1016/0008-6223(93)90034-8

Braun, J. L., Holtman, K. M., and Kadla, J. F. (2005). "Lignin-based carbon fibers: Oxidative thermostabilization of kraft lignin," *Carbon* 43(2), 385-394. DOI: 10.1016/j.carbon.2004.09.027

Bruijnincx, P. C. A., Rinaldi, R., and Weckhuysen, B. M. (2015). "Unlocking the potential of a sleeping giant: Lignins as sustainable raw materials for renewable fuels, chemicals and materials," *Green Chem.* 17(11), 4860-4861. DOI: 10.1039/C5GC90055G

Castellino, M., Rovere, M., Shahzad, M. I., and Tagliaferro, A. (2016) “Conductivity in carbon nanotube polymer composites: A comparison between model and experiment.” *Compos. Part A* 87, 237-242. DOI: 10.1016/j.compositesa.2016.05.002

Celzard, A., Marêché, J. F., Payot, F., and Furdin, G. (2002). "Electrical conductivity of carbonaceous powders," *Carbon* 40(15), 2801-2815. DOI: 10.1016/S0008-6223(02)00196-3

Çetin, N. S., and Özmen, N. (2002). "Use of organosolv lignin in phenol–formaldehyde resins for particleboard production: I. Organosolv lignin modified resins," *Int. J. Adhes. Adhes.* 22(6), 477-480. DOI: 10.1016/S0143-7496(02)00058-1

Chakar, F. S., and Ragauskas, A. J. (2004). "Review of current and future softwood kraft lignin process chemistry," *Ind. Crop. Prod.* 20(2), 131-141. DOI: 10.1016/j.indcrop.2004.04.016

Chatterjee, S., Saito, T., Rios, O., and Johs, A. (2014). "Lignin based carbon materials for energy storage applications," in: *Green Technologies for the Environment*, American Chemical Society, Washington, DC, pp. 203-218.

Chung, D. D. L. (2004). "Electrical applications of carbon materials," *J. Mater. Sci.* 39(8), 2645-2661. DOI: 10.1023/B:JMSC.0000021439.18202.ea

Das, T. K., and Prusty, S. (2012). "Review on conducting polymers and their applications." *Polym. Plastics Technol. Eng.* 51, 1487-1500. DOI: 10.1080/03602559.2012.710697

Doherty, W. O. S., Mousavioun, P., and Fellows, C. M. (2011). "Value-adding to cellulosic ethanol: Lignin polymers," *Ind. Crop. Prod.* 33(2), 259-276. DOI: 10.1016/j.indcrop.2010.10.022

Dresselhaus, M. S., Jorio, A., Hofmann, M., Dresselhaus, G., and Saito, R. (2010). "Perspectives on carbon nanotubes and graphene Raman spectroscopy," *Nano Lett.* 10(3), 751-758. DOI: 10.1021/nl904286r

Duval, A., and Lawoko, M. (2014). "A review on lignin-based polymeric, micro- and nano-structured materials," *React. Funct. Polym.* 85, 78-96. DOI: 10.1016/j.reactfunctpolym.2014.09.017

Foston, M., Nunnery, G. A., Meng, X., Sun, Q., Baker, F. S., and Ragauskas, A. (2013). "NMR a critical tool to study the production of carbon fiber from lignin," *Carbon* 52, 65-73. DOI: 10.1016/j.carbon.2012.09.006

Fu, S.-Y., Feng, X.-Q., Lauke, B., and Mai, Y.-W. (2008). "Effects of particle size, particle/matrix interface adhesion and particle loading on mechanical properties of particulate–polymer composites," *Compos. Part B-Eng.* 39(6), 933-961. DOI: 10.1016/j.compositesb.2008.01.002

García, A., Toledano, A., Serrano, L., Egüés, I., González, M., Marín, F., and Labidi, J. (2009). "Characterization of lignins obtained by selective precipitation," *Sep. Purif. Technol.* 68(2), 193-198. DOI: 10.1016/j.seppur.2009.05.001

Gindl-Altmutter, W., Fürst, C., Mahendran, A., Obersriebnig, M., Emsenhuber, G., Kluge, M., Veigel, S., Keckes, J., and Liebner, F. (2015). "Electrically conductive kraft lignin-based carbon filler for polymers," *Carbon* 89, 161-168. DOI: 10.1016/j.carbon.2015.03.042

Gonugunta, P., Vivekanandhan, S., Mohanty, A. K., and Misra, M. (2012). "A study on synthesis and characterization of biobased carbon nanoparticles from lignin," *World Journal of Nano Science and Engineering* 2(3), 148-153. DOI: 10.4236/wjnse.2012.23019

González-García, S., Moreira, M. T., Artal, G., Maldonado, L., and Feijoo, G. (2010). "Environmental impact assessment of non-wood based pulp production by soda-anthraquinone pulping process," *J. Clean. Prod.* 18(2), 137-145. DOI: 10.1016/j.jclepro.2009.10.008

Gosselink, R. J. A., de Jong, E., Guran, B., and Abächerli, A. (2004). "Co-ordination network for lignin—Standardisation, production and applications adapted to market requirements (EUROLIGNIN)," *Ind. Crop. Prod.* 20(2), 121-129. DOI: 10.1016/j.indcrop.2004.04.015

Hayashi, J., Kazehaya, A., Muroyama, K., and Watkinson, A. P. (2000). "Preparation of activated carbon from lignin by chemical activation," *Carbon* 38(13), 1873-1878. DOI: 10.1016/S0008-6223(00)00027-0

Huang, J.-C. (2002). "Carbon black filled conducting polymers and polymer blends," *Adv. Polym. Tech.* 21(4), 299-313. DOI: 10.1002/adv.10025

Jin, J., Lin, Y., Song, M., Gui, C., and S. Leesirisan (2013). “Enhancing the electrical conductivity of polymer composites,” *Eur. Polym. J.* 49(5), 1066-1072. DOI: 10.1016/j.eurpolymj.2013.01.014

Kadla, J. F., Kubo, S., Venditti, R. A., Gilbert, R. D., Compere, A. L., and Griffith, W. (2002). "Lignin-based carbon fibers for composite fiber applications," *Carbon* 40(15), 2913-2920. DOI: 10.1016/S0008-6223(02)00248-8

Kai, D., Tan, M. J., Chee, P. L., Chua, Y. K., Yap, Y. L., and Loh, X. J. (2016). "Towards lignin-based functional materials in a sustainable world," *Green Chem.* 18(5), 1175-1200. DOI: 10.1039/C5GC02616D

Köhnke, J., Fürst, C., Unterweger, C., Rennhofer, H., Lichtenegger, H. C., Keckes, J., Emsenhuber, G., Mahendran, A., Liebner, F., and Gindl-Altmutter, W. (2016). "Carbon microparticles from organosolv lignin as filler for conducting poly(lactic acid)," *Polymers* 8(6), 205-217. DOI: 10.3390/polym8060205

Köhnke, J., Rennhofer, H., Lichtenegger, H., Mahendran, A., Unterweger, C., Prats-Mateu, B., Gierlinger, N., Schwaiger, E., Mahler, A.-K., Potthast, A., *et al*. (2018). "Electrically conducting carbon microparticles by direct carbonization of spent wood pulping liquor," *ACS Sustain. Chem. Eng.* 6(3), 3385-3391. DOI: 10.1021/acssuschemeng.7b03582

Laurichesse, S., and Avérous, L. (2014). "Chemical modification of lignins: Towards biobased polymers," *Prog. Polym. Sci.* 39(7), 1266-1290. DOI: 10.1016/j.progpolymsci.2013.11.004

Li, F., Qi, L., Yang, J., Xu, M., Luo, X., and Ma, D. (2000). "Polyurethane/conducting carbon black composites: Structure, electric conductivity, strain recovery behavior, and their relationships," *J. Appl. Polym. Sci.* 75(1), 68-77. DOI: 10.1002/(SICI)1097-4628(20000103)75:1<68::AID-APP8>3.0.CO;2-I

Liu, W.-J., Jiang, H., and Yu, H.-Q. (2015). "Thermochemical conversion of lignin to functional materials: A review and future directions," *Green Chem.* 17(11), 4888-4907. DOI: 10.1039/C5GC01054C

Mansouri, N.-E. E., and Salvadó, J. (2006). "Structural characterization of technical lignins for the production of adhesives: Application to lignosulfonate, kraft, soda-anthraquinone, organosolv and ethanol process lignins," *Ind. Crop. Prod.* 24(1), 8-16. DOI: 10.1016/j.indcrop.2005.10.002

Norberg, I., Nordström, Y., Drougge, R., Gellerstedt, G., and Sjöholm, E. (2013). "A new method for stabilizing softwood kraft lignin fibers for carbon fiber production," *J. Appl. Polym. Sci.* 128(6), 3824-3830. DOI: 10.1002/app.38588

Pan, X., Arato, C., Gilkes, N., Gregg, D., Mabee, W., Pye, K., Xiao, Z., Zhang, X., and Saddler, J. (2005). "Biorefining of softwoods using ethanol organosolv pulping: Preliminary evaluation of process streams for manufacture of fuel-grade ethanol and co-products," *Biotechnol. Bioeng.* 90(4), 473-481. DOI: 10.1002/bit.20453

Rodríguez, A., Sánchez, R., Requejo, A., and Ferrer, A. (2010). "Feasibility of rice straw as a raw material for the production of soda cellulose pulp," *J. Clean. Prod.* 18(10-11), 1084-1091. DOI: 10.1016/j.jclepro.2010.03.011

Ruiz-Rosas, R., Bedia, J., Lallave, M., Loscertales, I. G., Barrero, A., Rodríguez-Mirasol, J., and Cordero, T. (2010). "The production of submicron diameter carbon fibers by the electrospinning of lignin," *Carbon* 48(3), 696-705. DOI: 10.1016/j.carbon.2009.10.014

Sadezky, A., Muckenhuber, H., Grothe, H., Niessner, R., and Pöschl, U. (2005). "Raman microspectroscopy of soot and related carbonaceous materials: Spectral analysis and structural information," *Carbon* 43(8), 1731-1742. DOI: 10.1016/j.carbon.2005.02.018

Sánchez-González, J., Macías-García, A., Alexandre-Franco, M. F., and Gómez-Serrano, V. (2005). "Electrical conductivity of carbon blacks under compression," *Carbon* 43(4), 741-747. DOI: 10.1016/j.carbon.2004.10.045

Shulga, G., Rekner, F., and Varslavan, J. (2001). "SW—Soil and water: Lignin-based interpolymer complexes as a novel adhesive for protection against erosion of sandy soil," *J. Agr. Eng. Res.* 78(3), 309-316. DOI: 10.1006/jaer.2000.0599

Sixta, H. (2006). *Handbook of Pulp*, Wiley-VCH Verlag GmbH, Weinheim, Germany.

Snowdon, M. R., Mohanty, A. K., and Misra, M. (2014). "A study of carbonized lignin as an alternative to carbon black," *ACS Sustain. Chem. Eng.* 2(5), 1257-1263. DOI: 10.1021/sc500086v

Song, K., Ganguly, I., Eastin, I., and Dichiara, A. B. (2017). "Lignin-modified carbon nanotube/graphene hybrid coating as efficient flame retardant," *Int. J. Mol. Sci.* 18(11), 2368-2381. DOI: 10.3390/ijms18112368

Suhas, Carrott, P. J. M., and Carrott, M. M. L. R. (2007). "Lignin—From natural adsorbent to activated carbon: A review," *Bioresource Technol.* 98(12), 2301-2312. DOI: 10.1016/j.biortech.2006.08.008

Tejado, A., Peña, C., Labidi, J., Echeverria, J. M., and Mondragon, I. (2007). "Physico-chemical characterization of lignins from different sources for use in phenol-formaldehyde resin synthesis," *Bioresource Technol.* 98(8), 1655-1663. DOI: 10.1016/j.biortech.2006.05.042

Thakur, V. K., Thakur, M. K., Raghavan, P., and Kessler, M. R. (2014). "Progress in green polymer composites from lignin for multifunctional applications: A review," *ACS Sustain. Chem. Eng.* 2(5), 1072-1092. DOI: 10.1021/sc500087z

Tuinstra, F., and Koenig, J. L. (1970). "Raman spectrum of graphite," *J. Chem. Phys.* 53(3), 1126-1130. DOI: 10.1063/1.1674108

Vainio, U., Maximova, N., Hortling, B., Laine, J., Stenius, P., Simola, L. K., Gravitis, J., and Serimaa, R. (2004). "Morphology of dry lignins and size and shape of dissolved kraft lignin particles by X-ray scattering," *Langmuir* 20(22), 9736-9744. DOI: 10.1021/la048407v

Wang, M., Leitch, M., and Xu, C. (2009). "Synthesis of phenol-formaldehyde resol resins using organosolv pine lignins," *Eur. Polym. J.* 45(12), 3380-3388. DOI: 10.1016/j.eurpolymj.2009.10.003

Woodruff, M. A., and Hutmacher, D. W. (2010). "The return of a forgotten polymer—Polycaprolactone in the 21st century," *Prog. Polym. Sci.* 35(10), 1217-1256. DOI: 10.1016/j.progpolymsci.2010.04.002

Xu, C., Arancon, R. A. D., Labidi, J., and Luque, R. (2014). "Lignin depolymerisation strategies: Towards valuable chemicals and fuels," *Chem. Soc. Rev.* 43(22), 7485-7500. DOI: 10.1039/C4CS00235K

Yang, D., Qiu, X., Zhou, M., and Lou, H. (2007). "Properties of sodium lignosulfonate as dispersant of coal water slurry," *Energ. Convers. Manage.* 48(9), 2433-2438. DOI: 10.1016/j.enconman.2007.04.007

Yi, X., He, W., Zhang, X., Yue, Y., Yang, G., Wang, Z., Zhou, M., and Wang, L. (2017). "Graphene-like carbon sheet/Fe_3O_4 nanocomposites derived from soda papermaking black liquor for high performance lithium ion batteries," *Electrochim. Acta* 232, 550-560. DOI: 10.1016/j.electacta.2017.02.130

Article submitted: June 7, 2018; Peer review completed: July 30, 2018; Revisions accepted: December 12, 2018; Published: December 13, 2018.
DOI: 10.15376/biores.14.1.1091-1109

II

Köhnke, J., Fürst, C., Unterweger, C., Rennhofer, H., Lichtenegger, H.C., Keckes, J., Emsenhuber, G., Mahendran, A.R., Liebner, F. and Gindl-Altmutter, W. (2019) "**Carbon Microparticles from Organosolv Lignin as Filler for Conducting Poly(Lactic Acid)**" *Polymers* 8, 205. DOI: 10.3390/polym8060205

polymers

MDPI

Article

Carbon Microparticles from Organosolv Lignin as Filler for Conducting Poly(Lactic Acid)

Janea Köhnke [1,*], Christian Fürst [2], Christoph Unterweger [2], Harald Rennhofer [3], Helga C. Lichtenegger [3], Jozef Keckes [4], Gerhard Emsenhuber [1], Arunjunai raj Mahendran [2], Falk Liebner [1] and Wolfgang Gindl-Altmutter [1]

[1] BOKU-University of Natural Resources and Life Science Vienna, Konrad Lorenz Strasse 24, A-3430 Tulln, Austria; gerhard.emsenhuber@boku.ac.at (G.E.); falk.liebner@boku.ac.at (F.L.); wolfgang.gindl-altmutter@boku.ac.at (W.G.-A.)

[2] Kompetenzzentrum Holz GmbH, Altenbergerstrasse 89, A-4020 Linz, Austria; c.fuerst@kplus-wood.at (C.F.); c.untergweger@kplus-wood.at (C.U.); a.mahendran@kplus-wood.at (A.R.M.)

[3] BOKU-University of Natural Resources and Life Science Vienna, Peter Jordan Strasse 82, A-1190 Vienna, Austria; harald.rennhofer@boku.ac.at (H.R.); helga.lichtenegger@boku.ac.at (H.C.L.)

[4] Department Materials Physics, University of Leoben, Jahnstrasse 12, A-8700 Leoben, Austria; jozef.keckes@unileoben.ac.at

* Correspondence: janea.koehnke@boku.ac.at; Tel.: +43-1-47654-89181

Academic Editors: Hyeonseok Yoon and Changsik Song
Received: 4 April 2016; Accepted: 20 May 2016; Published: 26 May 2016

Abstract: Carbon microparticles were produced from organosolv lignin at 2000 °C under argon atmosphere following oxidative thermostabilisation at 250 °C. Scanning electron microscopy, X-ray diffraction, small-angle X-ray scattering, and electro-conductivity measurements revealed that the obtained particles were electrically conductive and were composed of large graphitic domains. Poly(lactic acid) filled with various amounts of lignin-derived microparticles showed higher tensile stiffness increasing with particle load, whereas strength and extensibility decreased. Electric conductivity was measured at filler loads equal to and greater than 25% *w*/*w*.

Keywords: lignin; carbon; carbonisation; electric conductivity; SAXS; filled polymers; tensile testing

1. Introduction

Lignin is the second most abundant natural polymer. It is an amorphous, thermoplastic, three-dimensional, cross-linked and aromatic component of the cell wall, that consists of substituted phenylpropane units, whose pattern largely depends on the plant species. Formed by random radical dehydropolymerisation of the three main aromatic precursor compounds coumaryl, coniferyl and sinapyl alcohol, lignin has a great diversity of bonds and functional groups [1]. ß-O-4 bonds can account for up to 70 percent of all linkages between lignols, but other bond types play a crucial role with regard to lignin properties as well, such as ether and C–C bonds as found in ß-5 and 5-5′ structural units. This applies for the functional groups of lignin as well which comprise in particular methoxyl, carbonyl, carboxyl and hydroxyl groups [2].

Lignin is an essential component of lignocellulosic plant tissues where it acts as a connecting, stiffening matrix between cells, increases compression resistance, imparts hydrophobicity to the cell wall, and provides protection against microorganisms [3]. Lignocellulosic materials such as wood contain between about 15 and 40 percent lignin, which can be extracted to a large extent during wood pulping. Taking into consideration global pulp production, about 70 million tons of lignin are produced as a side product every year, dominated by kraft lignin, soda lignin and the various types of lignosulfonates [4]. Whilst the majority of lignin is still used as fuel despite its comparatively low heating value, only 1.7 percent of this valuable natural resource finds application in materials.

Recent studies have confirmed renewed interest in using lignin as feedstock for the production of materials such as dispersants, binders or bulking agents [4]. A particular focus is currently on lignin-derived carbon fibres [5–8], which are hoped to become a low-cost alternative to high-quality carbon fibres derived from polyacrylonitrile. The application envisioned for lignin-derived carbon fibres is in lighter and hence fuel saving transportation devices.

Besides carbon fibre, carbon black has become a material that is of great technological and industrial importance because of its unique mechanical, chemical and electrical properties [9–11]. On the one hand, carbon black may reduce the overall material costs as low-cost filler in polymers, and on the other hand carbon black as filler can significantly improve the overall properties of plastics and elastomers, especially electric conductivity [12,13]. Carbon black is obtained through incomplete combustion or thermal degradation of fossil resources in absence of oxygen. According to the International Carbon Black Association (http://www.carbon-black.org), more than 8 million metric tons of carbon black were produced worldwide in 2014, almost exclusively from fossil resources. Therefore, a viable bio-based alternative to fossil-derived carbon black is of great interest. It is proposed that lignin-derived carbon microparticles may represent such an alternative. In the present study we focus on organosolv lignin as a potential raw material for carbonisation. The organosolv pulping process, which is based on the lignin solubilisation ability of (acidic) aqueous alcohols at elevated temperature and pressure, is considered to have great potential for lignocellulose biorefinery as demonstrated by the pilot scale plant Leuna [14], even though commercial implementation has not happened yet. Numerous studies [15–18] have confirmed that organosolv lignins have superior quality because of their high purity, low molecular weight and narrow size distribution as well as their low sulfur and salt contents. In view of these advantageous properties, the feasibility of producing carbon microparticles from organosolv lignin will be evaluated together with selected properties of this novel material.

2. Materials and Methods

2.1. Materials

Organosolv lignin (Product number CP8068-03-9-BULK) was purchased from Chemical Point UG (Deisenhofen, Germany) (Element contents: C: 61.7%, H: 5.3%, N: 0.9%, S: 0%, O: 28.3%, rest: 3.81%. Chloroform (Purity: ⩾99.5% was obtained from Sigma-Aldrich (Vienna, Austria) and poly(lactic acid) grade 2003D was purchased from Natureworks LLC (Minnetonka Boulevard, Minnetonka, MN, USA).

2.2. Lignin Carbonisation

Prior to carbonisation, lignin was thermostabilised to prevent particles from fusing during pyrolysis and graphitisation. For this purpose, organosolv lignin was evenly distributed in a crucible and heated at a rate of 0.01 min^{-1} to 250 °C in ambient atmosphere using a drying oven. Carbonisation was conducted in a GERO HTK8 oven (volume 6 L) using an argon gas flow of 150 $\text{L}\cdot\text{h}^{-1}$. The oven was set to a heating rate of 1 $°\text{C}\cdot\text{min}^{-1}$ up to 500 °C (1 h holding step), 5 $°\text{C}\cdot\text{min}^{-1}$ up to 900 °C (1 h holding step) and finally 5 $°\text{C}\cdot\text{min}^{-1}$ up to 2000 °C (1 h holding step).

2.3. Characterisation of Lignin and Carbon Particles

For scanning electron microscopy (SEM) and energy dispersive X-ray analysis (EDX) the samples were placed on a carbon conductive double coated tab and sputter-coated with a thin film of gold. Microscopy was conducted in a QuantaTM 250 field-emission environmental scanning electron microscope (FEI Europe B.V., Vienna, Austria) with a Shottky field emission gun operating at 10 kV in high vacuum of 1×10^{-6} mbar. Differential scanning calorimetry (DSC) data of both, untreated and thermostabilised, lignins were obtained with a DSC 200F3 Maia device (NETZSCH, Graz, Austria) and a heating rate of 10 $\text{K}\cdot\text{min}^{-1}$. Termogravimetric analyses were carried out using a TA Instruments TGA Q5000 (Waters GmbH, UB TA Instruments, Eschborn, Germany) with a heating rate of 20 $\text{K}\cdot\text{min}^{-1}$.

Attenuated diffuse reflection Fourier transform infrared spectroscopy (ATR-FTIR) was performed on a Helios spectrometer (Ultrafast Systems BV, Amsterdam, The Netherlands) equipped with a Tensor 27 and a diamond crystal. Spectral resolution was 4 cm^{-1}. The spectra were baseline corrected. Specific electrical resistivity was measured as described in Sánchez-González *et al.* [19]. X-ray diffraction (XRD) of the samples was performed using a 5-circle X ray diffractometer (SmartLab from Rigaku Co., Ettlingen, Germany) equipped with Cu $K\alpha$ radiation, a parabolic multilayer mirror in the primary beam and a secondary graphite monochromator. The samples were measured using a 2θ step of 0.02 degrees and 4 s dwell time.

Small angle X-ray scattering (SAXS) was used to obtain information about the nanostructure of the samples. Measurements were carried out with a three pinhole SMAX-3000 SAXS camera (Rigaku Co, Ettlingen, Germany) equipped with a copper target micro focus X-ray tube (MM002+ source with a wavelength of λ = 0.1541 nm). Two dimensional scattering images were recorded with a TRITON 200 multi-wire X-ray detector. The scattering images were averaged azimuthally to gain information on the scattered intensity I(q) in dependence on the scattering vector q, which is related to the scattering angle 2θ and the wavelength λ by the Bragg-equation:

$$q = \frac{4\pi}{\lambda} \times \sin\theta$$

The obtained data were background corrected and analysed with respect to the pore structure.

At high q values the scattering intensity follows the Porod law:

$$\mathrm{I}\,(q) = Pq^{-n}$$

The exponent n is usually close to 4 for smooth surfaces and P the Porod constant is proportional to the pore surface. The scattering invariant Q is defined by

$$Q = \int_0^\infty q^2 I\,(q)\,dq$$

and is a measure of the total scattering of the sample, related to the volumes of pores and matrix material. The ratio P/Q is proportional to the specific inner surface $S^* = S/V$ of the sample with a proportionality factor given by the fractions of pores Φ_1 and the matrix material Φ_2, with $\Phi_1 = 1 - \Phi_2$:

$$\frac{P}{Q} = \frac{1}{\pi\Phi_1\Phi_2} S^*$$

The Guinier approximation was used at low q to evaluate a pore radius of spherical pores R from the radius of gyration R_g, by $R^2 = 5/3\ R_g^2$ with:

$$I\,(q) \sim I_0 e^{-q^2 R_g^2/3}$$

2.4. Preparation and Characterisation of Poly(Lactic Acid) Composites Containing Different Amounts of Lignin-Derived Carbon Microparticles

Poly(lactic acid) (PLA) was dissolved in chloroform to give a concentration of 100 $\text{g}\cdot\text{L}^{-1}$. Defined amounts of lignin derived carbon microparticles (0–35 wt % related to the mass of composite) were then dispersed under stirring (ultra-turrax) in 100 mL aliquots of the PLA solution. After transferring the dispersions into petri dishes, the solvent was allowed to evaporate, slowed down by filter paper put on top of the petri dishes to obtain smooth polymer films. After about 16 hours the formed films were removed from the petri dishes, folded right in the middle obtaining a double-layer of film and hot pressed at 150 °C. This procedure was repeated three-times in order to improve particle dispersion in the polymer. A final film thickness of 0.5 mm was obtained. Strips (6 mm × 60 mm) were cut and tested for tensile strength on a Zwick Roell 20 kN testing machine (Zwick GmbH & Co. KG, Ulm, Germany) equipped with a 2.5 kN load cell. Electrical resistivity of the composite films was determined according to EN ISO 3915 using the same type of strips.

3. Results and Discussion

3.1. Scanning Electron Microscopy (SEM)

Morphological investigation of the prepared lignin-derived carbon microparticles using SEM revealed a largely irregular shape and broad size distribution for all of the three types of particles studied, *i.e.*, untreated lignin, thermostabilised lignin, and carbonised lignin (Figure 1). However, it can be seen that the particle size distribution is significantly affected by both thermostabilisation and carbonisation, as smaller particles are obtained with increasing mass loss by thermal degradation.

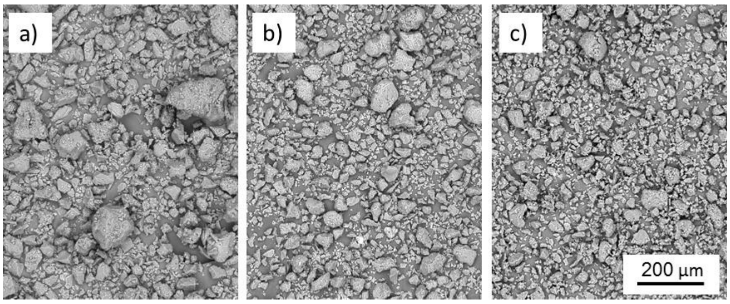

Figure 1. SEM micrographs of organosolv particles prior to (**a**) and after thermostabilisation (**b**) and carbonisation, respectively (**c**).

The average particle size of the native lignin was 9.1 ± 10.3 µm, dropping to 7.0 ± 7.5 µm for the stabilised particles. The smallest average particle size was obtained for the carbonised particles (5.3 ± 6.4 µm). Box and whisker plots visualize skewed sized distributions for all types of particles in favor of smaller particles (Figure 2). A few large outliers with dimensions above 14 µm are not shown in Figure 2, and their occurrence diminishes with every treatment step.

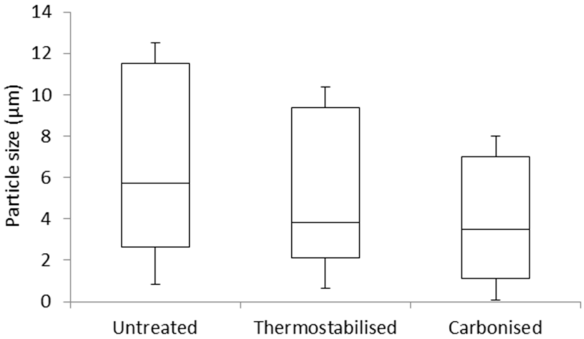

Figure 2. Particle size distribution of untreated, thermostabilised and carbonised organosolv lignin particles (outliers are not displayed; the box and whisker diagram is based on the minimum (lower whisker), the first quartile (bottom edge), the median (centre line), the third quartile (upper edge) and the maximum (upper whisker)).

Thermostabilisation (oxidative environment, $T \leqslant 250\ ^\circ\mathrm{C}$) and carbonisation (inert gas, $T \leqslant 2000\ ^\circ\mathrm{C}$) of organosolv lignin particles were accompanied by significant mass losses that accounted for 58% and 81%, respectively, of the starting material. In view of the only moderate reduction in particle size observed, the substantial mass loss measured points towards increased porosity of the particles after treatment. Compared to the literature, the reduction in particle size and the mass loss observed in the present study is less pronounced than in the case of carbonised lignosulfonate, where an overall carbon yield of only 7.3% was obtained [20].

3.2. Energy-Dispersive X-ray Spectroscopy (EDX)

The EDX results shown in Figure 3 confirm extensive carbonisation of lignin after treatment at 2000 °C, with more than 95% of sample mass converted to carbon. Besides oxygen and a trace of sodium, a small amount of silica was also detected. According to the silicon content of the parent material which was determined with 0.04 at % and the total mass yield of 19% there is a calculated total maximum of 0.2% silicon, which is in the same order of magnitude as EDX results. In good agreement with the fact that silica was detected in the carbonisation product, scanning electron microscopy revealed the presence of needle-shaped crystallites among the formed carbon particles (Figure 3). In these needles, reduced carbon content of 92.18 at % and oxygen and silicon contents of 5.06 at % and 2.37 at %, respectively, were found.

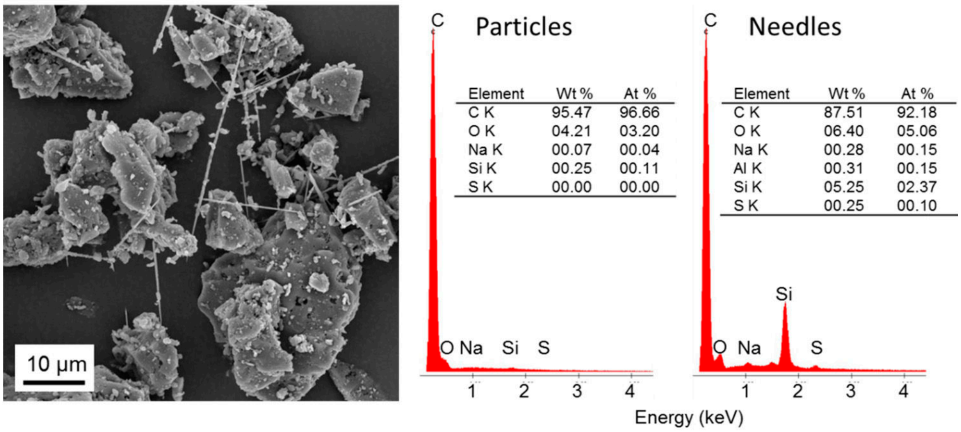

Particles

Element	Wt %	At %
C K	95.47	96.66
O K	04.21	03.20
Na K	00.07	00.04
Si K	00.25	00.11
S K	00.00	00.00

Needles

Element	Wt %	At %
C K	87.51	92.18
O K	06.40	05.06
Na K	00.28	00.15
Al K	00.31	00.15
Si K	05.25	02.37
S K	00.25	00.10

Figure 3. SEM image of carbonised lignin containing small amounts of needle-shape crystals (**left**) and results of EDX analyses (**right**) of both carbon particles and crystals.

It is well known that lignin of annual plants has a high content of silicates [21], so the organosolv lignin might be produced by annual plants such as grass or bamboo. Other studies showed that standard carbon black has a characteristic O/C atomic ratio of ⩽0.1, which is much lower than the measured O/C atomic ratio of our sample [22].

3.3. Attenuated Diffuse Reflection Fourier Transform Infrared Spectroscopy (ATR-FTIR)

The ATR-FTIR spectrum of unmodified organosolv lignin (Figure 4) as recorded in the vibration range of 4000–600 cm^{-1} (16 repetitions) was in good agreement with data published in Hage *et al.* [18]. Peak assignment based on the work of Norberg *et al.*, Sharma *et al.*, Braun *et al.* and Kubo *et al.* [23–26] confirmed the presence of hydroxyl groups due to phenolic or alcoholic components as shown in band (1) in the range of 3100 to 3500 cm^{-1}. Band (2) at wavenumber of 2934 cm^{-1} displays aliphatic and aromatic carbons, and band (3) at wavenumber of 1690 cm^{-1} shows unconjugated groups of carbonyls. Bands (4) and (5) are "the fingerprint region" which means that they are typical for ATR-FTIR spectra of lignin and are associated with the aromatic ring modes at wavenumbers 1596 and 1510 cm^{-1}, respectively. The band (6) at 1459 cm^{-1} represents C–H stretching of the aromatic skeletal, same as band (7) 1421 cm^{-1}. The bands (8), (9), and (11) at the wavenumbers 1328, 1212 and 1122 cm^{-1}, respectively, display syringyl and guaiacyl units. The band (10) at 1168 cm^{-1} represents conjugated esters. Finally, band (12) at 1028 cm^{-1} is due to lignin-linked hemicelluloses and band (13) at wavenumber 832 cm^{-1} is caused by aromatic C–H out of plane bending.

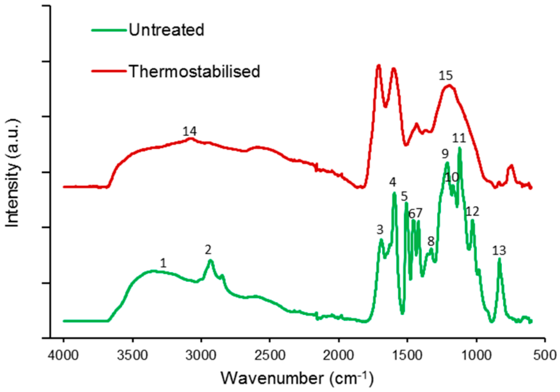

Figure 4. FTIR spectra of organosolv lignin particles before and after thermostabilisation.

After thermostabilisation, the FT-IR spectra lack peaks at bands (1) and (2) indicate a reduction of phenolic or alcoholic groups, and removal and methyl groups, respectively. In parallel, band (14) at wavenumber 3073 cm^{-1}, associated with aromatic hydrocarbon, increases in intensity in the thermostabilised variant. In the fingerprint region, a very significant increase is seen in band (3) associated with the stretch of unconjugated carbonyls, probably an indicator for rearrangement and radical reactions with introducing oxidised structures to the lignin. Furthermore, the number of distinct bands in the spectral region between 1500 and 700 cm^{-1} is much reduced, with a broad peak remaining at position (15) at 1199 cm^{-1}. This change in spectral features shows that carbonyl groups and methoxyl were removed during autoxidation reactions. Furthermore, crosslinking reactions in the C5 position of g-lignin units occur during the thermostabilisation. In summary, it can be said that there occurred dehydration and oxidation as well as carbonyl group formation and elimination during thermostabilisation in parallel to a decomposition of aliphatic units [27–30].

The thermal stabilisation process leads to lower content of oxygen, carbon and hydrogen caused by dehydration reactions, condensation, cross linking, autoxidation and elimination reactions. Byproducts of those reactions are water, carbon monoxide and carbon dioxide which are produced via formation of aromatic, keto, anhydride and ester linkages and formation of C–C and C=C bonds [25,31–34].

3.4. Differential Scanning Calorimetry (DSC) and Thermogravinetric Analysis (TGA)

Differential scanning calorimetry (DSC) and thermogravimetric analysis (TGA) were conducted to examine whether the thermostabilisation was effective in terms of eliminating thermoplasticity of the raw material. The DSC graphs of both untreated and thermostabilised lignin show an exothermal behaviour during heating from ambient temperature up to 300 °C (Figure 5a), which is more pronounced in the thermostabilised lignin compared to the untreated sample. A small but clear local minimum in the DSC curve of the untreated sample at a temperature of 230 °C indicates softening. As this local minimum vanishes entirely after thermostabilisation, this procedure is expected to be efficient in terms of preventing thermal fusing of the lignin during carbonisation.

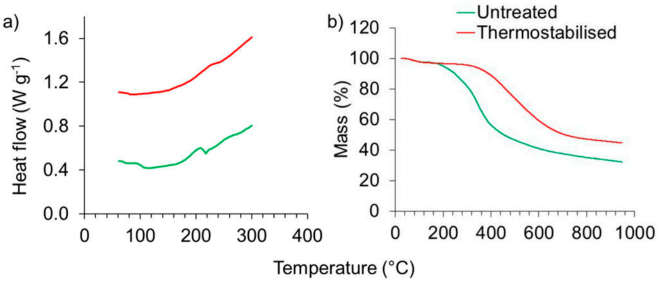

Figure 5. DSC (**a**) and TGA (**b**) curves of organosolv lignin particles prior to and after thermostabilisation.

TGA showed the mass loss, thermal and oxidation stability and the decomposition temperature of the lignin powders during heat treatment under nitrogen atmosphere (Figure 5b). There was an insignificant initial mass loss due to moisture removal [27]. The start of mass loss of the untreated lignin was detected at 170 °C. The thermogravimetry curve of the thermostabilised lignin shifted toward a higher temperature with the start of mass loss at 300 °C, which indicates an increasing thermal stability and longer temperature resistivity, longer stability and a later decomposition. The overall loss pattern was determined with 67% for the untreated lignin sample and in contrast to this the mass loss of the thermostabilised lignin was observed with 58% which approximates a total mass loss of 82% compared to the starting mass. The stagnation of the drop of the thermogravimetry curve shows that the decomposition of lignin terminates due to charring [35]. The results of TGA are in line with what was shown with DSC, the thermostabilisation was successfully conducted.

It should be mentioned here that it is known that the stabilisation process of lignin and the properties of the carbonised products largely depend on the lignin source (e.g., hardwood or softwood) because of important differences in composition and molecular weight distribution [36].

3.5. X-ray Powder Diffraction

Structural alterations of organosolv lignin as a result of thermostabilisation and carbonisation were confirmed by X-ray diffractometry (Figure 6).

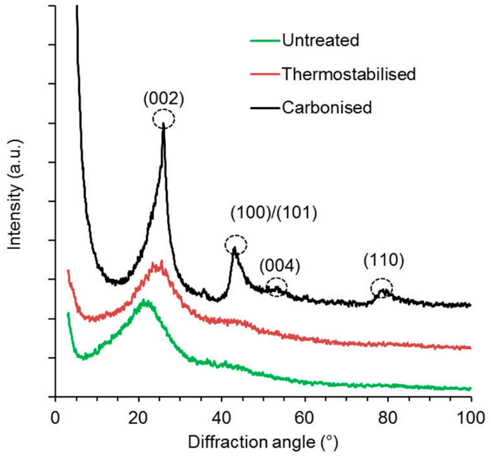

Figure 6. XRD patterns of organosolv lignin microparticles prior to and after thermostabilisation and carbonisation.

The XRD patterns of the untreated and the thermostabilised lignin powder are almost congruent and do not show well-defined peaks, which indicates a non-crystalline powder. After carbonisation, the XRD patterns show four peaks at diffraction angles of 26.7° (002), 43.2° (100)/(101), 54.7° (004) and 78.1° (110) confirming the occurrence of structural changes during carbonisation. Supramolecular rearrangement to partly graphitic structures is evident from sharpening of the (002) and (100)/(101) diffraction peaks and appearing of (004) and (110) peaks [37]. Graphite structures are formed during carbonisation by lignin dehydration, decarbonylation, decarboxylation as well as rearrangement and extension of the network of sp2 hybridised carbon formed by aromatic moieties inherent to lignin [24]. This takes place because the fundamental structure of the lignin is not affected for the most part, only side groups are cleaved and faded. Thus, graphene-like structures are built during carbonisation because of the dissociation of non-carbon atoms [6,38].

3.6. Small Angle X-ray Scattering

Small angle X-ray scattering experiments revealed a very similar morphology for the lignin particles prior to and after oxidative thermo-stabilisation, as evident from the similar decay of the scattering curves with increasing *q* values (Figure 7). Both curves can be fitted using an exponent close to four. The latter and the absence of any special feature suggest the material composed of poorly defined structures that feature very broad size distribution at the nano-scale. The existence of a slightly broader shoulder centered at about q = 0.5 nm^{-1} for the thermo-stabilised sample however is indicative for the development of some nano-porous structures during the oxidative activation step. In contrast, the broad peak of the scattering curve of the carbonised sample at a higher scattering vector ($0.6 \leqslant q \leqslant 4$) unambiguously reveals the formation of a highly nano-porous material of distinct size.

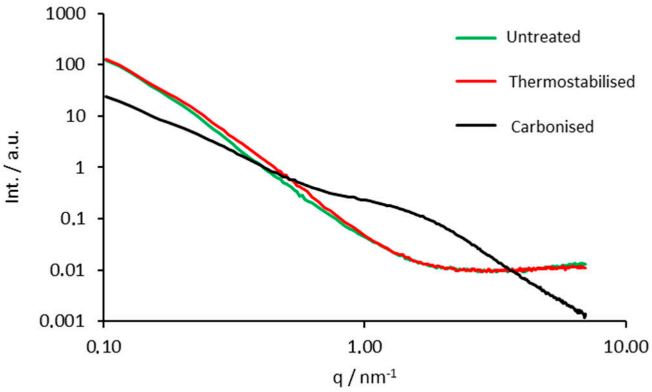

Figure 7. SAXS curves of the untreated, thermostabilised and carbonised organosolv lignin particles.

Application of the Guinier evaluation reveals a mean pore radius of R = (1.06 ± 0.04) nm for the carbonised lignin powder, assuming spherical pores. Also the exponent in the Porod regime is less than four, indicating a higher surface roughness. The P/Q ratio representing the total pore surface (open and closed pores) per volume increases slightly from 97 to 130 $\text{m}^2\cdot\text{cm}^{-3}$ during thermostabilisation but strongly from 130 to 770 $\text{m}^2\cdot\text{cm}^{-3}$ during carbonisation (*cf.* Table 1).

Table 1. Pore radius of the untreated, thermostabilised and carbonised lignin samples. Errors of the respective fit and calculations, respectively, are given in brackets.

Sample Name	n	P/Q ($\text{m}^2\cdot\text{cm}^{-3}$)	R/(nm)
untreated	−3.85(5)	97(20)	-
thermostabilised	−3.87(2)	130(30)	-
carbonised	−3.45(2)	770(50)	1.06(4)

In conclusion, the conducted SAXS experiments confirmed that the parent lignin powder had no defined pore structure at the nanoscale. Thermostabilisation did not alter the nanostructure significantly, only a slight increase of specific surface and indication for a somewhat higher nanoporosity was found (higher scattering intensity at respective q values). After carbonisation the material shows a clear pore structure, corresponding to the appereance of a distinct shoulder in the scattering curve, attributed to a pore size of about 1 nm and an increase of the specific surface by a factor of six (770 $\text{m}^{-2}\cdot\text{cm}^{-3}$), compared to the thermostabilised sample. The decreased exponent of the power law in the Porod regime of the scattering curve can be related to a higher surface roughness of the material.

3.7. Specific Electrical Resistivity

The specific electrical resistivity of the carbonised lignin particles was determined to evaluate their potential application for imparting organic polymers electro-conductivity. It can be seen in Figure 8 that the specific resistivity of carbon particles obtained in this study is in the range of 0.079 Ωm under atmospheric pressure, and 0.001 Ωm at a pressure of 0.51 MPa (Figure 8a). The resistivity diminishes with higher pressure. These findings are in good agreement with recent studies of electrical conductivity of carbon based particles derived from lignin [19,39–41]. It is known that heteroelements on the surface of carbonaceous materials can decrease total conductivity [39]. As mentioned, the carbon particles obtained in this study consisted of 96.66 at % of carbon and 3.20 at % of oxygen (*cf.* Figure 3). In comparison, carbon black particles obtained in a very similar way were reported to have an electrical resistivity of 0.004 Ωm under atmospheric pressure up to 0.025 Ωm at a pressure of 0.48 MPa, with a resistivity highly dependent on the extent of structural homogeneity of the prepared carbon blacks [19]. Increasing structural homogeneity generally translates into decreasing resistivity.

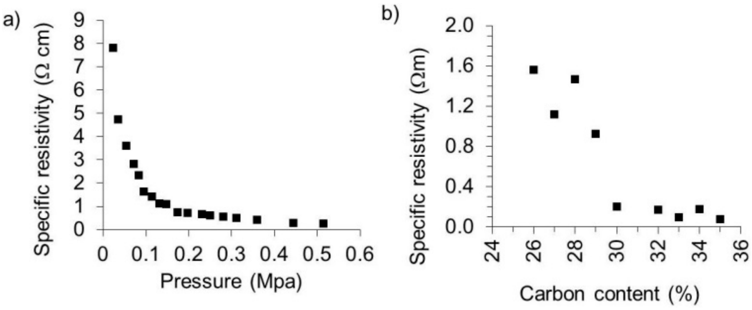

Figure 8. (**a**) Pressure dependence of specific resistivity for carbon particles made of organosolv lignin particles; (**b**) Effect of carbon microparticle content on specific resistivity of poly (lactic acid).

3.8. Conducting Poly(Lactic Acid) (PLA) Carbon Composites

Poly(lactic acid)/carbon composites were produced by incorporating different amounts of the lignin-derived carbon powders obtained in this study into diluted solutions of PLA in chloroform and subsequent evaporation of the organic solvent. PLA was chosen as matrix polymer because this polymer is easy to handle, biodegradable and thermoplastic. It has evoked a great interest and is one of the most interesting biopolymers. There is a wide range of applications for PLA, especially for medical and biological tasks as well as packaging [42]. The obtained composite materials were found to become electrically conductive above a carbon loading of 26% (Figure 8b). Beyond this percolation threshold, conducting pathways are increasingly established within the polymer as reflected by resistivity that dropped from 1.6 Ωm (26% loading) to 0.21 Ωm when 35 wt % of carbon particles were incorporated [43]. However, compared to other studies, carbon loading to achieve electro-conductivity is still very high. Carbon black for example has been reported to impart high electrical conductivity to high-density polyethylene (HDPE) already at loading of 3 wt % [44]. In a recent study it was demonstrated that graphitised carbon black as filler in Poly(L-lactide) (PLLA) caused a decrease of resistivity from 1.6×10^3 Ωm for unfilled PLLA to values lower than 1 Ωm with a concentration of carbon black of 10 wt % [45]. It is assumed that insufficiently homogeneous dispersion of particles (Figure 9) that were not surface-modified to improve compatibility with the PLA matrix may be one of the reasons for the high loadings required to reach the percolation threshold. The simple folding and hot-pressing method applied in our study clearly improved carbon dispersion in the PLA films cast from solution. However, further improvements could be achieved by proper melt-compounding by means of e.g. extrusion. It is known that the tunneling distance of electrons in carbon black-polymer systems depends on many factors and that there is no linear collective effect [9]. Liu *et al.* found that electrical resistance can be described by the tunneling conduction and percolation theory but that the electrical conductivity is dependent of the radius position [46]. In contrast, the tunneling distance of electrons in carbon nanotube polymer matrixes was found to be 1.8 nm [47]. The network of the carbon particles has to have smaller distance than this tunneling distance, otherwise there will be no electrical conductivity. The agglomeration of lignin-derived carbon powder in the PLA may be a reason for the need for high loadings of carbon powder. To reach a lower percolation threshold, the surface area can be enhanced, the structure should be higher and the volatile content should be the lowest possible [48].

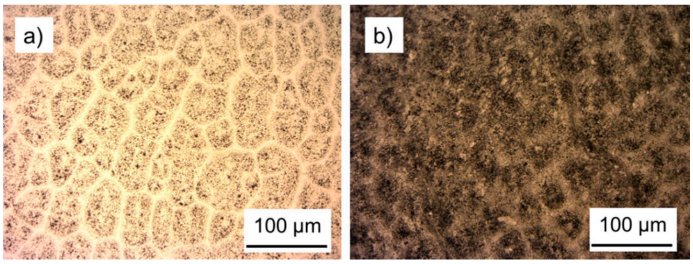

Figure 9. Optical micrographs of PLA films with 10% filler content showing (**a**) poor dispersion of carbon particles after casting from solution and (**b**) improved dispersion after repeated hot-pressing.

3.9. Mechanical Properties of Poly(Lactic Acid) (PLA) Carbon Composites

Tensile testing of PLA specimen loaded with different amounts of carbon particles revealed that both tensile strength and failure strain decreased with the addition of carbon particles to a certain extent (Figure 10). The tensile strength dropped from 25 MPa for PLA without lignin particles to 13 MPa for PLA filled with 5% carbonaceous lignin powder. For PLA filled with 5%–35% of the carbonaceous powder, the tensile strength is almost steady. Failure strain also decreased. Without carbon filling it was about 1.5%. After adding only 5% lignin derived carbon, the failure strain fell to 0.8%. Between 5% and 35% carbon loading, the failure strain was almost steady. Other studies found that the tensile strength increases with low loadings and decreases with high loadings. It was also found that the influence of carbon black particles differs a lot depending on the polymer matrix material [48]. In this case, agglomerates of the carbon particles can lead to imperfections in mechanical testing. The largest carbon particles, which were measured with 60 µm, can also lead to breakages.

In contrast to the decrease of tensile strength and failure strain, the Young modulus E seems to increase slightly at higher loadings. Overall, the effects of carbon filler on the mechanical performance of PLA are in agreement with other studies [49,50]. As outlined in a review on mechanics of particulate-filled polymers [51] an increase in composite stiffness in parallel with a reduction in tensile strength and extensibility is principally observed upon addition of particulate fillers. However, as shown in Figure 10, the PLA-carbon composites produced in the present study do not show a distinctly proportional relationship between filler content and change in mechanics, which one would expect. As with electrical conductivity of the PLA composites, it is proposed that improved filler dispersion by e.g. extrusion may lead to clearer relationships through reduced variability.

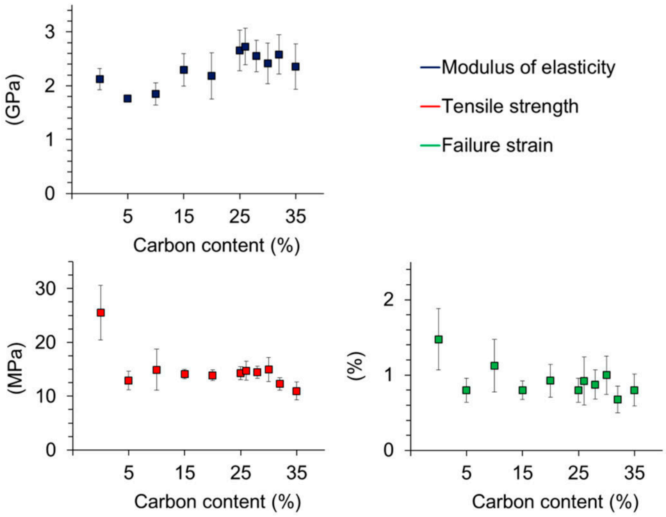

Figure 10. Relationship between mechanical properties and lignin-based carbon microparticle loading of poly(lactic acid) composites.

4. Conclusions

The results of this study are encouraging with respect to the production of conducting polymers using carbon particles derived from a specific technical lignin that is commercially available and produced by organosolv pulping of grass lignin. Even though reasonably low electrical resistivity was measured for the carbonised lignin particles, comparatively high carbon loadings were required to impart conductivity to poly(lactic acid), indicating that further research on lignin-based carbon particles is necessary.

Acknowledgments: Financial support by the Austrian Research Promotion Agency FFG, project 846543 is gratefully acknowledged.

Author Contributions: Janea Köhnke performed the majority of experiments and wrote the majority of the paper. Christian Fürst and Christoph Unterweger carried-out carbonisation. Jozef Keckes, Helga C. Lichtenegger, and Harald Rennhofer performed X-ray characterisation. Gerhard Emsenhuber performed electrical conductivity measurements. Arunjunai raj Mahendran carried-out thermal analysis. Falk Liebner and Wolfgang Gindl-Altmutter conceived the experiments, contributed significant parts to the paper, and supervised writing.

Conflicts of Interest: The authors declare no conflict of interest. The founding sponsors had no role in the design of the study; in the collection, analyses, or interpretation of data; in the writing of the manuscript, and in the decision to publish the results.

References

1. El Mansouri, N.-E.; Salvadó, J. Analytical methods for determining functional groups in various technical lignins. *Ind. Crop. Prod.* **2007**, *26*, 116–124. [CrossRef]
2. Belgacem, M.N.; Gandini, A. *Monomers, Polymers and Composites from Renewable Resources*; Elsevier Ltd.: London, UK, 2008.
3. Lin, S.Y.; Dence, C.W. *Methods in Lignin Chemistry*; Springer: Berlin, Germany, 1992.
4. Lora, J.H.; Glasser, W.G. Recent industrial applications of lignin: A sustainable alternative to nonrenewable materials. *J. Polym. Environ.* **2002**, *10*, 39–48. [CrossRef]
5. Baker, D.A.; Rials, T.G. Recent advances in low-cost carbon fiber manufacture from lignin. *J. Appl. Polym. Sci.* **2013**, *130*, 713–728. [CrossRef]
6. Chand, S. Carbon fibers for composites. *J. Mater. Sci.* **2000**, *35*, 1303–1313. [CrossRef]
7. Kadla, J.F.; Kubo, S.; Venditti, R.A.; Gilbert, R.D.; Compere, A.L.; Griffith, W. Lignin-based carbon fibers for composite fiber applications. *Carbon* **2002**, *40*, 2913–2920. [CrossRef]
8. Ruiz-Rosas, R.; Bedia, J.; Lallave, M.; Loscertales, I.G.; Barrero, A.; Rodríguez-Mirasol, J.; Cordero, T. The production of submicron diameter carbon fibers by the electrospinning of lignin. *Carbon* **2010**, *48*, 696–705. [CrossRef]
9. Balberg, I. A comprehensive picture of the electrical phenomena in carbon black-polymer composites. *Carbon* **2002**, *40*, 139–143. [CrossRef]
10. Geim, A.K.; Novoselov, K.S. The rise of graphene. *Nat. Mater.* **2007**, *6*, 183–191. [CrossRef] [PubMed]
11. Zhang, H.; Wang, C.; Zhang, Y. Preparation and properties of styrene-butadiene rubber nanocomposites blended with carbon black-graphene hybrid filler. *J. Appl. Polym. Sci.* **2015**, *132*. [CrossRef]
12. Ma, L.-F.; Bao, R.-Y.; Huang, S.-L.; Liu, Z.-Y.; Yang, W.; Xie, B.-H.; Yang, M.-B. Electrical properties and morphology of carbon black filled PP/EPDM blends: Effect of selective distribution of fillers induced by dynamic vulcanization. *J. Mater. Sci.* **2013**, *48*, 4942–4951. [CrossRef]
13. Feller, J.-F.; Petitjean, É. Conductive polymer composites(cpc): Influence of processing conditions, shear rate and temperature on electrical properties of poly(butylene terephthalate)/poly(amide12-b-tetramethyleneglycol)– carbon black blends. *Macromol. Symp.* **2003**, *203*, 309–316. [CrossRef]
14. Schulze, P.; Seidel-Morgenstern, A.; Lorenz, H.; Leschinsky, M.; Unkelbach, G. Advanced process for precipitation of lignin from ethanol organosolv spent liquors. *Bioresour. Technol.* **2016**, *199*, 128–134. [CrossRef] [PubMed]
15. Mansouri, N.-E.E.; Salvadó, J. Structural characterization of technical lignins for the production of adhesives: Application to lignosulfonate, kraft, soda-anthraquinone, organosolv and ethanol process lignins. *Ind. Crops Prod.* **2006**, *24*, 8–16. [CrossRef]

16. Zhang, K.; Pei, Z.; Wang, D. Organic solvent pretreatment of lignocellulosic biomass for biofuels and biochemicals: A review. *Bioresour. Technol.* **2016**, *199*, 21–33. [CrossRef] [PubMed]
17. Tejado, A.; Pena, C.; Labidi, J.; Echeverria, J.M.; Mondragon, I. Physico-chemical characterization of lignins from different sources for use in phenol-formaldehyde resin synthesis. *Bioresour. Technol.* **2007**, *98*, 1655–1663. [CrossRef] [PubMed]
18. El Hage, R.; Brosse, N.; Chrusciel, L.; Sanchez, C.; Sannigrahi, P.; Ragauskas, A. Characterization of milled wood lignin and ethanol organosolv lignin from miscanthus. *Polym. Degrad. Stab.* **2009**, *94*, 1632–1638. [CrossRef]
19. Sánchez-González, J.; Macías-García, A.; Alexandre-Franco, M.F.; Gómez-Serrano, V. Electrical conductivity of carbon blacks under compression. *Carbon* **2005**, *43*, 741–747. [CrossRef]
20. Gindl-Altmutter, W.; Fürst, C.; Mahendran, A.R.; Obersriebnig, M.; Emsenhuber, G.; Kluge, M.; Veigel, S.; Keckes, J.; Liebner, F. Electrically conductive kraft lignin-based carbon filler for polymers. *Carbon* **2015**, *89*, 161–168. [CrossRef]
21. Dwiyanti, M.S.; Stewart, J.R.; Yamada, T. Forages for feedstocks of biorefineries in temperate environments: Review of lignin research in bioenergy crops and some insight into miscanthus studies. *Crop Pasture Sci.* **2014**, *65*, 1199–1206. [CrossRef]
22. Kuo, D.T.F.; Vander Sande, J.B.; Gschwend, P.M. Characterization of black carbon in geosorbents at the nanometer scale by stem–edx elemental mapping. *Org. Geochem.* **2013**, *56*, 81–93. [CrossRef]
23. Norberg, I.; Nordström, Y.; Drougge, R.; Gellerstedt, G.; Sjöholm, E. A new method for stabilizing softwood kraft lignin fibers for carbon fiber production. *J. Appl. Polym. Sci.* **2013**, *128*, 3824–3830. [CrossRef]
24. Sharma, R.K.; Wooten, J.B.; Baliga, V.L.; Lin, X.; Geoffrey Chan, W.; Hajaligol, M.R. Characterization of chars from pyrolysis of lignin. *Fuel* **2004**, *83*, 1469–1482. [CrossRef]
25. Braun, J.L.; Holtman, K.M.; Kadla, J.F. Lignin-based carbon fibers: Oxidative thermostabilization of kraft lignin. *Carbon* **2005**, *43*, 385–394. [CrossRef]
26. Kubo, S.; Kadla, J.F. Hydrogen bonding in lignin: A fourier transform infrared model compound study. *Biomacromolecules* **2005**, *6*, 2815–2821. [CrossRef] [PubMed]
27. Yang, H.; Yan, R.; Chen, H.; Lee, D.H.; Zheng, C. Characteristics of hemicellulose, cellulose and lignin pyrolysis. *Fuel* **2007**, *86*, 1781–1788. [CrossRef]
28. Britt, P.F.; Buchanan, A.C., III; Malcolm, E.A. Thermolysis of phenethyl phenyl ether: A model for ether linkages in lignin and low rank coal. *J. Org. Chem.* **1995**, *60*, 6523–6536. [CrossRef]
29. Nimz, H. Über eine neuartige umlagerung in der ligninchemie. *Angew. Chem.* **1966**, *78*, 821–822. [CrossRef]
30. Schmidt, J.A.; Rye, C.S.; Gurnagul, N. Lignin inhibits autoxidative degradation of cellulose. *Polym. Degrad. Stab.* **1995**, *49*, 291–297. [CrossRef]
31. Drbohlav, J.; Stevenson, W.T.K. The oxidative stabilization and carbonization of a synthetic mesophase pitch, part I: The oxidative stabilization process. *Carbon* **1995**, *33*, 693–711. [CrossRef]
32. Drbohlav, J.; Stevenson, W.T.K. The oxidative stabilization and carbonization of a synthetic mesophase pitch, part II: The carbonization process. *Carbon* **1995**, *33*, 713–731. [CrossRef]
33. Matsumoto, T.; Mochida, I. A structural study on oxidative stabilization of mesophase pitch fibers derived from coaltar. *Carbon* **1992**, *30*, 1041–1046. [CrossRef]
34. Sahoo, S.; Seydibeyoğlu, M.Ö.; Mohanty, A.K.; Misra, M. Characterization of industrial lignins for their utilization in future value added applications. *Biomass Bioenergy* **2011**, *35*, 4230–4237. [CrossRef]
35. Wang, Y.; Xie, W. Synthesis of cationic starch with a high degree of substitution in an ionic liquid. *Carbohydr. Polym.* **2010**, *80*, 1172–1177. [CrossRef]
36. Saito, T.; Perkins, J.H.; Vautard, F.; Meyer, H.M.; Messman, J.M.; Tolnai, B.; Naskar, A.K. Methanol fractionation of softwood kraft lignin: Impact on the lignin properties. *Chemsuschem* **2014**, *7*, 221–228. [CrossRef] [PubMed]
37. Li, Z.Q.; Lu, C.J.; Xia, Z.P.; Zhou, Y.; Luo, Z. X-ray diffraction patterns of graphite and turbostratic carbon. *Carbon* **2007**, *45*, 1686–1695. [CrossRef]
38. Foston, M.; Nunnery, G.A.; Meng, X.; Sun, Q.; Baker, F.S.; Ragauskas, A. NMR a critical tool to study the production of carbon fiber from lignin. *Carbon* **2013**, *52*, 65–73. [CrossRef]
39. Pantea, D.; Darmstadt, H.; Kaliaguine, S.; Sümmchen, L.; Roy, C. Electrical conductivity of thermal carbon blacks. *Carbon* **2001**, *39*, 1147–1158. [CrossRef]

40. Celzard, A.; Marêché, J.F.; Payot, F.; Furdin, G. Electrical conductivity of carbonaceous powders. *Carbon* **2002**, *40*, 2801–2815. [CrossRef]
41. Chung, D.D.L. Electrical applications of carbon materials. *J. Mater. Sci.* **2004**, *39*, 2645–2661. [CrossRef]
42. Nampoothiri, K.M.; Nair, N.R.; John, R.P. An overview of the recent developments in polylactide (PLA) research. *Bioresour. Technol.* **2010**, *101*, 8493–8501. [CrossRef] [PubMed]
43. Li, F.; Qi, L.; Yang, J.; Xu, M.; Luo, X.; Ma, D. Polyurethane/conducting carbon black composites: Structure, electric conductivity, strain recovery behavior, and their relationships. *J. Appl. Polym. Sci.* **2000**, *75*, 68–77. [CrossRef]
44. Ren, D.; Zheng, S.; Wu, F.; Yang, W.; Liu, Z.; Yang, M. Formation and evolution of the carbon black network in polyethylene/carbon black composites: Rheology and conductivity properties. *J. Appl. Polym. Sci.* **2014**, *131*. [CrossRef]
45. Tsuji, H.; Kawashima, Y.; Takikawa, H.; Tanaka, S. Poly(L-lactide)/nano-structured carbon composites: Conductivity, thermal properties, crystallization, and biodegradation. *Polymer* **2007**, *48*, 4213–4225. [CrossRef]
46. Liu, X.; Kruckel, J.; Schubert, D.W. Building and testing a simple setup to investigate the electrical properties of polymer/carbon black composites. *Compos. Struct.* **2015**, *129*, 55–59. [CrossRef]
47. Li, C.Y.; Thostenson, E.T.; Chou, T.W. Dominant role of tunneling resistance in the electrical conductivity of carbon nanotube-based composites. *Appl. Phys. Lett.* **2007**, *91*. [CrossRef]
48. Huang, J.-C. Carbon black filled conducting polymers and polymer blends. *Adv. Polym. Technol.* **2002**, *21*, 299–313. [CrossRef]
49. Nerantzaki, M.; Papageorgiou, G.Z.; Bikiaris, D.N. Effect of nanofiller's type on the thermal properties and enzymatic degradation of poly(ε-caprolactone). *Polym. Degrad. Stab.* **2014**, *108*, 257–268. [CrossRef]
50. Kim, K.H.; Jo, W.H. A strategy for enhancement of mechanical and electrical properties of polycarbonate/multi-walled carbon nanotube composites. *Carbon* **2009**, *47*, 1126–1134. [CrossRef]
51. Fu, S.-Y.; Feng, X.-Q.; Lauke, B.; Mai, Y.-W. Effects of particle size, particle/matrix interface adhesion and particle loading on mechanical properties of particulate–polymer composites. *Compos. B Eng.* **2008**, *39*, 933–961.

III

Köhnke, J., Rennhofer, H., Lichtenegger, H., Mahendran, A.R.,, Unterweger, C., Prats-Mateu, B., Gierlinger, N., Schwaiger, E., Mahler, A.-K., Potthast, A. and Gindl-Altmutter, W. (2018) "**Electrically conducting carbon microparticles by direct carbonization of spent wood pulping liquor**" ACS Sustainable Chem. Eng. 6, 3385–3391. DOI: 10.1021/acssuschemeng.7b03582

ACS Sustainable Chemistry & Engineering

Research Article

Cite This: ACS Sustainable Chem. Eng. XXXX, XXX, XXX−XXX

pubs.acs.org/journal/ascecg

Electrically Conducting Carbon Microparticles by Direct Carbonization of Spent Wood Pulping Liquor

Janea Köhnke,[†] Harald Rennhofer,[†] Helga Lichtenegger,[†] Arunjunai raj Mahendran,[‡] Christoph Unterweger,[‡] Batirtze Prats-Mateu,[§] Notburga Gierlinger,[§] Elisabeth Schwaiger,[∥] Arnulf-Kai Mahler,[⊥] Antje Potthast,[#] and Wolfgang Gindl-Altmutter*[,†]

[†]Department of Materials Science and Process Engineering, BOKU-University of Natural Resources and Life Science, Konrad Lorenz Strasse 24, 3430 Tulln an der Donau, Austria

[‡]Kompetenzzentrum Holz GmbH, Altenbergerstrasse 69, 4040 Linz, Austria

[§]Department of Nanobiotechnology, BOKU-University of Natural Resources and Life Science, Muthgasse 11, 1190 Vienna, Austria

[∥]Mondi Frantschach GmbH, Frantschach 5, 9413 St. Gertraud, Austria

[⊥]Sappi Papier Holding GmbH, Brucker Strasse 21, 8101 Gratkorn, Austria

[#]Department of Chemistry, BOKU-University of Natural Resources and Life Science, Konrad Lorenz Strasse 24, 3430 Tulln an der Donau, Austria

ABSTRACT: Lignin is produced abundantly in wood pulping. Because it is currently mainly used for the generation of process energy and electrical energy by combustion, its isolation from processing liquor and subsequent purification for potential higher value uses is challenging. Therefore, the present study evaluates the feasibility of direct carbonization of spray-dried processing liquor from two relevant industrial pulping processes with the aim of obtaining electrically conducting carbon. Analysis of the carbonization process reveals significant differences in the thermal stability of spray-dried liquor from a sulfite pulping process compared to kraft liquor. As a result, kraft-derived carbon shows highly ordered graphitic structure and good electrical conductivity comparable to carbon black, whereas sulfite liquor derived carbon only shows modest conductivity.

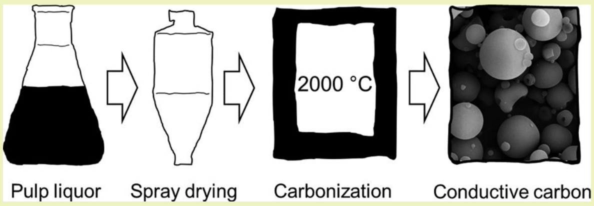

KEYWORDS: *Carbon, Electrical conductivity, Kraft lignin, Lignosulfonate, Microparticles*

INTRODUCTION

The production of cellulosic pulp fiber from wood is one of the major value chains in forest-based industry. Because of the composition of native wood, which consists of roughly 40% cellulose, 30% noncellulosic polysaccharides, and 30% lignin, substantial amounts of lignin arise during the production of pulp fiber. The industrially most important delignification technologies, that is, kraft pulping and sulfite pulping, involve the use of sulfur in some form, together with substantial amount of other inorganic process chemicals. Thus, the composition of lignin-containing liquor is highly variable depending on the technology applied. While currently used predominantly for the generation of process heat and power through combustion, lignin-containing liquor is in focus of substantial research efforts that look into new routes for generating added value from lignin. A number of recent publications[1−11] cite, for example, materials, fuels, solvents, and chemical building blocks based on lignin. It has been shown that the incorporation of biorefinery approaches for the generation of added value from wood pulping process streams may significantly benefit the economic profitability of the pulp and paper sector.[12] In parallel to the utilization of lignin for value-added products, also the technologies used for isolation and purification of lignin from process liquors, which may contain dissolved wood polysaccharides and inorganic salts besides lignin, has made significant progress, for example, with the LignoBoost boost process.[13] Among the potential materials to be produced from lignin, carbon fibers have received particular attention.[14−20] The overall rationale behind this route is in the production of low-cost carbon fiber with intermediate mechanical performance suitable for applications in automotive composite materials,[16] where the expectation of a cost advantage compared to current polyacrylonitrile (PAN)-based carbon fiber is founded on the low cost of lignin precursor. Even though major progress in the processes of separation, preparation, melt-spinning, and thermal stabilization needed for lignin-based precursor fibers has been made,[14,16] no commercial break-through has been achieved so far. As an alternative to micron-scale lignin-based carbon fiber, electrospun carbon fibers with submicron diameters open up new application scenarios in materials science,[14] among which electrode

Received: October 5, 2017
Revised: November 16, 2017
Published: January 17, 2018

DOI: 10.1021/acssuschemeng.7b03582

materials are being widely discussed, for example, in refs 21−24.

In addition to fibrous carbon, particulate carbon also presents opportunities for lignin-derived materials. It is well-known that globular lignin precipitates may arise during the washing of pulp fiber,[25,26] and such globular lignin particles of micro- and nanosize may also be produced in a controlled and reproducible fashion.[27−29] Carbon materials produced from such lignin microparticles show interesting properties in terms of electrical conductivity[30,31] or high surface area.[32,33] Recently it was shown that the electrical conductivity of lignin-derived carbon microparticles can be employed to sense deformation in polymer composites.[31]

All the carbon materials mentioned above are produced from lignin, which was separated from processing liquor via precipitation or filtration and, where necessary, purified from unwanted nonlignin residues. While this processing step allows recovery and valorization of dissolved polysaccharides and process chemicals, this process may also add cost to potential lignin-based products. Without performing a detailed analysis of economic advantages or disadvantages, the present study examines the technical feasibility and resulting material properties of direct carbonization of processing liquors. The liquors originate from two pulp plants using a Kraft process and a sulfite process, respectively, which represent the two industrially most relevant delignification technologies at present. Due to the very different chemical technologies applied in these processes, lignins arising from these processes are very different in terms of chemistry and molecular weight. Even though carbon fibers were produced successfully both from lignins isolated from kraft[15,34] and sulfite,[35] a systematic comparison of carbon derived from these two processes is lacking. Thus, in the present study, the processing liquors from both technologies were spray-dried and carbonized without any pretreatment other than diluting with water to a concentration suitable for spray-drying. Chemical and structural characterization is carried out in order to reveal potential differences in the carbon materials obtained.

■ EXPERIMENTAL SECTION

Liquors from a kraft mill (softwood mix) and from a sulfite mill (hardwood) with a solids content of 50−55% and a lignin content between 35% and 40% were obtained and spray-dried in a laboratory spray-dryer Büchi Mini Spray Dryer B-290. For spray-drying, the solids content of the liquors was set to 10% on a mass basis. Spray-drying was performed with an inlet temperature of 120 °C, aspirator of 100% and a feed rate of 400 mL/h.

Simultaneous thermogravimetric analysis (TGA) and differential scanning calorimetry (DSC) was performed with a Netzsch DSC 200 F3Maia. Under nitrogen atmosphere, open aluminum crucibles were used at a heating rate of 5 °C min^{-1}. Furthermore, TG-FTIR experiments were performed with identical samples in order to monitor the gas outflux during TGA. For this purpose a TA Instruments's Q5000 machine (New Castle, USA) coupled with a Nicolet 380 FTIR (from Thermo Scientific, Madison, USA) via a heated transfer line was used. The heating rate applied was 10 °C min^{-1} and measurements were carried out under nitrogen atmosphere with balance and sample flow rates set at 10 mL min^{-1} and 25 mL min^{-1}, respectively. The number of scans for a single FTIR spectrum was 24 s and samples were scanned at the interval of 30 s. OMNIC software was used to analyze FTIR spectra.

The spray-dried powder was thermostabilized by slow heating up to 250 °C at a heating rate of 0.01 °C min^{-1} at ambient atmosphere in a Memmert drying oven in order to prevent fusing of thermoplastic lignin during carbonization.[36] Thereafter, carbonization was carried out in a GERO HTK8 oven with a volume of 6 L. Argon atmosphere (150 L h^{-1}) was used and heating was performed at rates of 1 °C min^{-1} up to 500 °C (1 h holding step), 5 °C min^{-1} up to 900 °C (1 h holding step), and a final step up to 2000 °C at a rate of 5 °C min^{-1}, concluding with a final holding step of 1 h.

Scanning electron microscopy was carried out in a Quanta 250 FEG from FEI in high-vacuum secondary electron mode. For non-carbonized specimens, sputter-coating with a thin gold layer was carried out prior to SEM. Energy dispersive X-ray spectra were recorded from all specimens (entire field of view) using the same device, but without sputter-coating with gold. Signal was collected for 20 s and the detector was operated at 25 keV.

Elemental analysis was conducted with an EA 1108 CHNS-O elemental analyzer by Carlo Erba Instruments with tin capsules and temperatures of 1.020 °C up to 1.400 °C (oxygen flash combustion). For separation by gas chromatography helium is used as carrier gas, detection as well as quantification were done at a Thermal Conductivity Detector.

Wide angle X-ray diffraction was performed with a Rigaku SmartLab 5-Axis X-ray diffractometer using glass capillaries and Cu K alpha radiation with a wavelength of $\lambda = 0.15418$ nm. Intensity data were recorded in intervals of 0.02° between the scattering angles $2\theta = 5°$ and 50°. Small angle X-ray scattering (SAXS) was carried out with a Rigaku S-Max3000 3-pinhole SAXS camera with MM002+ source and a Triton 200 multiwire detector. Scattering images were recorded in the range from $q = 0.08$–8 nm^{-1}, with $q = 4\pi \sin \theta/\lambda$ the scattering vector, integrated and background corrected before further data evaluation.[30]

Raman spectra were acquired using a Raman microscope (alpha300RA, WITec GmbH, Germany) equipped with a green laser ($\lambda = 532$ nm), spectrometer with a 600 gmm^{-1} grating (UHTS 300 WITec, Germany) and a CCD camera (Andor DU401ABV, Belfast, North Ireland). The laser power was set to 5 mW and with an integration time of 0.05 s single spectra have been collected every 250 nm over a region of 20 × 20 μm2 (6400 spectra/region) using a 100× oil immersion objective (numerical aperture (NA) = 1.4). Finally average spectra of always three regions of the K and L samples have been calculated (19200 spectra/sample) and compared.

Finally, the electrical resistivity of pure carbon particle powders was measured at different pressure according to refs 37 and 38.

■ RESULTS AND DISCUSSION

The powders resulting from spray-drying of processing liquors consisted of spherical particles for both variants as revealed by SEM (Figure 1). Typically, the diameter of the particles was in the order of 4−6 μm, with smaller particles of diameters down to 1 μm occurring additionally. No significant differences were observed between particles originating from Kraft and sulfite liquor, respectively.

The composition of the spray dried powders as determined by element analysis is shown in Table 1. Major differences are seen in the carbon content, which is significantly higher for sulfite than for kraft, and in the content of inorganics, which is typical of the chemical delignification processes used in the respective pulp plants.

Thermostabilization of spray-dried powders at temperatures up to 250 °C under ambient atmosphere resulted in significant mass loss of 25.8% for kraft and 55.7% for sulfite. Thermostabilization of lignin is known to lead to mass loss due to oxidative processes.[36] The significantly lower mass loss of the kraft variant compared to sulfite may be primarily be explained by the high inorganics content of the kraft variant (Table 1), which is nonvolatile. The thermostabilized material was characterized by simultaneous thermal analysis (STA) and TG-FTIR in inert atmosphere in order to obtain some understanding of the different behavior of these materials during the carbonization process. However, technical limi-

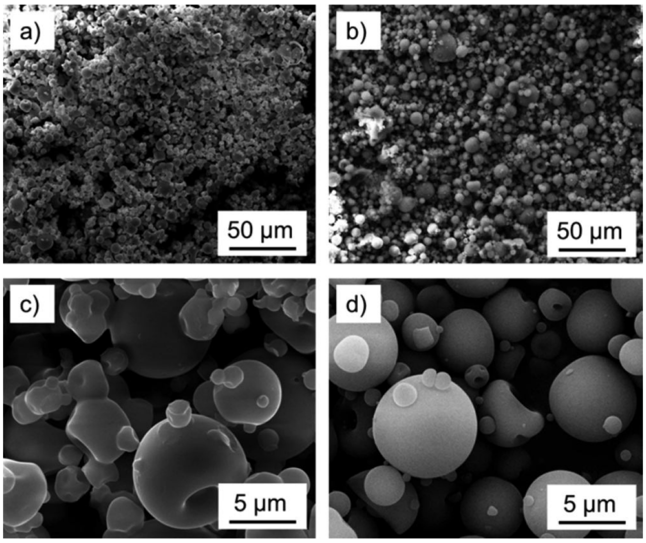

Figure 1. Scanning electron microscopy of spray-dried kraft (a, c) and sulfite (b, d) liquors.

tations of the characterization devices used allowed analysis only up to temperatures of 600 °C, whereas carbonization was carried out at temperatures up to 2000 °C. Thermogravimetric analysis (Figure 2a and b) shows major mass loss at temperatures above 200 °C for both specimens. Overall, mass loss is significantly more pronounced for the sulfite variant compared to Kraft, which confirms the different behavior of the two variants already observed as a result of thermostabilization. Differential scanning calorimetry of the same specimens (Figure 2a and d) reveals significant endothermal behavior at temperatures around 100 °C, which is typical of lignins and associated with loss in humidity.[39]

A major difference between the two variants of processing liquors studied arises at higher temperature, where a very strong exothermal region between 300 and 450 °C appears in the sulfite variant. Depending on its chemistry, a certain amount of SO_2 is released during thermal degradation of lignosulfonate,[40] which accounts for the strong exothermal peak seen in DSC. FTIR analysis of exhaust gas from TG (Figure 2e and f) shows a characteristic absorbance band at 2360 cm^{-1}, which may be attributed to the characteristic $O{=}C{=}O$ stretching vibration of CO_2.[41] In good agreement with TG and DSC, strong emission of CO_2 is observed for the sulfite variant, whereas only moderate emissions are shown with kraft. In summary, intense lignin degradation processes setting in at 300 °C were thus observed for the sulfite variant.

Carbonization at temperatures up to 2000 °C affected both the morphology and the structure and composition of spray-dried particles. In terms of morphology as revealed by SEM (Figure 3), two characteristics were affected: first, the characteristic particle diameter becomes smaller, with diameters primarily in the order of 3−4 μm instead of 5 μm before carbonization, and, second, the surface of the particles appears significantly rougher instead of the smooth appearance shown before carbonization (Figure 1). The rough appearance of the surface of particles is proposed to be a result of the intense structural conversion and evaporation of material during carbonization. Same as before carbonization, the morphology of both variants, i.e. Kraft and sulfite, is very similar. Energy-dispersive X-ray analysis confirms substantial structural reorganization of the specimen chemistry during carbonization. For both variants, the carbon content increases strongly (Table 2), whereas oxygen is no longer detected. Interestingly, sodium is completely removed from the Kraft variant, whereas the content of potassium remains constant. In the sulfite variant, the magnesium is still present, but reduced to approximately one-quarter of its original concentration. Residual metals may have some contribution to electrical conductivity of the carbon particles produced. In both variants, small amounts of sulfur persist also after carbonization. The mass loss observed during the carbonization step was very high, amounting to 94.5% for Kraft and 69.4% for sulfite particles, respectively. It is proposed that the loss of Na during high temperature treatment is one of

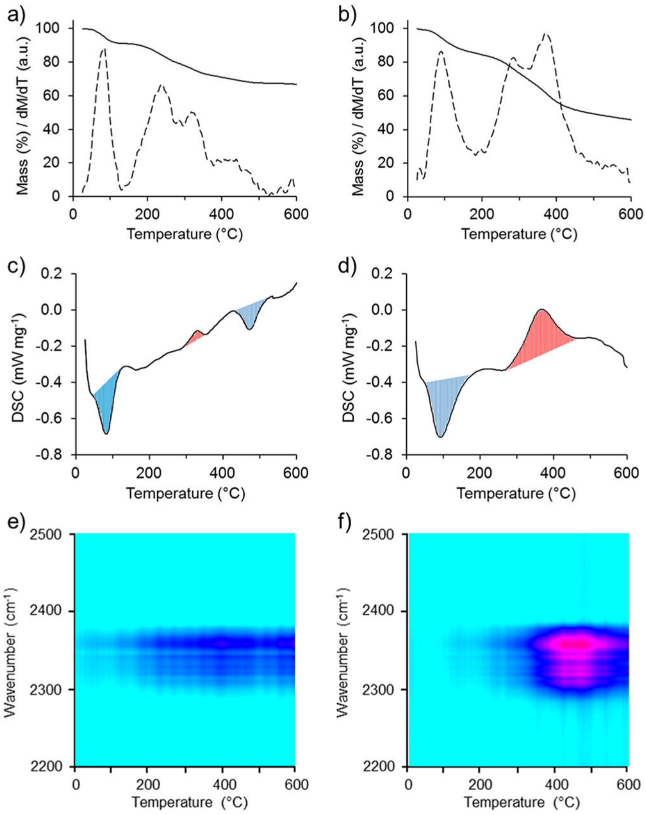

Figure 2. TG of spray dried kraft liquor (a) and sulfite liquor (b) together with DSC of the respective materials (c and d). Major endo- and exothermal peak regions in DSC are highlighted in blue and red, respectively. Panels e and f show 2D representations of the evolution of FTIR absorbance peaks attributed to CO_2 with increasing temperature for spray dried kraft liquor (e) and sulfite liquor (f).

Table 1. Elemental Analysis of Spray-Dried Pulp Liquors

	element (% w/w)								
material	C	H	N	S	O	Na	K	Ca	Mg
kraft	30.5	4.0	0.1	4.9	39.4	13.0	2.8	0.7	0.2
sulfite	46.9	5.8	0.2	5.2	36.6	0.1	0.4	0.7	1.8

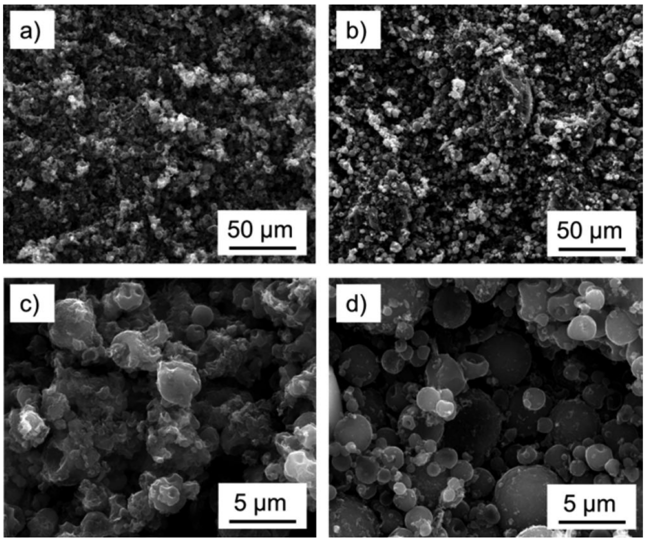

Figure 3. Scanning electron microscopy of spray-dried kraft (a, c) and sulfite (b, d) liquors after carbonization at 2000 °C.

Table 2. Element Distribution from EDAX Analysis of Spray-Dried Liquors and Carbon Derived Thereof

	element (atomic %)					
material	C	O	S	Mg	Na	K
kraft liquor	53.2	32.4	2.1		11.1	1.2
sulfite liquor	67.1	29.3	2.5	1.0		
carbon from kraft liquor	98.7		0.2			1.1
carbon from sulfite liquor	99.1		0.5	0.2		

the major contributors to the low yield observed for the Kraft variant compared to sulfite. During the whole process, including thermostabilization and carbonization, the total yield of carbon particles was thus 4.1% for the Kraft liquor and 13.6% for the sulfite liquor.

While the content of carbon derived from EDAX is similar for carbon particles derived from kraft and sulfite liquor, respectively (Figure 4, Table 2), the structure of carbon differs very significantly. X-ray diffraction (Figure 5) shows occurrence of clear graphitic structures for both variants, and also a substantial signal at small angles <10°, indicating nanoporosity. The most important graphitic diffraction peak is associated with the 002 lattice plane.[42] This peak is much more pronounced for the kraft, compared to the sulfite variant, indicating a significantly higher degree of supramolecular order in the first variant. This finding is supported by Raman spectroscopy (Figure 6). Raman spectra contain abundant information about the structure of carbon materials. In the present study, only two bands are discussed, that is, the G-band at ~1580 cm^{-1}, which is associated with an ideal, highly ordered graphitic lattice and the D-band at 1350 cm^{-1}, which represents signal from a disordered graphitic lattice.[43] As shown in Figure 6, the relative intensity of the G-band compared to the D-band is much stronger for the Kraft-derived carbon as opposed to the sulfite-derived carbon particles.

Small angle X-ray scattering curves (Figure 7) show nanoporosity, which is quite different for the Kraft and the sulfite derived particles, respectively. While the carbon particles from sulfite liquor feature well-defined nanopores with a mean pore radius of (1.41 ± 0.02) nm, which is evaluated from the prominent shoulder in the SAXS curve, the carbon particles from Kraft liquor show no distinct pore size. The rather single power law behavior[30] of the related SAXS curve indicates either a wide and even pore size distribution with no preferred size in the regime of pores accessible by the experiment, or pores bigger than 50 nm. The specific inner surface contributed from the nanopores smaller than about 50 nm could thus only be evaluated for the sulfite derived carbons with (860 ± 90) m^2 cm^{-3}. Both samples show a similar surface roughness indicated by the power law exponent of −3.2 ± 0.3, related to surface fractals. Pore structure and rough surfaces are usually expected as a result of carbonization processes, which open up pores due to material loss and induce rearrangement of graphite layers toward higher graphitic structures. Therefore it is surprising to find no pronounced nanopores smaller than 50 nm in the Kraft derived material, which has a clear 002 peak in the XRD, while the sulfite derived materials shows well-developed nanopores, but more amorphous structures.

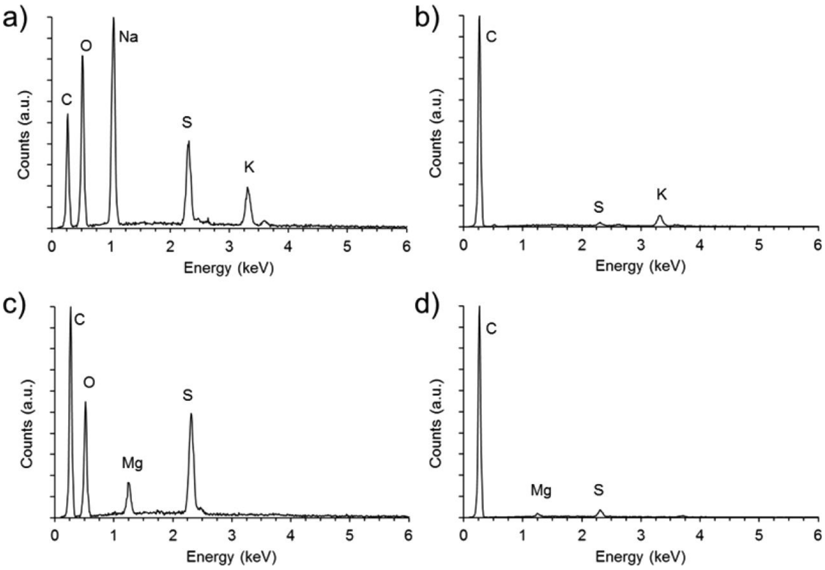

Figure 4. Energy-dispersive X-ray analysis of spray-dried kraft (a) and sulfite (c) liquor and their carbonized variants (b and d).

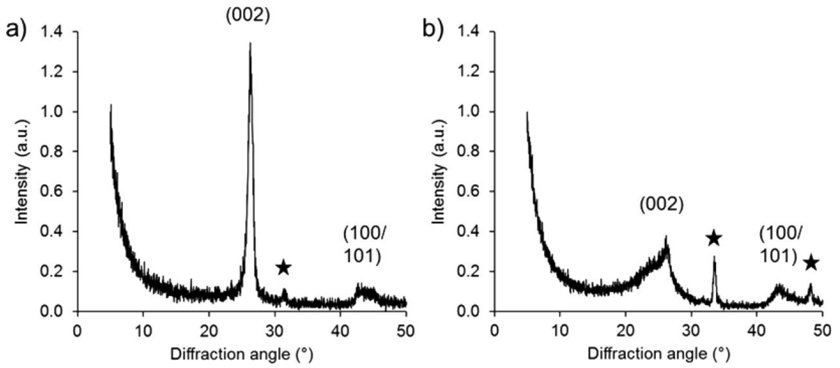

Figure 5. XRD of carbon particles derived from spray-dried kraft (a) and sulfite (b) liquor. Diffraction peaks are assigned with associated graphite lattice planes where possible. Nonidentified peaks are designated with an asterisk.

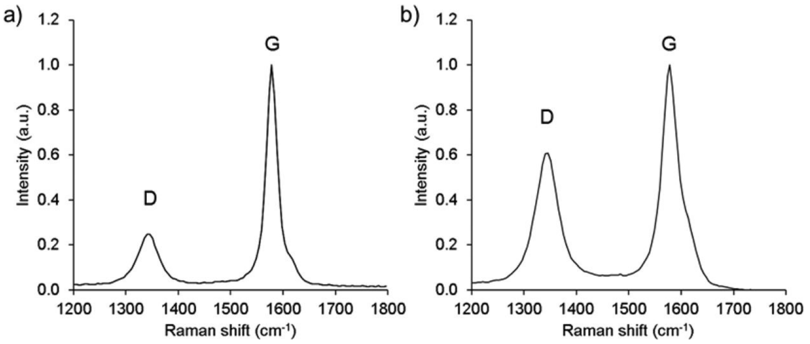

Figure 6. Raman shifts for carbon particles derived from spray-dried kraft (a) and sulfite (b) liquor.

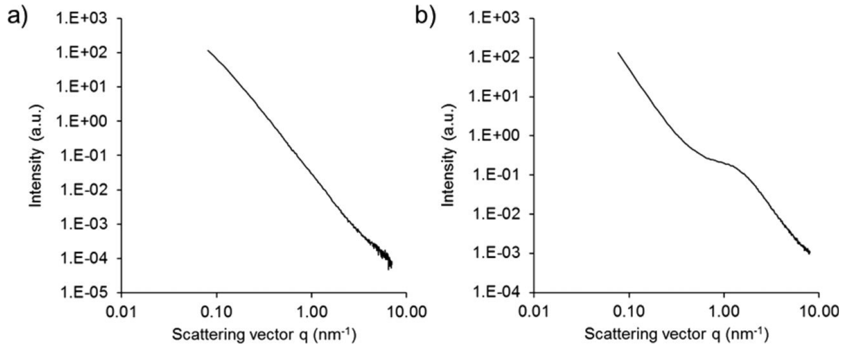

Figure 7. SAXS curves of carbon particles derived from spray-dried kraft (a) and sulfite (b) liquor.

In summary, structural characterization by means of XRD and Raman spectroscopy shows a much more ordered character for carbon particles produced from spray-dried Kraft liquor compared to sulfite liquor. Structural characterization by means of SAXS shows different morphology on the nanometer regime, i.e. nanopores of specific size for the sulfite derived carbons, which are not detected in the Kraft derived carbons. In good agreement with these structural differences, also the electrical resistivity measured for these carbon powders is significantly different (Figure 8). When using a pressure of 0.5 MPa for comparison, the resistivity of carbon from spray-dried sulfite liquor is roughly 5-fold the resistivity of carbon from spray-dried Kraft liquor. Electrically conductive carbon black is available with low and high structure, where the term structure refers to the envelope of a carbon particle at a given mass. A big envelope, i.e. high structure, of carbon particles reduces the mass of carbon needed in a polymer order to achieve electrical conductivity, whereas comparably higher filling with carbon is required when the envelope is small. At similar compaction pressure, different types of carbon black characterized in a comparable setup[38] yielded values of 0.004 Ωm for low-structure carbon black and 0.025 Ωm for high-structure carbon

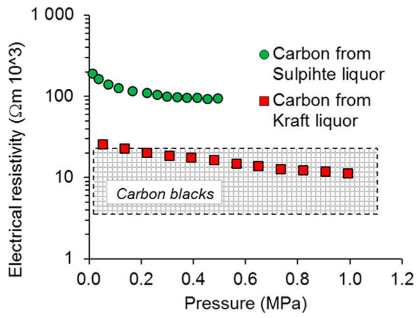

Figure 8. Electrical resistivity of carbon powders as a function of applied pressure.

black, respectively. Thus in terms of electrical resistivity, Kraft-type carbon is comparable with high-structure carbon black, whereas the resistivity of sulfite-type carbon is well above what is typical for carbon blacks. In terms of electrical conductivity, graphitic structure, particle morphology, and surface chemistry are important determinants.[44] The overall morphology is spherical for both carbons, with similar sizes of individual spheres, which why it is assumed that particle morphology does not contribute to the differences in resistivity observed. With regard to surface chemistry, where the presence of noncarbon elements may increase electrical resistivity,[44] differences are probably present (Table 2), but their significance cannot be assessed. As opposed to morphology and chemistry, differences in graphitic structure are very clear and it is proposed that these differences are responsible for the differences in electrical resistivity observed. The cause for the very different graphitic structure obtained from Kraft processing liquor as compared to sulfite processing liquor may be discussed in terms of the different chemistry and thermal behavior of Kraft lignin and lignosulfonate.[5] The Kraft process largely degrades the native lignin structure, which leads to a 2.5−3 times lower molar mass of the resulting lignin, in the present case the weight-average molar mass is 2700 g mol^{-1} for Kraft lignin, compared to 20.000 g mol^{-1} for the lignosulfonate.[45] In addition, the kraft lignin further condenses in the process of delignification, which leads to non-native new carbon−carbon bonds finally resulting in partial polycyclic aromatic structures which have recently been proposed.[46] The strong fluorescence of kraft lignins compared to LS is another indication of this pronounced precondensation process presence. The sulfur structure in kraft lignins is not well understood, but it can be assumed that sulfur residues are present in form of SH groups in the side chain. Lignosulfonates are generated in the sulfite cooking liquor by sulfonation, which occurs mainly at the C-3 side chain. The sulfonic acid groups introduced are highly ionic, that is, deprotonated, and lead to a dissolution of the lignin without significant fragmentation, which explains the higher molar mass. As to thermal degradation, substantial amounts of SO_2, which depolymerizes lignin, are being liberated from lignosulfonate prior to carbonization.[40] During the carbonization process lignosulfonate may thus degrade in a different way compared to the already degraded and precondensed kraft lignin. These particular features of lignosulfonate substantially impair the suitability of this raw material for electrically conducting carbon, as only poor structural order is obtained.

CONCLUSION

The results presented show that lignin-containing liquor from wood pulping processes may be converted to electrically conducting carbon without any pretreatment other than spray-drying and oxidative thermostabilization. Out of the two pulping processes studied, kraft lignin performed clearly better in terms of structural order and electrical conductivity, probably due to the presence of precondensed polycyclic aromatics in an overall more strongly degraded lignin, compared to lignin from a sulfite process. While the method described in the present study is attractive due to its simplicity, the very low carbon yield of roughly 5% to 15% for the two lignins studied may be prohibitive in economic terms, necessitating further optimization of the process. This also holds true for spray-drying. Here, further experiments with higher solids concentration will be required to minimize energy consumption.

AUTHOR INFORMATION

Corresponding Author

*E-mail: wolfgang.gindl@boku.ac.at. Phone: +43-1-47654-89111. Fax: +43-1-47654-89195.

ORCID

Helga Lichtenegger: 0000-0002-6624-1419
Antje Potthast: 0000-0003-1981-2271
Wolfgang Gindl-Altmutter: 0000-0002-8224-6762

Author Contributions

The manuscript was written through contributions of all authors. All authors have given approval to the final version of the manuscript.

Notes

The authors declare no competing financial interest.

ACKNOWLEDGMENTS

J.K., A.M., and W.G.-A. gratefully acknowledge funding from the Austrian Science Promotion Agency (FFG): Bridge Project 846543. N.G. and B.P.M. acknowledge funding of the Austrian Science Fund (FWF), START Project [Y-728-B16], and the European community (ERC-consolidator grant SCATAPNUT 681885). Dr. Jozef Keckes, University of Leoben, is gratefully acknowledged for providing XRD data. A.P. gratefully acknowledges support from the Austrian Science Promotion Agency (FFG): Project Flippr².

REFERENCES

(1) Ragauskas, A. J.; Beckham, G. T.; Biddy, M. J.; Chandra, R.; Chen, F.; Davis, M. F.; Davison, B. H.; Dixon, R. A.; Gilna, P.; Keller, M.; Langan, P.; Naskar, A. K.; Saddler, J. N.; Tschaplinski, T. J.; Tuskan, G. A.; Wyman, C. E. Lignin Valorization: Improving Lignin Processing in the Biorefinery. *Science* **2014**, *344*, 1246843.

(2) Kalami, S.; Arefmanesh, M.; Master, E.; Nejad, M. Replacing 100% of phenol in phenolic adhesive formulations with lignin. *J. Appl. Polym. Sci.* **2017**, *134*, 45124.

(3) Yuan, T. Q.; Xu, F.; Sun, R. C. Role of lignin in a biorefinery: separation characterization and valorization. *J. Chem. Technol. Biotechnol.* **2013**, *88*, 346−352.

(4) Laskar, D. D.; Yang, B.; Wang, H. M.; Lee, J. Pathways for biomass-derived lignin to hydrocarbon fuels. *Biofuels, Bioprod. Biorefin.* **2013**, *7*, 602−626.

(5) Laurichesse, S.; Avérous, L. Chemical modification of lignins: Towards biobased polymers. *Prog. Polym. Sci.* **2014**, *39*, 1266−1290.

(6) Rinaldi, R.; Jastrzebski, R.; Clough, M. T.; Ralph, J.; Kennema, M.; Bruijnincx, P. C. A.; Weckhuysen, B. M. Paving the Way for Lignin Valorisation: Recent Advances in Bioengineering, Biorefining and Catalysis. *Angew. Chem., Int. Ed.* **2016**, *55*, 8164−8215.

(7) Duval, A.; Lawoko, M. A review on lignin-based polymeric, micro- and nano-structured materials. *React. Funct. Polym.* **2014**, *85*, 78−96.

(8) Norgren, M.; Edlund, H. Lignin: Recent advances and emerging applications. *Curr. Opin. Colloid Interface Sci.* **2014**, *19*, 409−416.

(9) Rodríguez Correa, C.; Stollovsky, M.; Hehr, T.; Rauscher, Y.; Rolli, B.; Kruse, A. Influence of the Carbonization Process on Activated Carbon Properties from Lignin and Lignin-Rich Biomasses. *ACS Sustainable Chem. Eng.* **2017**, *5*, 8222−8233.

(10) Yang, Y.; Deng, Y.; Tong, Z.; Wang, C. Renewable Lignin-Based Xerogels with Self-Cleaning Properties and Superhydrophobicity. *ACS Sustainable Chem. Eng.* **2014**, *2*, 1729−1733.

(11) Xue, B.-L.; Wen, J.-L.; Sun, R.-C. Lignin-Based Rigid Polyurethane Foam Reinforced with Pulp Fiber: Synthesis and Characterization. *ACS Sustainable Chem. Eng.* **2014**, *2*, 1474−1480.

(12) Stern, T.; Ledl, C.; Braun, M.; Hesser, F.; Schwarzbauer, P. Biorefineries' impacts on the Austrian forest sector: A system dynamics approach. *Technol. Forecasting Social Change* **2015**, *91*, 311−326.

DOI: 10.1021/acssuschemeng.7b03582

(13) Fatehi, P.; Chen, J. Extraction of Technical Lignins from Pulping Spent Liquors, Challenges and Opportunities. In *Production of Biofuels and Chemicals from Lignin*; Fang, Z., Smith, J. R. L., Eds.; Springer: Singapore, 2016; pp 35−54.

(14) Fang, W.; Yang, S.; Wang, X.-L.; Yuan, T.-Q.; Sun, R.-C. Manufacture and application of lignin-based carbon fibers (LCFs) and lignin-based carbon nanofibers (LCNFs). *Green Chem.* **2017**, *19*, 1794−1827.

(15) Kadla, J. F.; Kubo, S.; Venditti, R. A.; Gilbert, R. D.; Compere, A. L.; Griffith, W. Lignin-based carbon fibers for composite fiber applications. *Carbon* **2002**, *40*, 2913−2920.

(16) Baker, D. A.; Rials, T. G. Recent advances in low-cost carbon fiber manufacture from lignin. *J. Appl. Polym. Sci.* **2013**, *130*, 713−728.

(17) Meek, N.; Penumadu, D.; Hosseinaei, O.; Harper, D.; Young, S.; Rials, T. Synthesis and characterization of lignin carbon fiber and composites. *Compos. Sci. Technol.* **2016**, *137*, 60−68.

(18) Hosseinaei, O.; Harper, D. P.; Bozell, J. J.; Rials, T. G. Role of Physicochemical Structure of Organosolv Hardwood and Herbaceous Lignins on Carbon Fiber Performance. *ACS Sustainable Chem. Eng.* **2016**, *4*, 5785−5798.

(19) Li, Q.; Xie, S. X.; Serem, W. K.; Naik, M. T.; Liu, L.; Yuan, J. S. Quality carbon fibers from fractionated lignin. *Green Chem.* **2017**, *19*, 1628−1634.

(20) Ogale, A. A.; Zhang, M.; Jin, J. Recent advances in carbon fibers derived from biobased precursors. *J. Appl. Polym. Sci.* **2016**, *133*, 43794.

(21) Cho, M. J.; Karaaslan, M. A.; Renneckar, S.; Ko, F. Enhancement of the mechanical properties of electrospun lignin-based nanofibers by heat treatment. *J. Mater. Sci.* **2017**, *52*, 9602−9614.

(22) Svinterikos, E.; Zuburtikudis, I. Tailor-Made Electrospun Nanofibers of Biowaste Lignin/Recycled Poly(Ethylene Terephthalate). *J. Polym. Environ.* **2017**, *25*, 465−478.

(23) Ruiz-Rosas, R.; Bedia, J.; Lallave, M.; Loscertales, I. G.; Barrero, A.; Rodríguez-Mirasol, J.; Cordero, T. The production of submicron diameter carbon fibers by the electrospinning of lignin. *Carbon* **2010**, *48*, 696−705.

(24) Shi, Z. Q.; Jin, G. Q.; Wang, J.; Zhang, J. Free-standing, welded mesoporous carbon nanofibers as anode for high-rate performance Li-ion batteries. *J. Electroanal. Chem.* **2017**, *795*, 26−31.

(25) Xu, Y.; Li, K.; Zhang, M. Lignin precipitation on the pulp fibers in the ethanol-based organosolv pulping. *Colloids Surf., A* **2007**, *301*, 255−263.

(26) Schmied, F. J.; Teichert, C.; Kappel, L.; Hirn, U.; Schennach, R. Analysis of precipitated lignin on kraft pulp fibers using atomic force microscopy. *Cellulose* **2012**, *19*, 1013−1021.

(27) Ago, M.; Tardy, B. L.; Wang, L.; Guo, J. Q.; Khakalo, A.; Rojas, O. J. Supramolecular assemblies of lignin into nano- and micro-particles. *MRS Bull.* **2017**, *42*, 371−378.

(28) Ago, M.; Huan, S.; Borghei, M.; Raula, J.; Kauppinen, E. I.; Rojas, O. J. High-Throughput Synthesis of Lignin Particles (similar to 30 nm to similar to 2 mu m) via Aerosol Flow Reactor: Size Fractionation and Utilization in Pickering Emulsions. *ACS Appl. Mater. Interfaces* **2016**, *8*, 23302−23310.

(29) Lievonen, M.; Valle-Delgado, J. J.; Mattinen, M. L.; Hult, E. L.; Lintinen, K.; Kostiainen, M. A.; Paananen, A.; Szilvay, G. R.; Setala, H.; Osterberg, M. A simple process for lignin nanoparticle preparation. *Green Chem.* **2016**, *18*, 1416−1422.

(30) Köhnke, J.; Fürst, C.; Unterweger, C.; Rennhofer, H.; Lichtenegger, H. C.; Keckes, J.; Emsenhuber, G.; Mahendran, A. R.; Liebner, F.; Gindl-Altmutter, W. Carbon microparticles from organosolv lignin as filler for conducting Poly(lactic acid). *Polymers* **2016**, *8*, 205.

(31) Gindl-Altmutter, W.; Fürst, C.; Mahendran, A. r.; Obersriebnig, M.; Emsenhuber, G.; Kluge, M.; Veigel, S.; Keckes, J.; Liebner, F. Electrically conductive kraft lignin-based carbon filler for polymers. *Carbon* **2015**, *89*, 161−168.

(32) Li, Z. L.; Ge, Y. Y.; Wan, L. Fabrication of a green porous lignin-based sphere for the removal of lead ions from aqueous media. *J. Hazard. Mater.* **2015**, *285*, 77−83.

(33) Kim, D.; Cheon, J.; Kim, J.; Hwang, D.; Hong, I.; Kwon, O. H.; Park, W. H.; Cho, D. Extraction and characterization of lignin from black liquor and preparation of biomass-based activated carbon therefrom. *Carbon Letters* **2017**, *22*, 81−88.

(34) Olsson, C.; Sjoholm, E.; Reimann, A. Carbon fibres from precursors produced by dry-jet wet-spinning of kraft lignin blended with kraft pulps. *Holzforschung* **2017**, *71*, 275−283.

(35) Yen, S. H.; Chang, F. C. Effects of Fiber Processing Conditions on the Yield, Carbon Content, and Diameter of Lignosulfonate-based Carbon Fibers. *BioResources* **2016**, *11*, 10158−10172.

(36) Norberg, I.; Nordström, Y.; Drougge, R.; Gellerstedt, G.; Sjöholm, E. A new method for stabilizing softwood kraft lignin fibers for carbon fiber production. *J. Appl. Polym. Sci.* **2013**, *128*, 3824−3830.

(37) Celzard, A.; Marêché, J. F.; Payot, F.; Furdin, G. Electrical conductivity of carbonaceous powders. *Carbon* **2002**, *40*, 2801−2815.

(38) Sánchez-González, J.; Macías-García, A.; Alexandre-Franco, M. F.; Gómez-Serrano, V. Electrical conductivity of carbon blacks under compression. *Carbon* **2005**, *43*, 741−747.

(39) Brebu, M.; Vasile, C. Thermal degradation of lignin—A review. *Cellulose Chem. Technol.* **2010**, *44*, 353−363.

(40) Jakab, E.; Faix, O.; Till, F.; Székely, T. The effect of cations on the thermal decomposition of lignins. *J. Anal. Appl. Pyrolysis* **1993**, *25*, 185−194.

(41) Wang, C. P.; Wu, Y. J.; Liu, Q.; Yang, H. R.; Wang, F. Y. Analysis of the behaviour of pollutant gas emissions during wheat straw/coal cofiring by TG-FTIR. *Fuel Process. Technol.* **2011**, *92*, 1037−1041.

(42) Li, Z. Q.; Lu, C. J.; Xia, Z. P.; Zhou, Y.; Luo, Z. X-ray diffraction patterns of graphite and turbostratic carbon. *Carbon* **2007**, *45*, 1686−1695.

(43) Sadezky, A.; Muckenhuber, H.; Grothe, H.; Niessner, R.; Pöschl, U. Raman microspectroscopy of soot and related carbonaceous materials: Spectral analysis and structural information. *Carbon* **2005**, *43*, 1731−1742.

(44) Pantea, D.; Darmstadt, H.; Kaliaguine, S.; Sümmchen, L.; Roy, C. Electrical conductivity of thermal carbon blacks. *Carbon* **2001**, *39*, 1147−1158.

(45) Sulaeva, I.; Zinovyev, G.; Plankeele, J. M.; Sumerskii, I.; Rosenau, T.; Potthast, A. Fast Track to Molar-Mass Distributions of Technical Lignins. *ChemSusChem* **2017**, *10*, 629−635.

(46) Crestini, C.; Lange, H.; Sette, M.; Argyropoulos, D. S. On the structure of softwood kraft lignin. *Green Chem.* **2017**, *19*, 4104−4121.

IV

Köhnke, J., Rennhofer, H., Unterweger, C., Gierlinger, N., Keckes, J., Zollfrank, C., Rojas, O.J., Gindl-Altmutter, W. (2019) “**Electrically-Conductive Sub-Micron Carbon Particles from Lignin: Elucidation of Nanostructure and Use as Filler in Cellulose Nanopapers**” Nanomaterials 8, 1055. DOI: 10.3390/nano8121055

nanomaterials

MDPI

Article

Electrically-Conductive Sub-Micron Carbon Particles from Lignin: Elucidation of Nanostructure and Use as Filler in Cellulose Nanopapers

Janea Köhnke [1], Harald Rennhofer [1], Christoph Unterweger [2], Notburga Gierlinger [3], Jozef Keckes [4], Cordt Zollfrank [5], Orlando J. Rojas [6] and Wolfgang Gindl-Altmutter [1,*]

[1] Department of Materials Science and Process Engineering, BOKU-University of Natural Resources and Life Science, Vienna, 3430 Tulln, Austria; janea.koehnke@boku.ac.at (J.K.); harald.rennhofer@boku.ac.at (H.R.)
[2] Wood K plus—Kompetenzzentrum Holz GmbH, 4040 Linz, Austria; c.unterweger@wood-kplus.at
[3] Department of Nanobiotechnology, BOKU-University of Natural Resources and Life Science, Vienna, 1190 Vienna, Austria; notburga.gierlinger@boku.ac.at
[4] Department of Materials Physics, Montanuniversität of Leoben, 8700 Leoben, Austria; keckes@unileoben.ac.at
[5] Chair for Biogenic Polymers, Technische Universität München, 94315 Straubing, Germany; cordt.zollfrank@tum.de
[6] Department of Bioproducts and Biosystems, School of Chemical Engineering, Aalto University, 00076 Aalto, Finland; orlando.rojas@aalto.fi
* Correspondence: wolfgang.gindl@boku.ac.at; Tel.: +46-1-47654-89111

Received: 20 November 2018; Accepted: 12 December 2018; Published: 15 December 2018

check for updates

Abstract: Carbon particles were produced from kraft lignin through carbonization of perfectly spherical, sub-micron beads obtained by aerosol flow. The structure of the resulting carbon particles was elucidated and compared to that derived from commercially available technical lignin powder, which is undefined in geometry. In addition to the smaller diameters of the lignin beads (<1 µm) compared to those of the lignin powder (100 µm), the former displayed a slightly higher structural order as revealed by X-ray diffraction and Raman spectroscopy. With regard to potential application in composite structures, the sub-micron carbon beads were clearly advantageous as a filler of cellulose nanopapers, which displayed better mechanical performance but with limited electrical conductivity. Compression sensing was achieved for this nanocomposite system.

Keywords: carbon particles; cellulose nanopaper; electrical conductivity; lignin

---

1. Introduction

Lignin is the second-most abundant plant bioresource after cellulose. Technical lignin arises as a by-product of the pulping process and is predominantly used for the production of energy. It has been shown that the pulp and paper sector may significantly benefit from a transition from a singular focus on pulp fiber production towards a broader utilization of lignocellulose in a biorefinery framework [1]. In order to enable this transition, value-added utilization pathways for lignin are urgently needed. In this context, the potential applications discussed are diverse and include production of bioaromatics, biopolymers, and biofuel [2–19]. In terms of lignin-derived materials, conversion by means of carbonization is attractive, due to the higher carbon content and yield of lignin, e.g., compared to those from cellulose, and the potentially high value of carbon materials obtained in the process [20]. Lignin-derived carbon fibers have been the subject of various studies [21–29], but lack mechanical performance relative to their fossil-derived counterparts. Even so, lignin-derived carbon fibers may be attractive as a low-cost and moderate performance alternative for widespread application in the automotive sector, where lightweight material alternatives to steel are needed to reduce fuel consumption [28]. Besides high mechanical performance, high specific surface area carbon materials, both fibrous and particulate, are highly attractive. A high specific surface area may be obtained by the electrospinning of lignin-containing aqueous solutions [22,25,30–34] or from particulate lignin [35–39], both of which can be carbonized. Potential applications of this class of materials lie predominantly in electrochemistry and filtration [7,20,40,41].

Lignin-derived and electrically conductive carbon has been discussed recently [42–44]. It has been demonstrated that, compared to fossil-based carbon black, moderate electrical conductivity may be obtained. In turn, when such materials are used as filler, they endow polymeric matrices with electrical conductivity. On the downside, however, lignin-derived carbon particles are expected to impair the mechanical performance of the composite materials, especially affecting their tensile strength [45]. According to composite micromechanics, such degradation in tensile strength upon addition of particulate filler diminishes with decreasing particle size [45]. The particle size of commercial, shape-amorphous lignin is in the order of 10 µm–100 µm [6,36,42,46], whereas the diameter of lignin particles obtained by spray-drying of pulping liquor is 1 µm–5 µm [43]. Several preparation procedures for submicron- to nano-scale lignin particles have been reported [6,9,46,47], and recently a high-throughput technology for submicron- and nanolignin synthesis via an aerosol flow reactor was introduced by Ago et al. [48], which has been shown to be cost-competitive and scalable [49]. Most relevantly, the method allows control of size, wettability, and surface morphology (wrinkled or smooth surfaces) [50]. In the present study, we obtained sub-micron carbon particles from spherical lignin beads according to this latter procedure [48] and compared the structures with commercially available (and amorphous) lignin powder, aiming to identify potential advantages of size diminution and shape toward the manufacture and use of carbon particles.

2. Materials and Methods

2.1. Materials

Indulin AT lignin was purchased from Meadwestvaco and used as received for reference purposes. The chemistry of this commercially available technical lignin is describes in detail in Reference [51]. Spherical and sub-micron lignin particles or beads were produced according to Ago et al. [48,49]. Briefly, the procedure involved the generation of small droplets of lignin solution in dimethylformamide via a jet atomizer that used nitrogen gas as the carrier, subsequent drying at 153 °C in a heated laminar flow reactor, and fractionation with a low-pressure impactor.

2.2. Carbonization

The two types of lignin powders were thermostabilized by slow heating at a rate of 0.01 °C min^{-1} from ambient temperature up to 250 °C in a Memmert oven. Slow heating in an ambient atmosphere induces oxidative changes in the lignin structure, resulting in the elimination of any thermoplastic behavior [52]. Thus, fusing of lignin particles during the initial heating phase of a carbonization process is prevented. Carbonization was carried out in a GERO HTK8 oven with a volume of 6 liters. An argon atmosphere (150 L h^{-1}) was used and heating was performed at rates of 1 °C min^{-1} up to 500 °C (1 h holding step), 5 °C min^{-1} up to 900 °C (1 h holding step), and a final step-up to 2000 °C at a rate of 5 °C min^{-1}, concluding with a final holding step of 1 h.

2.3. Preparation of Carbon-Filled Cellulose Nanopapers

In order to combine high strength and electrical conductivity, cellulose nanopapers with a carbon content of 15 wt.% were prepared by mixing the respective type of carbon particles with an aqueous cellulose nanofibril (CNF) suspension followed by filtration to remove water. The CNF was prepared from elementary chlorine free-bleached kraft pulp from spruce and pine wood and purchased as an aqueous suspension with a dry content of 5.9 wt.% from the Swiss Federal Laboratories for

Materials Science and Technology (EMPA). The suspension was diluted to 1.0 wt.% with deionized water and fibrillated by 100 passes at 700 bar in an APV 1000 high pressure homogenizer (SPX Flow Technology, Charlotte, NC, USA). For the preparation of the carbon/CNF mixtures, 42.5 g of the 1% CNF-suspension (equivalent to 0.425 g of dry CNF) and 0.075 g of oven dry carbon powder were poured into a beaker and filled up to a total of 200 g with deionized water. Relying on the known stabilizing function of nanocellulose on carbon nanomaterials [53], no additional dispersant was added. The resulting 0.25 wt.% suspension was homogenized with an Ultra-Turrax T10 (IKA-Werke, Staufen, Germany) basic disperser operated at 18,000 min^{-1} for 2 min. The suspension was then left to stand for 24 h after which it was again homogenized as described above. In order to optimize the dispersion of carbon particles, the suspension was sonicated using a Q500 Sonicator (QSonica, Newtown, CT, USA) equipped with a 0.5-inch diameter titanium probe. Sonication was carried out at a frequency of 20 kHz in pulse mode (50% output intensity) for a total of 3 min. The suspension was filtrated by means of a 1000 mL DURAN glass filtration apparatus equipped with a hydrophilic PVDF membrane filter (Merck No. DVPP09050) with a pore size of 0.65 µm. After filtration, the still wet CNF cake was carefully removed from the filter disc, sandwiched between two PVDF membrane filters and vacuum-dried at 93 °C and 0.1 bar for around 15 min in a Rapid-Koethen paper sheet former (Frank-PTI, Birkenau, Germany). The resulting carbon/CNF films had a diameter of 78 mm and a thickness of 0.2 ± 0.05 mm.

2.4. Characterization

Scanning electron microscopy was performed in a Quanta™ 250 FEG from FEI in high-vacuum secondary electron mode. For non-carbonized lignin specimens and carbon-filled cellulose nanopapers, sputter-coating with a thin gold layer was carried out prior to SEM. The electrical resistivity of pure carbon particle powders was measured at different pressures according to References [54–56]. Briefly, a volume of 0.2 cm^{-3} carbon powder as produced in the carbonization oven was placed into a polycarbonate cylinder sealed with a conducting aluminum sheet at its bottom. A steel piston was then inserted into the top end of the cylinder. The electrical conductivity of the powder was determined between the bottom and the top end of the cylinder while simultaneously exerting pressure on the piston. The first conductivity value was taken at a pressure of 0.05 MPa.

Wide angle X-ray diffraction was performed with a Rigaku SmartLab 5-Axis X-ray diffractometer using glass capillaries and Cu K alpha radiation with a wavelength of $\lambda = 0.15418$ nm. Intensity data were recorded in intervals of 0.02° between the scattering angles $2\theta = 5°$ and 50°. Small angle X-ray scattering (SAXS) was carried out with a Rigaku S-Max3000 3-pinhole SAXS camera with MM002+ source and a Triton 200 multiwire detector. Scattering images were recorded in the range from $q = 0.08$–8 nm^{-1}, with $q = 4 \sin\theta/\lambda$ the scattering vector, integrated and background corrected before further data evaluation.

Raman spectra were acquired using a Raman microscope (alpha300RA, WITec GmbH, Ulm, Germany) equipped with a green laser ($\lambda = 532$ nm), spectrometer with a 600 gmm^{-1} grating (UHTS 300 WITec, Ulm, Germany) and a CCD camera (Andor DU401ABV, Belfast, UK). The laser power was set to 5 mW and with an integration time of 0.05 s single spectra were collected every 250 nm over a region of 20 × 20 µm^2 (6400 spectra/region) using a 100× oil immersion objective (numerical aperture (NA) = 1.4). Finally, average spectra of three regions of the K and L samples were calculated (19,200 spectra/sample) and compared.

Cellulose nanopapers were characterized by means of tensile testing in a Zwick-Roell 20 kN universal testing machine equipped with a 10 kN load cell. Parallel strips with a width of 8 mm and a free length of 50 mm were strained at a rate of 1 mm min^{-1} until fracture. The suitability of carbon-filled cellulose nanopaper for compression sensing was evaluated by sandwiching nanopapers between steel foils and compressing them along their z-axis while measuring electric resistivity via the steel foil sandwich, which was electrically insulated from the testing machine.

3. Results and Discussion

3.1. Morphology

The morphology of sub-micron lignin-derived carbon particles is shown in comparison to carbon particles derived directly from as-received Indulin AT (Figure 1). Characteristically, Indulin AT yields geometrically undefined carbon particles with sizes between 10 µm and 100 µm. The surface of these particles was rough and internal cavities were typical. While a small fraction of particles was spherical, most of them presented irregular shapes. In comparison, sub-micron particles with characteristic size in the order of 50 nm to several 100 nm were nearly perfectly spherical in shape and smooth on the surface (note that wrinkle particles can be obtained with the same setup but were not considered in this investigation [50]). No signs of cavities were observed for these particles and it can be assumed that they were solid.

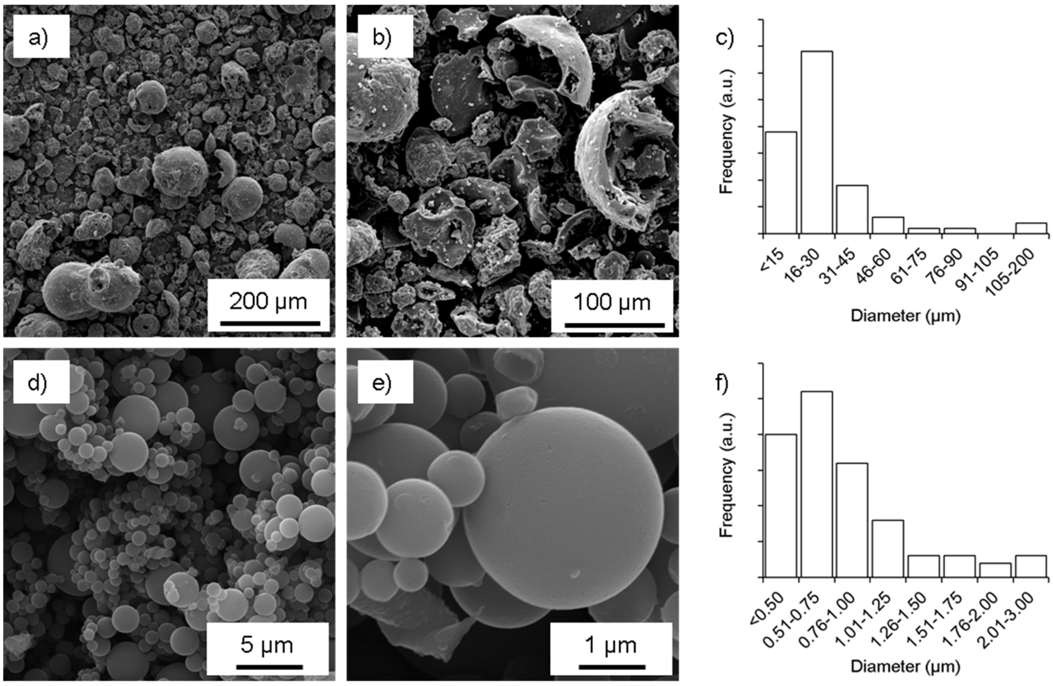

Figure 1. Scanning electron microscopy and diameter distribution (number frequency) of carbon particles derived from Indulin AT (**a**–**c**) and sub-micron lignin particles (**d**–**f**).

3.2. Structural Features

The results of extensive structural characterization of the two types of lignin-derived carbon particles are shown in Figure 2. X-ray diffraction (Figure 2a,b) reveals the presence of graphitic domains in both particle types, as indicated by the characteristic 002 diffraction peak originating from the stacking of graphene sheets in graphite [57]. When comparing the two carbon particles, this peak was more intense for the sub-micron spherical lignin-derived carbon. However, when compared to carbon derived directly from spray dried kraft black liquor in a different study [43], the ordered graphitic character was rather low. In the latter study, unpurified process liquors were carbonized. Small-angle X-ray scattering provides information about the internal pore structure of carbon materials. No significant differences were found in the scattering intensity distribution of the two types of carbon particles tested (Figure 2c,d). The pore radius was 1.09 ± 0.06 nm for Indulin AT carbon and 1.02 ± 0.04 for sub-micron lignin carbon. The corresponding surface area calculated from the scattering curves was 950 ± 140 m^2 cm^{-3} for Indulin AT and 860 ± 100 m^2 cm^{-3} for sub-micron lignin carbon.

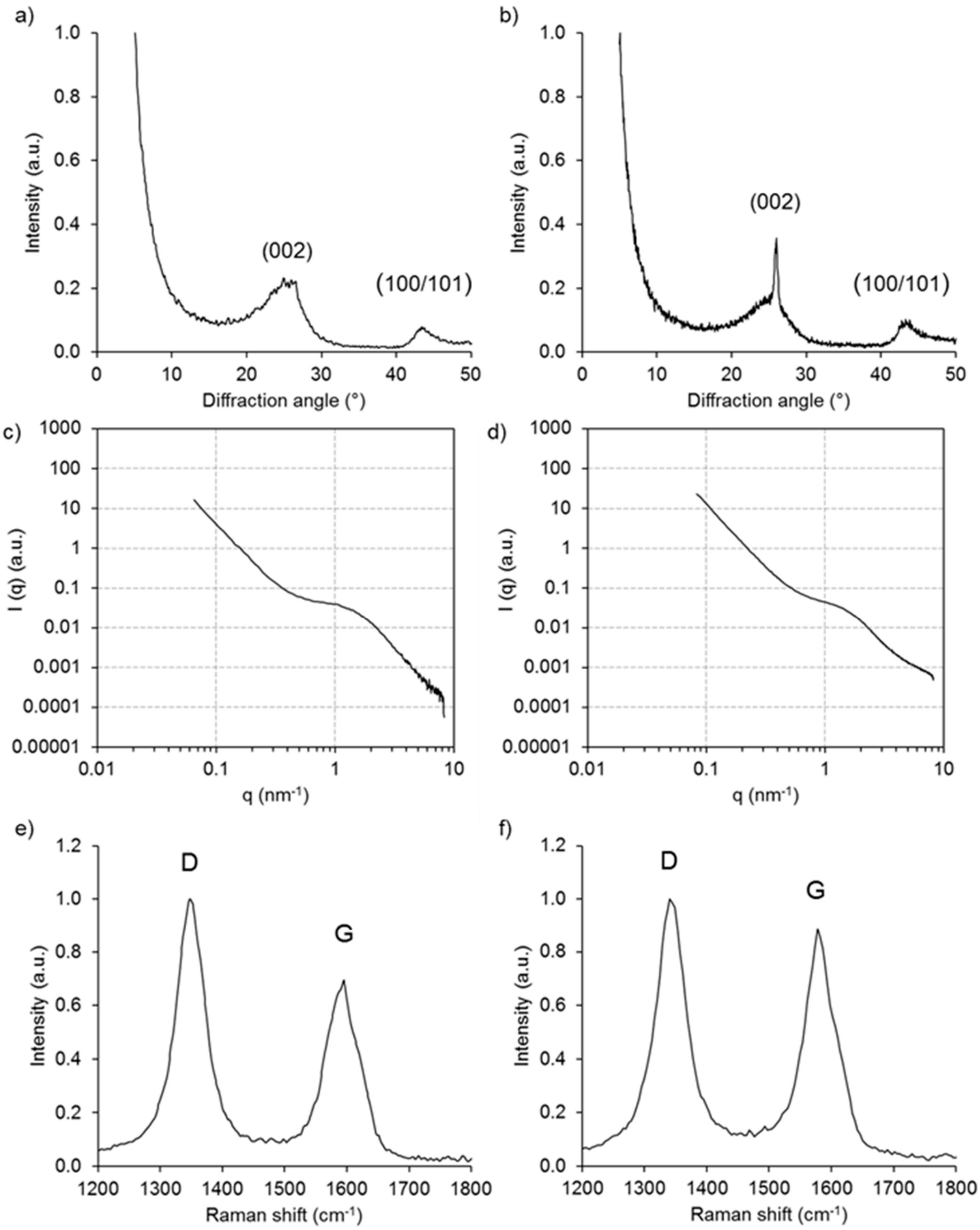

Figure 2. X-ray diffraction (**a**,**b**), small angle X-ray scattering (**c**,**d**), and Raman spectroscopy (**e**,**f**) of carbon particles derived from Indulin AT (**a**,**c**,**e**) and sub-micron lignin particles (**b**,**d**,**f**).

The finding of only moderately ordered graphitic structure for the carbons produced in the present study was corroborated by Raman spectroscopy (Figure 2e,f). Here, the G-band at ~1580 cm^{-1}, which is associated with a highly ordered graphitic lattice, and the D-band at 1350 cm^{-1}, which represents signal from a disordered graphitic lattice [58], were evaluated. While in highly ordered graphite the G band is usually much more intense than the D band, this was not the case for the materials studied here. On the contrary, for both carbon particles the D band was the most intense, indicating only a low content of ordered graphitic domains. Using the ratio between the peak intensities of the D and G peak as an indicator, I_D/I_G was 1.13 for Indulin-derived carbon and 1.45 for sub-micron lignin derived carbon. This is similar in magnitude compared to I_D/I_G values of 1.25–1.26 obtained for mesoporous carbon obtained from lignin nanofiber networks [59], but significantly higher than I_D/I_G of 0.25 and 0.60 obtained for carbon produced by direct carbonization of kraft and sulphite pulping liquors, respectively. Nevertheless, both X-ray diffraction and Raman spectroscopy of the sub-micron lignin-derived carbon showed a tendency towards higher graphitic order compared to carbon prepared directly from Indulin AT powder.

3.3. Electrical Conductivity

The electrical conductivity of the obtained carbon materials is of primary interest within the present study. As shown in Figure 3, sub-micron lignin carbon showed significantly less conductivity than that derived from Indulin AT. While the latter showed conductivity in a range comparable to earlier results with lignin-derived carbon [42–44], sub-micron lignin carbon clearly showed poor performance. In this context, however, it has to be considered that the density of both carbon powders was significantly different during this experiment. During the conductivity measurement, the density of Indulin AT derived carbon was between 0.50 g cm^{-3} and 0.51 g cm^{-3}, whereby density increased linearly as increasing pressure was applied. For the sub-micron lignin derived carbon, the density was only between 0.28 g cm^{-3} and 0.29 g cm^{-3}. Thus, on the basis of mass, the conductivity difference between both powders was still present, but was less pronounced.

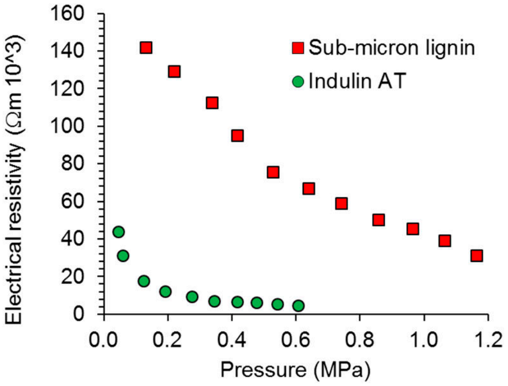

Figure 3. Pressure-dependent electrical resistivity of the two types of lignin-derived carbon powder.

3.4. Carbon-Filled Cellulose Nanopapers

Electrically conducting carbon may be used to endow a polymeric matrix with strain-sensing capability [44]. For this purpose, the matrix is filled with conducting filler at a content above the electric percolation threshold [60]. Tensile strain is then applied, which leads to an increasing distance between conductive filler particles and hence decreased electrical conductivity. In order not to impair the mechanical performance of the polymeric matrix, a small filling ratio is usually desired. In view of the relatively poor electrical conductivity of lignin-derived carbon obtained in the present study, this approach was deemed unsuitable because a high filling ratio of >20% would be required, as inferred from the percolation threshold of 20% carbon content determined in an earlier paper [44].

Instead, we evaluated the potential of the carbon particles as fillers in a setup used to assess the suitability of bio-based carbon in the manufacture of cellulose nanopaper for compression sensing. As shown in Figure 4, the presence of 15 wt.% carbon particles in CNF nanopaper significantly diminished the mechanical performance of this material. While pure CNF nanopaper showed a tensile modulus of 6.8 ± 0.32 GPa and strength of 195 ± 19 MPa, these values were reduced to 3.0 ± 0.08 GPa and 75 ± 3 MPa for sub-micron carbon, and 1.7 ± 0.01 GPa and 36 ± 1 MPa for Indulin AT carbon, respectively.

The results were as expected; namely, the carbon filler diminished the mechanical properties of cellulose nanopapers since there was a clear lack of interfacial adhesion between the carbon and the cellulose fibrils. Even so, nano-scale lignin may be beneficial to cellulose nanopaper mechanics, as it enhances the colloidal stability and dispersity of CNF in aqueous dispersions, and suppresses fibril aggregation during film formation [61]. What was surprising was the remarkably better performance of the sub-micron carbon over Indulin AT carbon. Clearly, the reduced particle size of the carbon filler, to the sub-micron size range, is an advantage [45]. Inquiring more deeply into the reasons for these observations, scanning electron microscopy (Figure 5) revealed a smooth surface for pure cellulose nanopaper. In contrast, the surface of nanopaper filled with Indulin AT carbon appeared rough, with several individual carbon particles with a diameter of 70–100 µm clearly visible. Sub-micron carbon filled nanopaper also appeared more structured than the smooth surface of pure cellulose nanopaper. However, the small sub-micron carbon particles appeared quite homogeneously distributed at this level of magnification. Images of fracture surfaces taken after tensile testing confirmed severe structural disorder due to the presence of comparably large carbon particles in Indulin AT filled nanopaper. By comparison, the structure of sub-micron lignin filled nanopaper appears much less disturbed due to the small size of carbon particles of this variant.

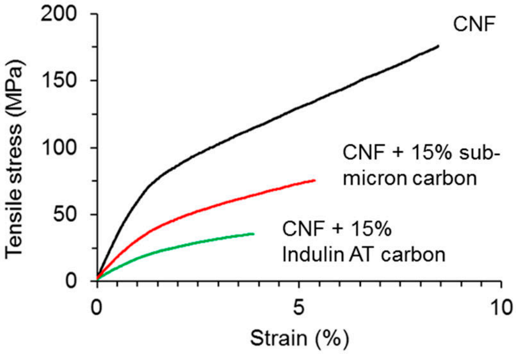

Figure 4. Representative stress-strain curves from tensile tests with pure cellulose nanopaper (CNF) and nanopaper filled with 15 wt.% carbon particles.

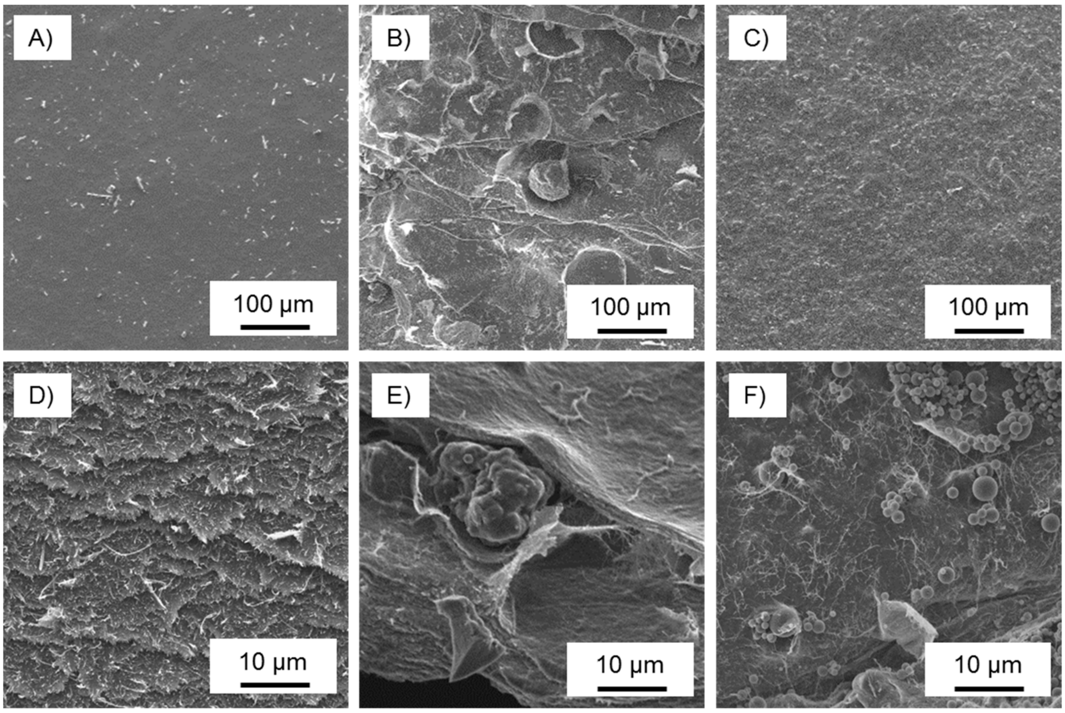

Figure 5. Scanning electron microscopy of the surface of pure cellulose nanopaper (**A**), nanopaper filled with 15 wt.% Indulin AT carbon (**B**), nanopaper filled with 15 wt.% sub-micron carbon (**C**), and corresponding fracture surfaces (**D**–**F**).

Most remarkably, compared to the values of electrical resistivity determined for the neat carbon powders, the resistivity of carbon-filled cellulose nanopapers was orders of magnitude higher.

The nanopapers filled with 15 wt.% carbon showed electrically insulating behavior at the beginning of a compression experiment (Figure 6); electrical current was registered starting from 25 MPa pressure for Indulin AT carbon and from 50 MPa onwards for nanopapers filled with sub-micron lignin carbon. Thus, in principle, composite material configurations such as the carbon-filled nanopaper might serve as compression sensors with moderate sensitivity at high loads, but their practical usefulness has yet to be determined.

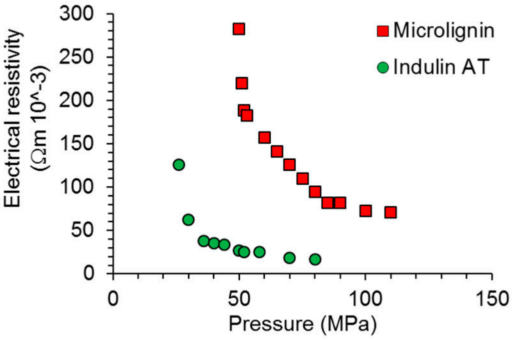

Figure 6. Pressure-dependent electrical resistivity along the out-of-plane direction of cellulose nanopapers filled with the two types of lignin-derived carbon particles.

4. Conclusions

The results presented above show that carbon particles with partially ordered graphitic structure and limited electrical conductivity can be produced from sub-micron lignin particles. Overall, sub-micron lignin derived carbon did not show significant differences in terms of structure and electrical conductivity compared to carbon produced from as-received Indulin AT lignin, with particle sizes ranging from 10 µm to 100 µm. The only very clear advantage of sub-micron lignin-derived carbon particles compared to their larger counterparts lies in their positive effect on tensile behavior. At a filler content of 15 wt.% sub-micron carbon filled cellulose nanopapers performed twice as well in terms of tensile strength and stiffness compared to nanopaper filled with Indulin AT-derived carbon.

Author Contributions: Investigation, J.K. (Janea Köhnke), C.U., H.R., N.G. and J.K. (Jozef Keckes); Writing—original draft preparation, J.K. (Janea Köhnke) and W.G.-A.; Writing—review and editing, O.J.R., C.Z., and W.G.-A.

Funding: J.K. (Janea Köhnke), C.Z., and W.G.-A. received funding from the Austrian Science Promotion Agency (FFG): Bridge Project 846543; N.G. received funding from the Austrian Science Fund (FWF): START Project Y-728-B16 and the European Research Council (ERC) under the European Union's Horizon 2020 research and innovation programme under grant agreement No 681885; C.U. received funding from the European Regional Development Fund (EFRE) and the province of Upper Austria through the program IWB 2014-2020 (project BioCarb-K).

Acknowledgments: All authors gratefully acknowledge access to infrastructure provided by the CEITEC Nano Research Infrastructure financed by the Ministry of Education, Youth and Sports of the Czech Republic (MEYS CR).

Conflicts of Interest: The authors declare no conflicts of interest. The funders had no role in the design of the study; in the collection, analyses, or interpretation of data; in the writing of the manuscript, or in the decision to publish the results.

References

1. Stern, T.; Ledl, C.; Braun, M.; Hesser, F.; Schwarzbauer, P. Biorefineries' impacts on the Austrian forest sector: A system dynamics approach. *Technol. Forecast. Soc. Chang.* **2015**, *91*, 311–326. [CrossRef]
2. Sahoo, S.; Seydibeyoğlu, M.Ö.; Mohanty, A.K.; Misra, M. Characterization of industrial lignins for their utilization in future value added applications. *Biomass Bioenergy* **2011**, *35*, 4230–4237. [CrossRef]
3. Laurichesse, S.; Avérous, L. Chemical modification of lignins: Towards biobased polymers. *Prog. Polym. Sci.* **2014**, *39*, 1266–1290. [CrossRef]

4. Schutyser, W.; Renders, T.; Van den Bosch, S.; Koelewijn, S.F.; Beckham, G.T.; Sels, B.F. Chemicals from lignin: An interplay of lignocellulose fractionation, depolymerisation, and upgrading. *Chem. Soc. Rev.* **2018**, *47*, 852–908. [CrossRef] [PubMed]
5. Fatehi, P.; Chen, J. Extraction of technical lignins from pulping spent liquors, challenges and opportunities. In *Production of Biofuels and Chemicals from Lignin*; Fang, Z., Smith, J.R.L., Eds.; Springer: Singapore, 2016; pp. 35–54.
6. Zhao, W.; Simmons, B.; Singh, S.; Ragauskas, A.; Cheng, G. From lignin association to nano-/micro-particle preparation: Extracting higher value of lignin. *Green Chem.* **2016**, *18*, 5693–5700. [CrossRef]
7. Chatterjee, S.; Saito, T.; Rios, O.; Johs, A. Lignin based carbon materials for energy storage applications. In *Green Technologies for the Environment*; American Chemical Society: Washington, DC, USA, 2014; Volume 1186, pp. 203–218.
8. Ragauskas, A.J.; Beckham, G.T.; Biddy, M.J.; Chandra, R.; Chen, F.; Davis, M.F.; Davison, B.H.; Dixon, R.A.; Gilna, P.; Keller, M.; et al. Lignin valorization: Improving lignin processing in the biorefinery. *Science* **2014**, *344*, 1246843. [CrossRef] [PubMed]
9. Tian, D.; Hu, J.; Bao, J.; Chandra, R.P.; Saddler, J.N.; Lu, C. Lignin valorization: Lignin nanoparticles as high-value bio-additive for multifunctional nanocomposites. *Biotechnol. Biofuels* **2017**, *10*, 192. [CrossRef] [PubMed]
10. Norgren, M.; Edlund, H. Lignin: Recent advances and emerging applications. *Curr. Opin. Colloid Interface Sci.* **2014**, *19*, 409–416. [CrossRef]
11. Tondi, G.; Link, M.; Kolbitsch, C.; Gavino, J.; Luckeneder, P.; Petutschnigg, A.; Herchl, R.; Van Doorslaer, C. Lignin-based foams: Production process and characterization. *Bioresources* **2016**, *11*, 2972–2986. [CrossRef]
12. Rojas, O.J.; Bullon, J.; Ysambertt, F.; Forgiarini, A.; Salager, J.-L.; Argyropoulos, D.S. Lignins as emulsion stabilizers. In *Materials, Chemicals, and Energy from Forest Biomass*; Argyropoulos, D.S., Ed.; American Chemical Society: Washington, DC, USA, 2007; Volume 954, pp. 182–199.
13. Brodin, M.; Vallejos, M.; Opedal, M.T.; Area, M.C.; Chinga-Carrasco, G. Lignocellulosics as sustainable resources for production of bioplastics—A review. *J. Clean. Prod.* **2017**, *162*, 646–664. [CrossRef]
14. Beckham, G.T.; Johnson, C.W.; Karp, E.M.; Salvachua, D.; Vardon, D.R. Opportunities and challenges in biological lignin valorization. *Curr. Opin. Biotechnol.* **2016**, *42*, 40–53. [CrossRef] [PubMed]
15. Laskar, D.D.; Yang, B.; Wang, H.M.; Lee, J. Pathways for biomass-derived lignin to hydrocarbon fuels. *Biofuels Bioprod. Biorefin.-Biofpr* **2013**, *7*, 602–626. [CrossRef]
16. Rinaldi, R.; Jastrzebski, R.; Clough, M.T.; Ralph, J.; Kennema, M.; Bruijnincx, P.C.A.; Weckhuysen, B.M. Paving the way for lignin valorisation: Recent advances in bioengineering, biorefining and catalysis. *Angew. Chem. Int. Ed.* **2016**, *55*, 8164–8215. [CrossRef] [PubMed]
17. Duval, A.; Lawoko, M. A review on lignin-based polymeric, micro- and nano-structured materials. *React. Funct. Polym.* **2014**, *85*, 78–96. [CrossRef]
18. Kai, D.; Tan, M.J.; Chee, P.L.; Chua, Y.K.; Yap, Y.L.; Loh, X.J. Towards lignin-based functional materials in a sustainable world. *Green Chem.* **2016**, *18*, 1175–1200. [CrossRef]
19. Bruijnincx, P.C.A.; Rinaldi, R.; Weckhuysen, B.M. Unlocking the potential of a sleeping giant: Lignins as sustainable raw materials for renewable fuels, chemicals and materials. *Green Chem.* **2015**, *17*, 4860–4861. [CrossRef]
20. Borghei, M.; Lehtonen, J.; Liu, L.; Rojas, O.J. Advanced biomass-derived electrocatalysts for the oxygen reduction reaction. *Adv. Mater.* **2018**, *30*, 1703691. [CrossRef]
21. Olsson, C.; Sjoholm, E.; Reimann, A. Carbon fibres from precursors produced by dry-jet wet-spinning of kraft lignin blended with kraft pulps. *Holzforschung* **2017**, *71*, 275–283. [CrossRef]
22. Yen, S.H.; Chang, F.C. Effects of fiber processing conditions on the yield, carbon content, and diameter of lignosulfonate-based carbon fibers. *Bioresources* **2016**, *11*, 10158–10172. [CrossRef]
23. Kadla, J.F.; Kubo, S.; Venditti, R.A.; Gilbert, R.D.; Compere, A.L.; Griffith, W. Lignin-based carbon fibers for composite fiber applications. *Carbon* **2002**, *40*, 2913–2920. [CrossRef]
24. Braun, J.L.; Holtman, K.M.; Kadla, J.F. Lignin-based carbon fibers: Oxidative thermostabilization of kraft lignin. *Carbon* **2005**, *43*, 385–394. [CrossRef]
25. Fang, W.; Yang, S.; Wang, X.-L.; Yuan, T.-Q.; Sun, R.-C. Manufacture and application of lignin-based carbon fibers (lcfs) and lignin-based carbon nanofibers (lcnfs). *Green Chem.* **2017**, *19*, 1794–1827. [CrossRef]

26. Li, Q.; Xie, S.X.; Serem, W.K.; Naik, M.T.; Liu, L.; Yuan, J.S. Quality carbon fibers from fractionated lignin. *Green Chem.* **2017**, *19*, 1628–1634. [CrossRef]
27. Ogale, A.A.; Zhang, M.; Jin, J. Recent advances in carbon fibers derived from biobased precursors. *J. Appl. Polym. Sci.* **2016**, *133*. [CrossRef]
28. Baker, D.A.; Rials, T.G. Recent advances in low-cost carbon fiber manufacture from lignin. *J. Appl. Polym. Sci.* **2013**, *130*, 713–728. [CrossRef]
29. Vincent, S.; Prado, R.; Kuzmina, O.; Potter, K.; Bhardwaj, J.; Wanasekara, N.D.; Harniman, R.L.; Koutsomitopoulou, A.; Eichhorn, S.J.; Welton, T.; et al. Regenerated cellulose and willow lignin blends as potential renewable precursors for carbon fibers. *ACS Sustain. Chem. Eng.* **2018**, *6*, 5903–5910. [CrossRef]
30. Cho, M.J.; Karaaslan, M.A.; Renneckar, S.; Ko, F. Enhancement of the mechanical properties of electrospun lignin-based nanofibers by heat treatment. *J. Mater. Sci.* **2017**, *52*, 9602–9614. [CrossRef]
31. Shi, Z.Q.; Jin, G.Q.; Wang, J.; Zhang, J. Free-standing, welded mesoporous carbon nanofibers as anode for high-rate performance li-ion batteries. *J. Electroanal. Chem.* **2017**, *795*, 26–31. [CrossRef]
32. Tao, L.; Zheng, Y.W.; Zhang, Y.H.; Ma, H.; Di, M.W.; Zheng, Z.F. Liquefied walnut shell-derived carbon nanofibrous mats as highly efficient anode materials for lithium ion batteries. *RSC Adv.* **2017**, *7*, 27113–27120. [CrossRef]
33. Ruiz-Rosas, R.; Bedia, J.; Lallave, M.; Loscertales, I.G.; Barrero, A.; Rodríguez-Mirasol, J.; Cordero, T. The production of submicron diameter carbon fibers by the electrospinning of lignin. *Carbon* **2010**, *48*, 696–705. [CrossRef]
34. Svinterikos, E.; Zuburtikudis, I. Tailor-made electrospun nanofibers of biowaste lignin/recycled poly(ethylene terephthalate). *J. Polym. Environ.* **2017**, *25*, 465–478. [CrossRef]
35. Pang, J.; Zhang, W.F.; Zhang, J.L.; Zhang, H.M.; Cao, G.P.; Han, M.F.; Yang, Y.S. Oxygen and nitrogen co-enriched sustainable porous carbon hollow microspheres from sodium lignosulfonate for supercapacitors with high volumetric energy densities. *Chemelectrochem* **2018**, *5*, 1306–1320. [CrossRef]
36. Kim, D.; Cheon, J.; Kim, J.; Hwang, D.; Hong, I.; Kwon, O.H.; Park, W.H.; Cho, D. Extraction and characterization of lignin from black liquor and preparation of biomass-based activated carbon therefrom. *Carbon Lett.* **2017**, *22*, 81–88.
37. Li, Z.L.; Ge, Y.Y.; Wan, L. Fabrication of a green porous lignin-based sphere for the removal of lead ions from aqueous media. *J. Hazard. Mater.* **2015**, *285*, 77–83. [CrossRef] [PubMed]
38. Rodríguez Correa, C.; Stollovsky, M.; Hehr, T.; Rauscher, Y.; Rolli, B.; Kruse, A. Influence of the carbonization process on activated carbon properties from lignin and lignin-rich biomasses. *ACS Sustain. Chem. Eng.* **2017**. [CrossRef]
39. Beisl, S.; Friedl, A.; Miltner, A. Lignin from micro- to nanosize: Applications. *Int. J. Mol. Sci.* **2017**, *18*, 2367. [CrossRef] [PubMed]
40. García-Negrón, V.; Phillip, N.D.; Li, J.; Daniel, C.; Wood, D.; Keffer, D.J.; Rios, O.; Harper, D.P. Processing–structure–property relationships for lignin-based carbonaceous materials used in energy-storage applications. *Energy Technol.* **2017**, *5*, 1311–1321. [CrossRef]
41. Khan, A.; Nair, V.; Colmenares, J.C.; Glaser, R. Lignin-based composite materials for photocatalysis and photovoltaics. *Top. Curr. Chem.* **2018**, *376*, 20. [CrossRef]
42. Köhnke, J.; Fürst, C.; Unterweger, C.; Rennhofer, H.; Lichtenegger, H.C.; Keckes, J.; Emsenhuber, G.; Mahendran, A.R.; Liebner, F.; Gindl-Altmutter, W. Carbon microparticles from organosolv lignin as filler for conducting poly(lactic acid). *Polymers* **2016**, *8*, 205. [CrossRef]
43. Köhnke, J.; Rennhofer, H.; Lichtenegger, H.; Mahendran, A.R.; Unterweger, C.; Prats-Mateu, B.; Gierlinger, N.; Schwaiger, E.; Mahler, A.-K.; Potthast, A.; et al. Electrically conducting carbon microparticles by direct carbonization of spent wood pulping liquor. *ACS Sustain. Chem. Eng.* **2018**, *6*, 3385–3391. [CrossRef]
44. Gindl-Altmutter, W.; Fürst, C.; Mahendran, A.R.; Obersriebnig, M.; Emsenhuber, G.; Kluge, M.; Veigel, S.; Keckes, J.; Liebner, F. Electrically conductive kraft lignin-based carbon filler for polymers. *Carbon* **2015**, *89*, 161–168. [CrossRef]
45. Fu, S.-Y.; Feng, X.-Q.; Lauke, B.; Mai, Y.-W. Effects of particle size, particle/matrix interface adhesion and particle loading on mechanical properties of particulate–polymer composites. *Compos. Part B Eng.* **2008**, *39*, 933–961. [CrossRef]
46. Beisl, S.; Miltner, A.; Friedl, A. Lignin from micro- to nanosize: Production methods. *Int. J. Mol. Sci.* **2017**, *18*, 1244. [CrossRef] [PubMed]

47. Lievonen, M.; Valle-Delgado, J.J.; Mattinen, M.L.; Hult, E.L.; Lintinen, K.; Kostiainen, M.A.; Paananen, A.; Szilvay, G.R.; Setala, H.; Osterberg, M. A simple process for lignin nanoparticle preparation. *Green Chem.* **2016**, *18*, 1416–1422. [CrossRef]
48. Ago, M.; Huan, S.; Borghei, M.; Raula, J.; Kauppinen, E.I.; Rojas, O.J. High-throughput synthesis of lignin particles (similar to 30 nm to similar to 2 mu m) via aerosol flow reactor: Size fractionation and utilization in pickering emulsions. *ACS Appl. Mater. Interfaces* **2016**, *8*, 23302–23310. [CrossRef] [PubMed]
49. Abbati de Assis, C.; Greca, L.G.; Ago, M.; Balakshin, M.Y.; Jameel, H.; Gonzalez, R.; Rojas, O.J. Techno-economic assessment, scalability, and applications of aerosol lignin micro- and nanoparticles. *ACS Sustain. Chem. Eng.* **2018**, *6*, 11853–11868. [CrossRef] [PubMed]
50. Kämäräinen, T.; Ago, M.; Seitsonen, J.; Raula, J.; Kauppinen, E.I.; Ruokolainen, J.; Rojas, O.J. Harmonic analysis of surface instability patterns on colloidal particles. *Soft Matter* **2018**, *14*, 3387–3396. [CrossRef]
51. Constant, S.; Wienk, H.L.J.; Frissen, A.E.; de Peinder, P.; Boelens, R.; van Es, D.S.; Grisel, R.J.H.; Weckhuysen, B.M.; Huijgen, W.J.J.; Gosselink, R.J.A.; et al. New insights into the structure and composition of technical lignins: A comparative characterisation study. *Green Chem.* **2016**, *18*, 2651–2665. [CrossRef]
52. Norberg, I.; Nordström, Y.; Drougge, R.; Gellerstedt, G.; Sjöholm, E. A new method for stabilizing softwood kraft lignin fibers for carbon fiber production. *J. Appl. Polym. Sci.* **2013**, *128*, 3824–3830. [CrossRef]
53. Hajian, A.; Lindström, S.B.; Pettersson, T.; Hamedi, M.M.; Wågberg, L. Understanding the dispersive action of nanocellulose for carbon nanomaterials. *Nano Lett.* **2017**, *17*, 1439–1447. [CrossRef]
54. Sánchez-González, J.; Macías-García, A.; Alexandre-Franco, M.F.; Gómez-Serrano, V. Electrical conductivity of carbon blacks under compression. *Carbon* **2005**, *43*, 741–747. [CrossRef]
55. Celzard, A.; Marêché, J.F.; Payot, F.; Furdin, G. Electrical conductivity of carbonaceous powders. *Carbon* **2002**, *40*, 2801–2815. [CrossRef]
56. Pantea, D.; Darmstadt, H.; Kaliaguine, S.; Sümmchen, L.; Roy, C. Electrical conductivity of thermal carbon blacks. *Carbon* **2001**, *39*, 1147–1158. [CrossRef]
57. Li, Z.Q.; Lu, C.J.; Xia, Z.P.; Zhou, Y.; Luo, Z. X-ray diffraction patterns of graphite and turbostratic carbon. *Carbon* **2007**, *45*, 1686–1695. [CrossRef]
58. Sadezky, A.; Muckenhuber, H.; Grothe, H.; Niessner, R.; Pöschl, U. Raman microspectroscopy of soot and related carbonaceous materials: Spectral analysis and structural information. *Carbon* **2005**, *43*, 1731–1742. [CrossRef]
59. Ago, M.; Borghei, M.; Haataja, J.S.; Rojas, O.J. Mesoporous carbon soft-templated from lignin nanofiber networks: Microphase separation boosts supercapacitance in conductive electrodes. *RSC Adv.* **2016**, *6*, 85802–85810. [CrossRef]
60. Pan, Y.; Weng, G.J.; Meguid, S.A.; Bao, W.S.; Zhu, Z.H.; Hamouda, A.M.S. Percolation threshold and electrical conductivity of a two-phase composite containing randomly oriented ellipsoidal inclusions. *J. Appl. Phys.* **2011**, *110*, 123715. [CrossRef]
61. Liu, Y. Strong and flexible nanocomposites of carboxylated cellulose nanofibril dispersed by industrial lignin. *ACS Sustain. Chem. Eng.* **2018**, *6*, 5524–5532. [CrossRef]